UNIVERSITÀ DEGLI STUDI DI MILANO

PhD degree in Systems Medicine

Dept. Of Oncology and Emato-Oncology

DISSECTING THE ROLE OF GOLGI TRAFFIC IN BRAIN DEVELOPMENT ACROSS HEALTH AND DISEASE: A LESSON FROM COG5-CDG STUDIES

MEDS-02/A

Martina Polenghi
Matr. R13497
ORCID n. 0009-0003-6358-3901

Elena Taverna

DIEGO PASINI

A.A. 2024-2025

Acknowledgments

This work would not have been possible without the support of Dr. Elena Taverna, under whose supervision I began to work on this project and to grow as a researcher. I am very grateful that you had the openness and believed in me enough to take me on as a young researcher with little experience in the neurodevelopmental field.

I would like to deeply thank Dr. Elena Restelli for committing so much time to teach me almost all the experimental skills I own today and for constantly helping and providing support when I felt lost or confused.

Of course, I cannot thank enough my science colleagues and dearest friends, Valentina and Giulia, without whom my PhD would have been darker. You have been and really are my happiness during the bad days and the good days. Thanks for your constant support, for the help and for all the inspiring discussions that we always have. You are the fil rouge of my days and I'm incredibly fortunate to call you my friend. Also, thanks for standing and sharing my insane passion for animals, and dogs especially.

Finally, but not for importance, I would like to thank my mum, that supported me throughout all the decisions I've made during these years, that has always been and will always be my safe and happy place to go to. You have always inspired me to pursue my interests and to develop every project that came to my mind. You always make me feel in the right place and loved. No words on a page can express my gratitude for everything you have done for me. I hope that this work makes you proud. A special thank to Margot, my beloved dog, for all the furry supportive hugs.

Abstract

Neurons forming the neocortex are generated during embryonic development from two main classes of neural progenitor cells: apical and basal progenitors (APs and BPs, respectively). The cell fate switch from AP to BP is accompanied by changes in polarization and intracellular architecture. Interestingly, Golgi apparatus (GA) is differentially positioned in APs and BPs. GA is the main hub for glycosylation and defects in GA and associated glycosylation are observed in a group of rare multi system diseases collectively referred to as Congenital Disorders of Glycosylation (CDGs). Notably, brain development impairments, such as primary microcephaly, are described in most CDG patients. Despite the increased number of diagnosed patients, the cell biological mechanisms linking defective Golgi glycosylation and neurodevelopmental manifestations are currently unknown.

Here we try to fill this gap by investigating the influence of GA on cell identity and fate transition during brain development.

In this study we show that pharmacologically induced GA fragmentation results in a premature cell fate switch from apical to basal progenitors, prompting to a link between Golgi apparatus homeostasis and cell identity and fate in brain development. Using ML-guided automated microinjection we prove that the premature cell fate switch is caused by an increase in symmetric differentiative divisions of AP cells.

To specifically study GA polarization in APs and GA-related glycosylation in physiology and disease in humans, we select COG5 as a target for functional manipulation. COG5 is a subunit of the Conserved Oligomeric Golgi Complex (COG) whose mutation is associated with primary microcephaly and glycosylation impairments.

We first use electroporation in organoids to knock down COG5 and we observe that depletion of COG5 affects Golgi integrity and causes an increase in BPs and in Ctip2+ neurons suggesting that targeted GA perturbation influences the program of cell proliferation vs differentiation.

To gain more insights into the cellular logic linking GA and cell fate switch we generate human brain organoids from two patients harboring a novel COG5 mutation that causes reduced levels of COG5 protein and of its COG7 interactor. Concomitantly, reduction of glycosphingolipid (GSL) subtypes is observed.

In the brain organoids of the COG5 CDG patients, an impairment on APs Golgi structure is observed. This is paralleled by changes in the apical progenitor cells division plane, that ultimately affect NPCs and neuronal populations abundance. These observations are consistent with the microcephalic clinical phenotype described for the two patients.

Finally, we show that COG5 mutation can differentially regulate cell fate switch trajectories, possibly by influencing signaling pathways determinants trafficking, and we specifically propose a role of ACBD3-mediated Notch/Numb pathway.

In conclusion, our data suggest that GA is linked to cell fate switch during brain development and that GA is crucial for the control of cell proliferation vs differentiation possibly by influencing the trafficking of cell fate determinants.

TABLE OF CONTENTS

INTRODUCTION 10

BRAIN DEVELOPMENT 10
NEURAL STEM CELL TYPES IN THE DEVELOPING BRAIN 10
APICAL PROGENITORS 11
BASAL PROGENITORS 12
NEURONS 13
INTRACELLULAR TRAFFICKING PATHWAYS 13
THE ENDOPLASMIC RETICULUM 14
THE GOLGI APPARATUS 15
THE GOLGI APPARATUS AND HUMAN DISEASES 16
GLYCOSYLATION 17
CELL POLARITY 18
POLARITY IN APICAL PROGENITORS 18
INTRECELLULAR ARCHITECTURE OF CELL FATE TRANSITION 20
CONGENITAL DISORDERS OF GLYCOSYLATION (CDGS) 21
Classification *22*
CDG mutations, symptoms and treatments *22*
TRANSPORT IN THE GOLGI APPARATUS 24
THE COG COMPLEX 25
COG5 ..... *26*
HUMAN NEURODEVELOPMENTAL DISORDERS IN A DISH: THE IPSCS REVOLUTION 27
PATHOLOGY, ONE CELL AT THE TIME 28

MATERIALS & METHODS 30

MICE 30
Hemisphere rotating culture (HERO) and pharmacological treatment *30*
2D CELL CULTURE 30
HeLa *30*
Fibroblasts *31*
Fibroblast reprogramming *31*
BFA treatment of HeLa and fibroblasts *32*
ORGANOIDS AND IPSCS 32
Thawing iPSCs *32*
iPSCs culture *32*
iPSCs maintenance *32*
Freezing iPSCs *33*
KO line production *33*
Organoids culture *33*
SCRNASEQ 34
scRNAseq data analysis *35*
Functional enrichment analysis *36*
LIPID GLYCOMICS 36
PHARMACOLOGICAL TREATMENT ON HUMAN BRAIN ORGANOIDS 37
EDU LABELING ON HUMAN BRAIN ORGANOIDS 37
PREPARATION OF ORGANOTYPIC TISSUE SLICES FROM HUMAN BRAIN ORGANOID AND MOUSE EMBRYONIC BRAIN TISSUE 37

MICROINJECTION FOR LINEAGE TRACING 37
Fixation, embedding, and sectioning of microinjected organoids and mouse tissue 38
Brain organoids clearing for whole mount analysis 38
IMMUNOFLUORESCENCE STAINING 39
IMAGE ACQUISITION 40
IMAGE ANALYSIS 40
Image analysis for the reconstruction of single cell intracellular architecture 41
SHRNA PLASMID PREPARATION 41
SHRNA VALIDATION ON HELA CELLS 42
ELECTROPORATION 42
WESTERN BLOT 42
Western blot on lectins 43
AUTOMATIC ANNOTATION 44
TARGET ANNOTATION AND TISSUE EDGE DETECTION 44
RESULTS 48
DEVELOPING TECHNOLOGY FOR SINGLE CELL MANIPULATION IN TISSUE 48
Autoinjector set up 49
Calibration automation 49
Automated tissue annotation 50
Robotic microinjection performance in mouse brain slices and human brain organoids 51
Reconstructing intracellular architecture using microinjection 53
HUMAN BRAIN ORGANOIDS TO MODEL BRAIN DEVELOPMENT IN A DISH 55
GA IN THE HUMAN DEVELOPING BRAIN 57
ACUTE GA DISASSEMBLY FAVORS AP-TO-BP FATE TRANSITION 58
GA DISASSEMBLY AFFECTS FATE TRANSITION BY FAVORING SYMMETRIC DIFFERENTIATIVE DIVISION OF APICAL PROGENITORS 62
COG5 KNOCK DOWN AFFECTS CELL IDENTITY AND FATE OF NEURAL PROGENITOR CELLS 65
COG5 IS LOCALIZED AT THE GOLGI APPARATUS IN NEURAL PROGENITOR CELLS 65
GENETIC PERTURBATION OF COG5 IN HUMAN BRAIN ORGANOIDS USING SHRNA ELECTROPORATION RESULTS IN THE DISASSEMBLY OF THE GOLGI APPARATUS 67
THE ACUTE KNOCK-DOWN OF COG5 IN HUMAN BRAIN ORGANOIDS FAVOURS THE GENERATION OF BPS 69
MODELING THE NEURODEVELOPMENTAL MANIFESTATIONS OF COG5-CDG USING HUMAN BRAIN ORGANOIDS 72
Identification of two COG5-CDG patients harboring new COG5 mutations 72
COG5-CDG human brain organoids reveal defects in the COG complex 75
COG5-CDG mutations affect GA architecture in apical progenitors 76
Brain organoids from COG5-CDG patients show impaired growth and general architecture 77
COG5-CDG alters the mode of division of apical progenitors 83
The analysis of scRNAseq transcriptional make up reveals premature switch to neuron generation 84
Pathways analysis in APs reveals alterations in Notch pathways 91
COG5-CDG shows a change in the subcellular distribution of Numb/Notch upstream regulators 94
Pathways analysis in BPs 96
Pathways analysis in neurons 100
Glycans profiles in COG5-CDG human brain organoids 102
Glyco-lipidomics in COG5-CDG human brain organoids 104
DISCUSSION 106

A machine learning-guided microinjection robot to target and study single cells in the developing brain 106
Polarized localization of the GA in human apical progenitors 107
Acute GA fragmentation induces a cell fate switch 108
Leveraging the genetics of CDGs to understand the mechanisms linking GA function to neural stem cell identity 108
COG5 mutations affect cell fate and identity during brain organoid development 109
COG5 mutations affect the mode of division of APs 110
ACBD3 distribution in COG5 mutant brain organoids 111
Divergent cellular and molecular phenotypes in COG5-CDG patients 111
Considerations on the effects of COG5-KO on neural stem cells 113
Are glycolipids a main molecular target in COG5-CDG? 113
Conclusions 114
APPENDIX 115
Introduction 115
Materials and methods 116
Organoids *116*
Cryopreservation protocol *116*
Organoids dissociation *117*
Fixation, embedding, and sectioning of microinjected organoids *117*
Immunofluorescence *117*
Preliminary Results 121
Characterization of thawed organoids *121*
Neurons from cryopreserved organoids *122*
Conclusions and discussion 125
BIBLIOGRAPHY 126

FIGURES AND TABLES

FIGURE 1. NEURAL STEM CELLS IN THE DEVELOPING MOUSE AND HUMAN BRAIN. 11
FIGURE 2. CONVENTIONAL AND UNCONVENTIONAL TRAFFICKING ROUTES IN APS 20
FIGURE 3.LOCALIZATION OF TRAFFICKING ORGANELLES IN APS AND BPS 21
FIGURE 4. SCHEMATIC REPRESENTATION OF BRAIN ORGANOID GENERATION PROTOCOL. 34
FIGURE 5. AUTOINJECTOR SET UP.. 49
FIGURE 6. AUTOMATED CALIBRATION AND TISSUE ANNOTATION. 51
FIGURE 7. ML-GUIDED MICROINJECTION OF SINGLE NEURONS IN EMBRYONIC MOUSE BRAIN TISSUE. 52
FIGURE 8. APPLICATION OF THE ML-GUIDED AUTOINJECTOR ON HUMAN BRAIN ORGANOIDS-DERIVED NEURONS. 53
FIGURE 9. ML-GUIDED AUTOINJECTOR ALLOWS TO RECONSTRUCT CELLULAR MORPHOLOGY AND INTRACELLULAR ARCHITECTURE OR INJECTED CELLS IN HUMAN BRAIN ORGANOIDS. 55
FIGURE 10. HUMAN BRAIN ORGANOIDS RECAPITULATE BRAIN DEVELOPMENT IN VITRO. 57
FIGURE 11. GOLGI APPARATUS IS LOCALIZED IN THE APICAL PROCESS OF APICAL PROGENITORS IN HUMAN BRAIN ORGANOIDS. 58
FIGURE 12. DRUG TREATMENT-INDUCED GA FRAGMENTATION. 60
FIGURE 13. ACUTE GOLGI-DISASSEMBLING PHARMACOLOGICAL TREATMENT INCREASES THE NUMBER OF TBR2+ BPS IN BOTH EMBRYONIC MOUSE BRAIN AND HUMAN BRAIN ORGANOIDS. 62
FIGURE 14.LINEAGE TRACING USING THE ML-GUIDED AUTOINJECTOR REVEALS THAT DRUG TREATMENT-INDUCED GOLGI APPARATUS FRAGMENTATION FAVORS SYMMETRIC DIFFERENTIATIVE DIVISION OF APICAL PROGENITORS. 64
FIGURE 15. COG5 IS EXPRESSED ACROSS CELL TYPES IN BRAIN DEVELOPMENT AND COLOCALIZES WITH GOLGI APPARATUS. 66
FIGURE 16. COG5 KD IN HELA CELLS COMPROMISES GOLGI INTEGRITY. 68
FIGURE 17. KNOCK DOWN OF COG5 IN HUMAN BRAIN ORGANOIDS AFFECTS THE INTEGRITY OF GOLGI APPARATUS AND AFFECTS DEVELOPMENTAL TRAJECTORIES. 70
FIGURE 18. COG5 KD DOES NOT AFFECT THE NUMBER OF CYCLING CELLS. 71
FIGURE 19. CHARACTERIZATION OF A NOVEL COG5 MUTATION IN TWO CDG PATIENTS. 73
FIGURE 20. COG5 MUTATION AFFECTS THE STRUCTURE OF GOLGI APPARATUS. 75
FIGURE 21. COG5 MUTATION DECREASES COG5 AND COG7 PROTEIN LEVELS. 76
FIGURE 22. GOLGI APPARATUS STRUCTURAL INTEGRITY IS AFFECTED BY COG5 MUTATION AND COG5 KO 77
FIGURE 23. HUMAN BRAIN ORGANOIDS RECAPITULATE THE MICROCEPHALIC PHENOTYPE OF THE TWO PATIENTS. 79
FIGURE 24. COG5 MUTATION AND KO DIFFERENTIALLY IMPAIR BRAIN DEVELOPMENT BY ALTERING PROGENITORS AND NEURONS COMPOSITION. 80
FIGURE 25. COG5 MUTATION DECREASES THE THICKNESS OF THE VENTRICULAR AREA AND OF THE NEURONAL LAYER IN BRAIN ORGANOIDS. 81
FIGURE 26. COG5 KO ALTERS THE NUMBER OF CYCLING CELLS. 82
FIGURE 27. COG5 MUTATION AFFECTS THE CELL DIVISION PLANE IN APICAL PROGENITOR CELLS 84
FIGURE 28. IDENTIFICATION OF NPCS AND NEUORONAL CLUSTERS WITH SCRNA SEQ ANALYSIS OF PATIENT DERIVED HUMAN BRAIN ORGANOIDS. 85
FIGURE 29. COG5 MUTATION REDUCES NPCS IN THE COG53 PATIENT. 86
FIGURE 30. COG5 MUTATION AFFECTS BOTH NPCS AND NEURONS IN COG52 FEMALE PATIENT 89
FIGURE 31. DIFFERENTIAL ABUNDANCE ANALYSIS REVEALS AN OVERALL DEPLETION OF ALL NPCS RELATED CELL CLUSTERS IN A COMPARISON BETWEEN COG53 AND COG52. 90
FIGURE 32. PATHWAYS ANALYSIS IN APS REVEALS ALTERATIONS IN CELL DIFFERENTIATION VS PROLIFERATION DECISION AND NEURONAL DEVELOPMENT PATHWAYS. 93
FIGURE 33. ACBD3 PROTEIN TRAFFICKING IN COG5 PATIENTS AND IN KO ORGANOIDS. 95
FIGURE 34. PATHWAYS ANALYSIS IN BPS REVEALS ALTERATIONS IN CNS DIFFERENTIATION AND AXONAL GUIDANCE PATHWAYS 98

FIGURE 35.NOTCH PATHWAY IS INHIBITED IN CLUSTER 7 CELLS FROM COG53 PATIENT ORGANOIDS. 99
FIGURE 36. ANALYSIS OF NEURONAL CLUSTERS REVEAL ACTIVATION OF NEURONAL DEVELOPMENTAL RELATED PATHWAY..... 101
FIGURE 37. SNA DISTRIBUTION IS IMPAIRED IN COG5-CDG PATIENTS BRAIN ORGANOIDS. 103
FIGURE 38. . LIPID GLYCOSYLATION ANALYSIS OF PATIENT DERIVED HUMAN BRAIN ORGANOIDS. 105
FIGURE 39. CRYOPRESERVED ORGANOIDS MAINTAIN THE INTERNAL STRUCTURE AND CELLULAR COMPOSITION AFTER THAWING..... 123
FIGURE 40. CRYOPRESERVED ORGANOIDS CAN BE DISSOCIATED INTO NPCS AND NEURONS. 124

TABLE 1. ANTIBODIES USED AND DILUTIONS 45
TABLE 2. ANTIBODIES USED FOR PROTOCOL SET UP. 120

ABBREVIATIONS

AJ	Apical Junction
AP	Apical Progenitor
aRG	apical Radial Glia
BFA	Brefeldin A
BP	Basal Progenitor
bRG	basal Radial Glia
BSA	Bovine Serum Albumin
CATCHR	Complexes Associated with Tethering Containing Helical Rods
CCT	Coiled-Coils Tether
CDG	Congenital Disorders of Glycosylation
Cer	Ceramide
CIMM	CO2-Independend microinjection medium
COG	Conserved Oligomeric Golgi complex
ConA	Concanavalin A
CP	Cortical Plate
CSF	Cerebrospinal Fluid
DM	Differentiation Medium
DMEM	Dulbecco's Modified Eagle Medium
DMSO	Dimethyl Sulfoxide
DNA	Deoxyribonucleic Acid
E	Embryonic
EB	Embryoid Bodies
ECM	Extracellular Matrix
ER	Endoplasmic Reticulum
ERGIC	ER-Golgi Intermediate Compartment
EtOH	Ethanol
FOV	Field of View
GA	Golgi Apparatus
GalNAc	N-acetylgalactosamine
GPI	Glycosylphosphatidylinositols
GSL	Glycosphingolipids
GUI	Graphic
GW	Gestational Week

HERO	Hemisphere Rotating culture
HRP	Horseradish Peroxidase
IF	Immunofluorecence
INM	Interkinetic Nuclear Migration
IP	Intermediate Progenitor
iPSC	Induced Pluripotent Stem Cells
ISVZ	Inner Subventricular Zone
KD	Knock down
KO	Knock out
MEM NEAA	MEM Non-Essential Amino Acids
ML	Machine Learning
MTC	Multisubunit Tethering Complex
MTOC	Microtubule Organizing Center
NE	Neuroepithelial Cells
NPC	Neural Progenitor Cells
o/n	Overnight
oRG	outer Radial Glia
OST	Oligosaccharyltransferase
OSVZ	Outer Subventricular Zone
PFA	Paraformaldhyde
PM	Plasma Membrane
PTFE	Polytetrafluoroethylene
PTM	Post Translational Modification
PVDF	Polyvinylidene Fluoride
RER	Rough Endoplasmic Reticulum
RNA	Ribonucleic Acid
RT	Room Temperature
SCM	Slice Culture Medium
SER	Smooth Endoplasmic Reticulum
SVZ	Subventricular Zone
TGN	Trans Golgi Network
VZ	Ventricular Zone
WGA	Wheat Germ Agglutinin

INTRODUCTION

Brain development

The mammalian brain, and the human brain in particular, is a complex organ that possess high-level network-like organization crucial for its function.

From an evolutionary point of view, the neocortex is the youngest part of the cerebral cortex and accounts for the acquisition of higher-order cognitive functions (Rakic 2009). Neocortex forms during embryonic development through a very precise sequence of symmetric and asymmetric division of neural progenitor cells (NPCs) (Noctor et al. 2004). NPCs' divisions are either proliferative or self-renewing and generate - in a direct or indirect way – neurons. NPCs' divisions are tightly regulated in order to ensure a controlled tissue organization in space and time. Newly formed neurons migrate radially to the basal part of the cortex where they form, along with supporting glial cells, the six-layered cortical plate (CP) (Harris et al. 2015). The development of cognitive abilities is thought to be linked to an increase in NPCs' diversity and number within the neocortex and a complexification of neurodevelopmental trajectories (Rakic 1995; Fish et al. 2008).

A key concept in brain development is cellular polarization, which is defined as the process through which cellular components and compartments are differentially localized within the cell (Buckley and St Johnston 2022). The acquisition and maintenance of cell identity and fate during brain development is crucial and it's linked to cellular polarization.

Neural stem cell types in the developing brain

Neurons that populate the neocortex are formed during brain development from NPCs. Two main classes of neural progenitors have been defined: apical progenitors (APs) and basal progenitors (BPs). This broad classification is based on the localization of the cell body within the developing neocortex and refers to the location where these cells undergo mitosis in (Taverna and Huttner 2010; Kosodo et al. 2011).

The developmental trajectories in the neocortex are directed from the apical side of the tissue -delimited by the ventricle- to the basal lamina that is directly in touch with the meninges.

APs are found in the apical most part of the developing cortex, in a region defined as ventricular zone (VZ), and they undergo mitosis at the apical surface lining the ventricle. BPs instead mostly reside in the subventricular zone (SVZ), located more basally, where they also divide.

APs and BPs own different morphologies and polarity cues, which make the process of cell fate switch from AP to BP particularly interesting to study, as it closely resemble an epithelial to mesenchymal transition (EMT) (Fietz and Huttner 2011).

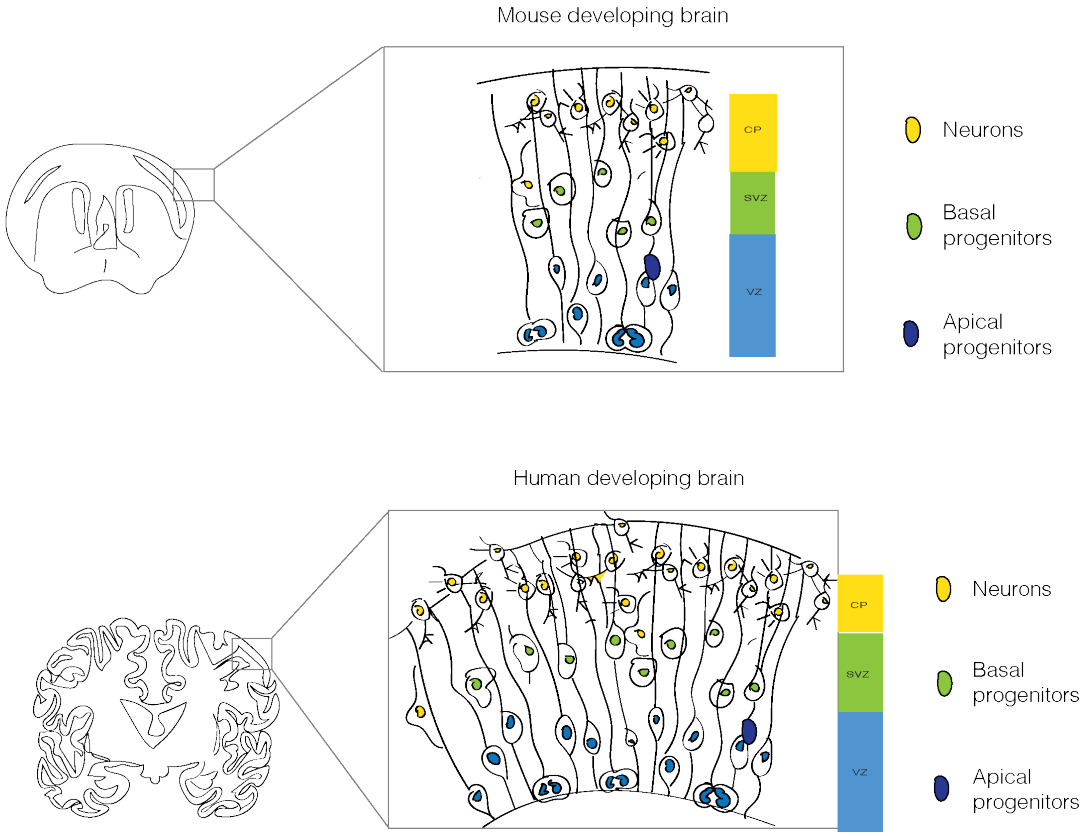


Figure 1. Neural stem cells in the developing mouse and human brain.

Scheme illustrating the neural stem cells that populate the developing mouse (up) and human (down) brain. Apical progenitors (APs, blue), are epithelial cells that occupy the ventricular zone (VZ) spanning the whole thickness of the developing neocortex. Basal progenitors (BPs, green) occupy the subventricular zone (SVZ) and represent the main source of neurons (yellow) in the developing mammalian brain

Apical progenitors

APs are very elongated epithelial cells that span the entire thickness of the cortical wall. They have a very small apical plasma membrane (1%-2% of the total plasma membrane) that contacts the ventricle, and a very elongated basolateral plasma membrane that reaches the basal lamina. This elongation can reach up to several millimeters as in the case of primate developing brain.

APs can be subdivided into two subclasses, neuroepithelial cells (NEs) and apical radial glia cells (aRGs).

NEs are the first stem cell type appearing early during neurogenesis (Kintner 2002); these cells span throughout the whole thickness of the developing cortex, and possess both an apical and a basal process separated by junctions; NEs cells form a pseudostratified epithelium and undergo interkinetic nuclear migration (INM), a process during which the nucleus moves along the apico-basal axis of the cell in concert with cell cycle progression. This process restricts mitosis to the apical surface, whereas S-phase takes place in the basal

most part of the VZ. As the founder cells of the central nervous system, NEs divide in a symmetric proliferation mode that expands the pool of NPCs (Götz and Huttner 2005).
At mid neurogenesis, NEs gives then rise to apical radial glia (aRG). aRGs retain many of the features of neuroepithelial cells. aRGs display radial glial markers and they are even more elongated than NE cells. Furthermore, similarly to NEs, aRG undergo INM. Of note, unlike NEs, aRGs develop a long basal process that crosses the SVZ and forming neuronal layer, and that keep the contact with the basal lamina. aRGs typically divide through asymmetric self-renewing division, giving rise to an aRG and a BP (Paridaen and Huttner 2014; Arai and Taverna 2017).
BPs delaminate from the ventricular surface by losing the apical attachment. The switch from symmetric to asymmetric division mode is paralleled and favored by a change in the cleavage angle of mitotic APs: a vertical division plane is associated to the symmetric cell divisions of NEs, while a diagonal or horizontal cleavage is associated with the asymmetric divisions of aRGs, that give rise to daughter cells with two different fates. Changes in division plane are paralleled by symmetric vs asymmetric distribution of determinants that influence the outcome of the mitotic division.

Basal progenitors

At mid neurogenesis APs start to give rise to BPs. New-born BPs undergo a process called delamination that allow them to disengage from the apical junctional belt. As a consequence of delamination, BPs lack the apical contact that characterizes APs (Tavano et al. 2018) . This process is reminiscent of epithelial-to-mesenchymal transition and is paralleled by the reorganization of the intracellular architecture occurs (Sokpor et al. 2022). In line with that, APs and BPs differ not only for their positioning and morphology but also for polarity cues that specify these cells' intracellular architecture.
BPs are a very heterogeneous class of progenitors that occupy a distinct region within the developing cortex, the sub ventricular zone (SVZ) where they undergo mitosis. BPs are a very heterogeneous and are subdivided into intermediate progenitors (IPs) and basal radial glia cells (bRGs) (Florio and Huttner 2014; Namba and Huttner 2017). BP subtypes differ in proliferative capacity and molecular landscape, as well as in morphology and polarity. The occurrence and type of basal polarity cues, for example the presence of one or more basal process, allows further classification of BPs into distinct subclasses (Kalebic and Huttner 2020).
Intermediate progenitors are the most abundant BP class in mouse developing brain and lack both an apical and a basal process and as such they are classified as non-polar cells. bRGs instead can have one or more basal attachments and in few cases, they also retain apical polarity cues, such as an apical directed process. Furthermore, while IPs are more likely to undergo differentiative divisions to give rise to neurons, bRGs retain the ability of self-renewing. This feature is believed to be directly linked to the expansion of the neocortex in gyrencephalic species, which is accompanied by an increase in the number of cells produced from NPCs. In these species the abundance and variety of bRGs lead to a further separation of the developing tissue into an inner subventricular zone (ISVZ) and an outer

subventricular zone (OSVZ) further expanding the overall volume of the proliferative zones in the developing neocortex (Kalebic et al. 2019).

Neurons

The VZ and the SVZ represent the site of origin for pyramidal neurons. These neurons migrate along the radial glial cells basal processes in an outward fashion to form the six-layered cortical plate (Budday et al. 2015). It has been observed that pyramidal neurons pause in the SVZ for up to 24h before resuming their migration, suggesting that the SVZ synchronizes the migration of pyramidal neurons and interneurons (Lui et al. 2011). The preplate is a structure that forms prior to neuronal radial migration, and it is populated by cells of different type that migrate tangentially to become inhibitory neurons (Del Rio 2000). Overall, cortical development is governed by coordinated radial and tangential growth. This interplay, together with species-specific gradients, underlies connectivity, gyrification, and eventual myelination patterns.

Cortical layers develop in an inside-out sequence, with early-born deep-layer neurons derived mainly from apical progenitors, and later-born superficial layers arising from SVZ-derived progenitors. This laminar organization proceeds along a temporal gradient, first appearing rostrally and later dorsocaudally (Noctor et al. 2004; Budday et al. 2015).
In humans, between GW9–18, the proliferative zones thin as neurons migrate outward. By GW18, the six-layered architecture becomes distinguishable, though superficial neurons remain immature. After GW22, cortical plate differentiation predominates: the VZ reduces to a thin ependymal layer, the SVZ persists as the main proliferative zone. By GW28, layer I is fully developed, migration ceases, radial glia transform into astrocytes, and tangential interneuron migration continues (Budday et al. 2015). The differentiation of specific neuronal types and their location within the nascent CP is critical for function. The major types of cortical projection neurons can be defined basing on their connectivity and projection schemes. For example commissural, callosal projection neurons are localized primarily in layers II/III, V and VI. These neurons, identified by different fate markers, Tbr1, Satb2, Ctip2, project their axons from one hemisphere to neurons on the controlateral hemisphere (Mukhtar and Taylor 2018; Greig et al. 2013).
Given the high connectivity of neurons within an hemisphere and from one hemisphere to the other, the regulation of neuron subtype formation and the temporospatial control of neurogenesis is critical for brain function.

Intracellular trafficking pathways

The secretory pathway allows proteins and lipids to be posttranslational modified, folded and delivered to the target compartment where they work. The final destination of cargos coming from the trafficking pathway can be (i) the plasma membrane, where a protein or a lipid with the appropriate post translational modifications (PTMs) are inserted, as in the case of receptors; (ii) the extracellular environment, where the protein can be released, and either

work in signaling pathways or as part of the extracellular matrix (ECM); (iii) Intracellular organelles, among which the organelles that constitute the secretory pathway.
The secretory pathway starts at the Endoplasmic Reticulum (ER) where a protein while or right after being translated undergoes a first subset of PTMs and then, packed into COPII coated vesicles, is delivered to the cis Golgi (Sato and Nakano 2007). When the cargo moves from the cis, to the intermediate and finally the trans Golgi, more rounds of PTMs take place to ensure that at the exit site of the GA the protein (or lipid) is folded and functional.
One of the main and most well studied PTMs that are operated in the secretory pathway is glycosylation, a process that consists in the addition of sugar moieties to proteins or lipids. The addition of glycans ultimately form a specific complex chain that allows the compound to acquire structural and functional stability; furthermore, glycosylation is also involved in signaling processes and cell-cell recognition events (He et al. 2024a).
Glycosylation is a key step in the secretory pathway, in line with that, defects in glycosylation are associated to a group of rare diseases collectively called Congenital Disorders of Glycosylation (CDGs; see below for an in-depth description). Glycosylation events can be divided based on the aminoacid residue the sugar is attached to. N-glycosylation is the addition of a mannose rich chain of sugars on the asparagine residue, and takes place in the ER, and later in the GA. O-glycosylation refers to the addition of sugars to the OH group of a serine or threonine, and it is operated entirely in the GA (He et al. 2024a).
The trafficking route ER→GA→Plasma membrane (PM) is referred to as conventional secretion pathway. However, this route is sometimes replaced by an unconventional secretory pathway (USP) that bypasses the GA step (Nickel and Rabouille 2018). In the USP proteins are only modified in the ER and directly delivered to the plasma membrane. Interestingly USP has been found to be used by neurons for the delivery at the PM of receptors involved in synaptic processes (Hanus et al. 2016).

The Endoplasmic Reticulum

The endoplasmic reticulum (ER) is formed by network of interconnected tubular structures in continuity with the nuclear envelope. The ER is functionally and morphologically divided in two types: the rough endoplasmic reticulum (RER) and the smooth endoplasmic reticulum (SER). In the RER glycosylation of lipids and proteins starts with the addition of N-acetylglucosamine on a dolichol phosphate for lipids and on asparagine for proteins. Then these compounds undergo rounds of preliminary modifications and if not correctly folded or modified, they are delivered back to the cytoplasm for proteasomal degradation(Haynes et al. 2004; Ninagawa et al. 2021). Interestingly, failure to degrade misfolded proteins, triggers ER stress responses that have been found to be linked to defects in cortical developmental processes (Laguesse et al. 2015).
Of note, between the ER and the GA an intermediate organelle has been observed, the ER-Golgi intermediate compartment, or ERGIC. ERGIC is a vesiculo-tubular organelle that mediates the anterograde and retrograde transport between ER and GA. Though ERGIC is understudied, some observations propose a central role of this organelle in mediating the

communication of GA-derived compounds with GA-depleted in neurons (Breuza et al. 2004; Appenzeller-Herzog and Hauri 2006; Zhang et al., n.d.; De Los Ángeles Juricic Urzúa et al. 2021).

The Golgi Apparatus

The GA is composed of multiple cisternae packed together to form a stack. GA is normally localized in a perinuclear position, close to the ER and to another organelle, the centrosome. GA cisternae progress from the cis-Golgi, close to the ER, through the medial and then trans Golgi, where modified proteins or lipids enter the trans Golgi network (TGN), to be then ultimately directed to their target compartment. In mammalian cells GA adjacent stacks are interconnected by tubular membranes to form a ribbon-like structure. Vesicles bud and fuse along the cisternae to ensure the correct delivery of structural proteins and glycosylation enzymes within the GA (D'Souza et al. 2020; Glick and Luini 2011; Park et al. 2021). The Golgi matrix supports the Golgi ribbon formation and maintenance and is composed by several proteins such as golgins and Golgi Reassembly Stacking Proteins (GRASPs) whose main function is to maintain the structure of the ribbon and to mediate the trafficking of vesicles along the cisternae (Volchuk et al. 2004; Park et al. 2021); mutations to these proteins lead to Golgi disruption and impaired secretory pathway. For example, in mouse neurons the KO of GM130, a member of the group of Golgi matrix proteins, results in GA architecture and positioning disruption and subsequent secretory cargo trafficking impairment associated with cerebellar atrophy (Nakamura 2010; Liu et al. 2021).

In addition, Golgi resident proteins are also important for the organelle's structural and functional integrity: SNAREs mutations impair the docking and fusion of vesicles, with consequences on brain functionality, specifically on the sorting of neurotransmitter receptors at synapses (Malsam and Sollner 2011; Jahn et al. 2024; Liu et al. 2021). Importantly, among the resident Golgi proteins ATPases were found to help maintaining Golgi luminal ion concentration, such as Ca^{2+} and Mn^{2+}, which in turns affects the optimal activity of glycosyltransferases and trafficking of cargoes (De Bie et al. 2007). Finally, kinases, methyltransferases and GTPases also play a crucial for Golgi structural organization and functional integrity (Short et al. 2005).

The actin-microtubule cytoskeleton interacts with GA-resident structural proteins ensuring the organelle's integrity and trafficking. Of note, GA disassembly, a process that is crucial for cell cycle entry, is also regulated by the cytoskeleton dynamics and represents a checkpoint for the cell cycle progression (Colanzi et al. 2003; Ayala and Colanzi 2017). Another silent player of the secretory pathway is represented by the cytoskeleton railway, that not only allows the trafficking and transport of vesicles, but also governs the structural integrity of the Golgi apparatus.

In this context, it is worth mentioning that besides the most known functions within the secretory pathway, the GA also influences cell behavior and homeostasis. GA can act as a non centrosomal microtubule organizing center (MTOC) by nucleating microtubules. GA-MTOC has been shown to be relevant for directional protein transport (Gavilan et al. 2018). In brain development GA-MTOC are crucial for NPCs as they regulate and fine tune the

architecture and function of the cytoskeleton, influencing fate choice by affecting spindle dynamics and orientation (Ori-McKenney et al. 2012).

As the ER, Golgi has also a role in proteostasis. In fact, three Golgi-associated stress pathways have been described up to date: (i) CREB3 pathway, (ii) TFE3 pathway, and (iii) HSP47 mediated pathway. It has been observed that upon GA fragmentation using brefeldin A, golgicide A or monensin, triggered a ARF4 and CREB3-mediated stress response. Upon activation through proteolytic cleavage CREB3 translocates from the Golgi membranes to the nucleus, where it activates its target pro-apoptotic genes (Taniguchi and Yoshida 2017). During stress responses TFE3 is translocated to the nucleus, where it regulates glycosylation genes involved in sialylation and fucosylation (Sasaki et al. 2019; D'Souza et al. 2020). HSP47 pathway, identified by Miyata et al. (2013) and Sasaki et al. (2019), is activated by BenzylGalNAc a Golgi stress inducer which causes reduction of mucin-type glycosylation (Miyata et al. 2013; Sasaki et al. 2019).
Recently, another route has been explored: upon glycans-induced stress, GA starts a response leading to the activation of glycosylation enzymes for proteoglycans (Sasaki et al. 2019; Polenghi and Taverna 2023). Finally, GA has also been found to respond to DNA HR repair (Galea et al. 2022): in HeLa cells RAD51C, a regulatory HR protein, shuttles from the Golgi membranes to the perinuclear region following a DNA stress. RAD51 is linked to the golgin GM130 whose expression is controlled by TFE3 and was reported to be defective in some neuromuscular syndromes present in concert with microcephaly (Dinter and Berger 1998; Passemard et al. 2019; Polenghi and Taverna 2023).

The Golgi apparatus and human diseases

Golgipathies are a group of diseases assciated with defects in Golgi apparatus. Over 40% of GA-related genes defects are associated with central and peripheral nervous system clinical manifestations (Jaeken and Matthijs, n.d.; Freeze et al. 2014).
Such mutations typically impare Golgi structure, integrity and functional maintenance. As mentioned before, the organization of the Golgi apparatus (GA) into stacked cisternae relies on structural proteins including golgin-45, GM130, Giantin, and GRASPs, as well as regulatory GTPases such as RABs, ARFs, ARLs, and the TRAPP complexes. TRAPP functions as a guanine nucleotide exchange factor for RAB1, promoting the recruitment of golgins and GM130 at the cis-Golgi to mediate vesicle tethering. TRAPPC9 also links COPII-coated carriers to dynein for cytoskeletal transport. Mutations in TRAPP subunits are implicated in neurodevelopmental disorders: TRAPPC9 loss-of-function causes MRT13, characterized by postnatal microcephaly, callosal thinning, hypotonia, and obesity, while TRAPPC12 variants lead to progressive encephalopathy and microcephaly (Mochida et al. 2009; Milev et al. 2017; Marin-Valencia et al. 2018; Shamseldin et al. 2016; Banworth and Li 2018; Sakamoto et al. 2021). Pathology can also arise from defects in other regulators, such as CDC42 in Takenouchi-Kosaki syndrome, disrupting Golgi trafficking and cargo sorting (Flynn et al. 2021). As another example, factors like LGALS3BP highlight how GA-dependent trafficking

influences brain development through effects on receptors and extracellular matrix components, both of which are heavily glycosylated (Kyrousi et al. 2021).
Golgipathies can also be caused by mutations on genes associated with the GA glycosylation machinery. CDGs are a broad group of disorders caused by mutations on functional or structural components of GA tht ultimately impair glycosylation process. CDGs are classified based on the which organelle and on which step of glycosylation pathway the mutation is on. As a general feature, severe congenital malformationa associated with CDGs include brain related phenotypes, such as microcephaly, macrocephaly and brain atrophy.
CDGs will be discussed more thoroghly later on in a separate pharagraph.

Glycosylation

Though glycosylation is not the only PTM operated in the secretory pathway, it is for sure one of the most well studied modifications. Glycosylation is a central post-translational, essential for protein folding, stability, trafficking, and recognition, as well as for the structural and functional diversification of lipids. Two predominant types of protein glycosylation are N-linked and O-linked, which differ in the acceptor residue, the organelle in which the modification in catalysed, and the enzymes involved.

N-linked glycosylation. N-linked glycosylation initiates during protein translation in the endoplasmic reticulum (ER). A lipid-linked oligosaccharide precursor is assembled on dolichol phosphate within the ER membrane. Sequential addition of N-acetylglucosamine, mannose, and glucose residues occurs through the action of specific glycosyltransferases. Once the precursor is completed, the oligosaccharyltransferase (OST) complex transfers it to the amide nitrogen of an asparagine side chain located within the canonical consensus sequence Asn-X-Ser/Thr. Immediately following transfer, glucose residues are trimmed by glucosidases I and II, enabling quality control via the calnexin/calreticulin cycle. Further processing continues in the ER and, after export to the Golgi apparatus, involves extensive remodeling: trimming of mannoses by mannosidases and subsequent addition of N-acetylglucosamine, galactose, fucose, and sialic acid residues by specific glycosyltransferases. This yields high-mannose, hybrid, or complex N-glycans, which modulate protein folding, half-life, and cell–cell communication (He et al. 2024b; Esmail and Manolson 2021; Breitling and Aebi 2013).

O-linked glycosylation. O-linked glycosylation occurs predominantly in the Golgi apparatus and is generally a post-translational event. Unlike N-glycans, O-glycans are not transferred as preassembled units. Instead, glycosyltransferases add monosaccharides directly and sequentially to the OH group of serine or threonine residues. The most common initial modification is the attachment of N-acetylgalactosamine (GalNAc). This core can be further elongated by the addition of galactose, N-acetylglucosamine, sialic acids, or fucose, giving rise to diverse O-glycan structures (Van Tol et al. 2019). Of note, recent studies suggest that some types of glycosylation, as O-GalNacylation, is a feature of organelles secreted by

neurons and glia to expand inflammatory response and exerting a neuroprotective action (Lee et al. 2021).

Lipid Glycosylation. Glycosylation of lipids gives rise to glycosphingolipids and glycosylphosphatidylinositols (GPIs). Glycosphingolipids are synthesized in the Golgi by sequential transfer of sugars onto ceramide, forming lactosylceramide as a central precursor. This can be extended into gangliosides, globosides, or other complex glycolipids with distinct tissue-specific distributions and signaling roles. GPIs, in contrast, are glycolipid anchors assembled in the ER, starting with the addition of N-acetylglucosamine to phosphatidylinositol, followed by sequential mannose additions, phosphoethanolamine bridges, and remodeling of the lipid tail. The mature GPI anchor is ultimately attached to the C-terminus of specific proteins via a transamidase complex, yielding GPI-anchored proteins critical for membrane localization and signaling (Jáñez Pedrayes et al. 2024; Hirata et al. 2022).
Together, protein N- and O-glycosylation and lipid glycosylation constitute fundamental biosynthetic processes that shape the molecular interface of cells, regulate interactions, and sustain development, immunity, and homeostasis.

Cell polarity

Polarity refers to an asymmetric distribution of cellular structures, subcellular compartments and molecular components within the cell. Polarity allows for compartmentalization of functions and it's crucial for the ability of the cell to interact with and respond to the extracellular environment (Glotzer and Hyman, 1995).
The compartmentalization of components allows for example the different parts of the cell to interact with different environments by integrating and responding to specific signals. A prime example of polarity is represented by epithelial cells and by neuronal cells.
Epithelial cells are polarized cells that posses at least two different compartments: an apical and a basal compartments, facing respectively the lumen and the basal lamina.
Polarity is not only specific for epithelial cells, as one of the most relevant examples of polar cells are neurons. Neurons have two distinct compartments (the axon and the dendrites, and the pre- and post-synaptic compartmens) that send and sense signals during the synaptic transmission (Takano et al. 2019) .
Changes in polarity are critical as they lead to changes in the repertoire of signals the cell is exposed to, and it can also be accompained by whole tissue remodeling through migration of cells to different destination.

Polarity in apical progenitors

In the context of brain development, APs represent an excellent example of polarized cells. Apical progenitors in fact are extremely elongetd epithelail cells, with an apical process that contact the apical surface lining the ventricle, and a long basal process that touches the pial

surface. The lumen of the ventricle is filled with cerebrospinal fluid (CSF), with signaling molecules such as FGF, IGF, Shh, retinoic acid, BMP and Wnts, whose action is thought to happen via their interaction with receptors at the apical plasma membrane (Lehtinen et al. 2011; Long et al. 2016; Wang et al. 2016). On the other end, at the basal lamina, APs receive signals from the meninges and the newly developed blood vessels (Siegenthaler et al. 2009; Janesick et al. 2015). All of these determinants play important roles in cell fate programs and orchestrate the correct brain development.

Interestingly, APs show a compartmentalization of trafficking organelles and most notably of GA. While in APs the ER is prensent in both processes, the apical and the basal, the Golgi apparatus is confined to the apical process and it's absent from the basal process (Taverna et al. 2016).

Unlike in other mammalian cells, in APs the GA displays a non-canonical organization as it is not pericentrosomal, not perinuclear and it shows stacks that are not assembled in the ribbon-like structure typical of mammalian cells. Furthermore, stacks are organized perpendicular to the apicobasal axis of the cell, with a TGN surface parallel to the basolateral PM. Live imaging experiments have shown that during all cell cycle phases, the GA remains apical to the nucleus, with only a small fraction found to be close to it (Taverna et al. 2016).

This apical confinement is maintained via the activity of PITPNA and PITPNB, two phosphatidylinositol 4-phosphate transfer proteins that recruit GOLPH3 as an adaptor to link the cisternae with the actin cytoskeleton (Xie et al. 2018). It has been observed that when the APs' nucleus moves during the cell cycle progression, GA is stretched and elongated in G1, reaches its maximum apical-to-basal extension in S phase and then it is compressed in G2 before being fragmented as the mitotic process starts (Xie et al. 2018; Passemard et al. 2019). This accordion like dynamics appear to be a peculiar feature of APs, and it was observed in the developing zebrafish retina as well (Guet et al. 2014).

The confinment of the GA to one process of the cell but not the other, has consequences for the organization and composition of the plasma membrane. Indeed the plasma membrane is populated by proteins and lipids that come from the secretory pathway and that use a conventional or an unconventional secretory pathway to be glycosylated by both the ER and the GA or by the ER solely.

The use of single cell labeling techniques coupled with the staining with ConA and WGA (two lectins that specifically recognize ER- and GA-derived glycans respectively) allowed to observe that the basolateral membrane of APs is subdivided into two domains according to their differences in glycosylation state. The apical process textending in the VZ contains both ER and GA-derived glycans, consistently with the precence of both organelles in this compartement. The basal process traversing the SVZ and the CP instead contains almost only ER-derived glycans, suggesting that an unconventional secretory pathway is used in the basal process to encompass the absence of the GA within this compartment (Taverna et al. 2016).

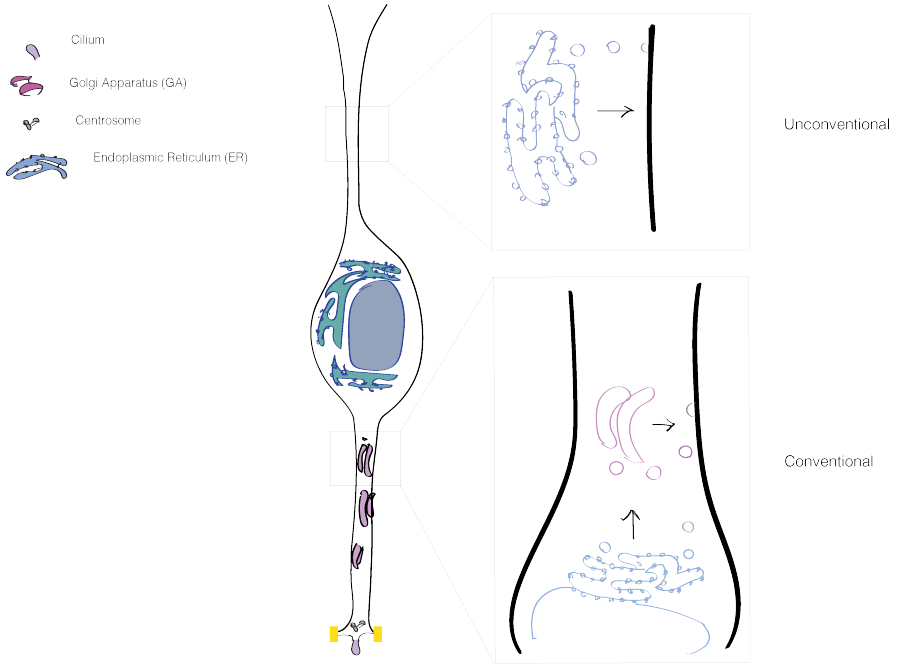


Figure 2. Conventional and unconventional trafficking routes in APs

(Adapted from Polenghi et al. 2023). In apical progenitors (APs) the apical process contains both the Endoplasmic reticulum (ER in blue) and the Golgi Apparatus (GA, in purple). The basal process of APs intead only contains the ER. This suggest that the apical process relies on conventional traffic routes, while the basal process utilizes unconventional secretion. Consequently, GA-derived glycans are asymmetrically distributed in APs, being enriched only in the apical process.

Intrecellular architecture of cell fate transition

Upon cell fate transition, from AP to BP, a deep reorganization of the intracellular compartments is observed, among which the cilium and the centrosome and -of particular interest for this project- the GA. During cell fate transition not only the Apical Junction (AJ) components cadherins and catenins were found to play a role in the delamination process, but also a link between AJ complex and Wnt/b catenin signaling has been proposed to exert a pro proliferative signaling function on cortical progenitor cells (Arai and Taverna 2017).

One of the first detectable differences that accompaines cell fate switch of NPCs is the change in the location of the primary cilium.

Cilia are important sensory organelles and in APs they protrude in the ventricle from the apical plasma membrane (Youn and Han 2018). Upon AP to BP transition, the cilium is repositioned abventricularly, above the AJ belt. The relocation of the cilium could remove nascent BPs

from the exposure to signals originating from the ventricle in favor of signals originating into more basal location within the VZ (Wilsch-Bräuninger et al. 2012; Taverna and Huttner 2019).

Interestingly, in newborn BPs upon delamination the GA is reorganized and positioned to a more canonical position, close to the nucleus and close to the centrosome (as typically observed in mammalian cells) (Taverna et al. 2016). Though it is not known whether this reorganization is a cause or a consequence of cell fate switch, some studies have reported that interfering with post-Golgi traffic affects the number of BPs, suggesting that traffic might directly influence cell fate.

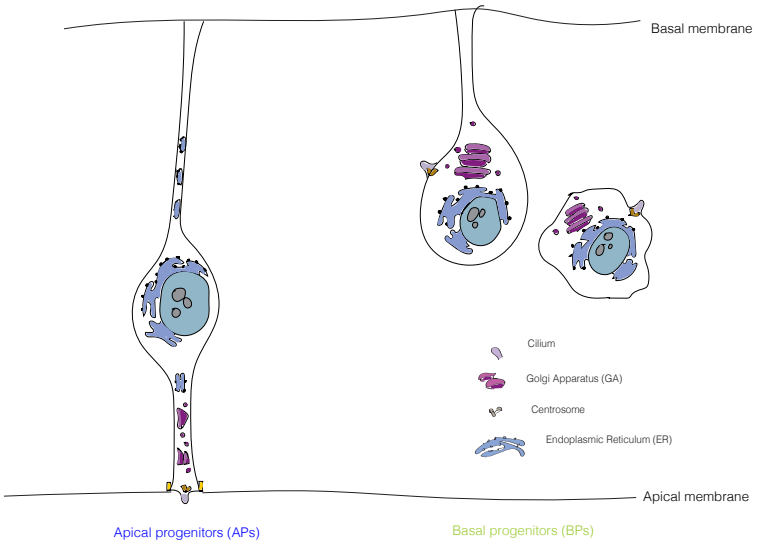


Figure 3.Localization of trafficking organelles in APs and BPs

(Adapted from Polenghi and Taverna, 2023). Golgi Apparatus (GA, in purple) is formed by separate stacks localized in the apical process of APs. In BPs GA is perinuclear and close to the centrosome. Centrosome is represented in brown, ER in blue and ciliary membrane in pink.

Congenital Disorders of Glycosylation (CDGs)

Congenital disorders of glycosylation are a complex and heterogeneous group of rare disorders that occur upon impairments in the glycosylation process. CDGs arise following mutations on structural or functional components of the secretory pathway, such as the ER and the Golgi apparatus, that ultimately interfere with glycoproteins and glycolipids assembly and remodeling (Freeze et al. 2022; Chang et al. 2018; Jaeken and Matthijs, n.d.).
Glycans are crucial for the correct functioning of these proteins and lipids, and defects are associated with consequences at multi organ level, causing various symptoms with different severity based on the mutation. The severity of clinical expression extends from perinatal death (and probably also miscarriage) to mild adult involvment (Altassan et al. 2019).

Interestingly, the most frequent clinical manifestations associated with CDG are at the level of the central nervous system (CNS) and its development (Francisco et al. 2023). This observation might not be surprising considering that both NPCs and neurons rely on heavy supply of membrane components through the secretory pathway and are involved in active signaling processes that require functional receptors, usually glycosylated, to interact with other cells and with the extracellular environment.
Although CDGs are rare, heterogeneity is found not only in terms of phenotypes and organ involvment, but also in terms of the frequency of mutations. For some CDGs only few patients have been described (ultra-rare CDGs), for others instead, as PMM2-CDG, more that a thousand patients have been diagnosed to date (Francisco et al. 2023).
CDGs genetic transmission is usually autosomal recessive. However 7% of the clinical manifestation display an autosomal dominant inheritance and 6% are instead X-linked (Francisco et al. 2023).
The serum transferrin isoelectrofocusing (IEF) represents the first-line biochemical screening for CDGs diagnosis, though it can result normal for some types of CDGs such as those caused by O-glycosylation defects (Guillard et al. 2011). As complementary tests, total N-glycan profiling from serum or plasma and exome or genome sequencing can be used, to better clarify and identify the presence of a CDG-causing mutation (Weixel et al. 2024).

Classification

The IEF pattern allowed, in a first attempt to provide a classification for CDGs, to identify two types of CDGs, the Type I and Type II, based on the glycosylation pathway step that the mutated protein is working in.
Following this classification, Type I CDGs were caused by defects in the association of the first oligosaccharide to the lipids anchor at the level of the ER or in the cytoplasm. Type II CDGs were instead associated with defects on the ER or on the GA in the glycosylation process or on the remodeling of N-glycans.
However, as of 2008 the number of reported CDGs exponentially increases, this nomenclature have been replaced by a novel system that comprises the name of the gene of the individual CDG diagnosis (e.g. COG5-CDG) (Jaeken et al. 2008; 2009). Nevertheless, still a classification based on the glycosylation pathway that is affected is maintained and distinguishes between N-linked, O-linked, GPI biosynthesis, lipid or multiple glycosylation defects. Different types of defective glycosylation are differentially responsible for symptoms in different organs, for example, defects at the CNS mostly account for multiple and N-linked glycosylation defects, while for skeletal muscle multiple as well as O-linked defects are the dominant causes for defects.

CDG mutations, symptoms and treatments

So far 163 genetic defects have been associated with CDGs, encompassing 193 phenotypes (Francisco et al. 2023). Phenotypes can be more complex because glycosylation is not specific for one cell type or one organ and thus multi organ defects must be expected

following trafficking pathway mutations. Furthermore, multiple glycosylation pathway defects can affect more strongly the outcome since more organelles are involved.

As mentioned, severe congenital malformations linked to CDGs can manifest as microcephaly, macrocephaly, ventriculomegaly or hydrocephalus, defects in myelination, abnormalities of the corpus callosum, and brain atrophy (Paprocka et al. 2021) . In contrast, O-linked CDGs, which primarily affect secreted proteins, are more often associated with neuronal migration defects, as exemplified by muscular dystrophy-dystroglycanopathy (MDDG) syndrome (Nguyen et al. 2013).These findings imply that correct deposition of extracellular matrix components is crucial for neuronal migration. Conversely, plasma membrane-anchored glycans appear to modulate intrinsic transcriptional programs that govern cell identity, likely due to their frequent role as receptors in signaling pathways (Varki 2017).

The biosynthesis of N-glycans initiates in the ER, where ALG family enzymes sequentially attach sugar residues to dolichol phosphate (Dol-P). Dol-P, in turn, is synthesized from GDP-mannose by the multi-subunit dolichol-phosphate-mannose (DPM) complex (Gandini et al. 2017). ALG1, ALG3, and ALG11 encode a β1,4 mannosyltransferase, an α1,3 mannosyltransferase, and an asparagine-linked glycosylation protein 11, respectively, and function at the ER level in the early glycosylation process (Rasika et al. 2018; Paprocka et al. 2021).Consistently, mutations in DPM2, ALG11, ALG1, ALG3, or members of the SLC35A family cause CDGs with microcephaly and other neurodevelopmental abnormalities. For example, pathogenic variants in the X-linked UDP-galactose transporter SLC35A2 impair protein galactosylation in the GA, leading to CDG phenotypes (Quelhas et al. 2021).

Once assembled, N-glycans are transferred by oligosaccharyltransferase (OST) to asparagine residues on proteins before entering the GA for further remodeling by mannosidases and fucosyltransferases (e.g., FUT). Defects at this stage can result in diverse neurological pathologies: mutations in MGAT2, encoding an N-acetylglucosaminyltransferase, lead to CDG type II with hydrocephalus and neurological dysfunction while INPP5E variants are associated with cerebellar abnormalities (Rasika et al. 2018). Additionally, Ng et al. (2018) reported FUT8 mutations in three unrelated children who presented with developmental delay, neurological impairment, growth retardation, and respiratory issues (Ng et al. 2018).

Within the GA, complex-type glycans are formed through the addition of residues such as fucose, sialic acid, or sulfates, which increase structural diversity. Hence, both structural and functional perturbations of the GA can give rise to distinct clinical presentations of CDG. O-glycosylation, on the other hand, also occurs within the GA, where enzymes such as POMT1 and POMT2 add sugars to serine or threonine residues of proteins destined primarily for secretion. Mutations in POMT1/2 are associated with intellectual disability and muscular dystrophy (Vajsar and Schachter 2006).

Treatments available to date are nearly exclusively symptomatic and include the use dietary supplements such as mannose or galactose (Verheijen et al. 2020). However, the fact that most CDGs includes impairments at the brain level, leads to significant challenges for treatments to surpass the blood brain barrier and reach the brain. Overall, the number of

CDGs with neurological manifestations has been steadily growing, underscoring the tight relationship between trafficking pathway homeostasis and neurodevelopment. Despite this, the precise mechanisms through which trafficking and glycosylation regulate neural stem cell behavior and, ultimately, brain development remain largely a mistery.

Transport in the Golgi apparatus

The secretory pathway is sustained by an intense and dynamic trafficking of vesicles, that ensure to deliver proteins and lipids to the target compartment. The process of vesicle formation is initiated by the activation of small GTPases belonging to the Arf/Sar1 family, that bind to the membrane and recruit coating proteins. Coat proteins polymerize and form a cage-like structure that, by enhancing the curvature of the membrane, starts the process of vesicle budding from the membrane (Pucadyil and Schmid 2009; D'Souza-Schorey and Chavrier 2006).

Coat proteins can be defined in three subclasses that exert their function at different locations, included the GA: COPI, COPII and clathrin (Bonifacino and Lippincott-Schwartz 2003; Blackburn et al. 2019).

COPI proteins are mostly used for retrograde transport within the GA cisternae and from the GA to the ER; COPII coated vesicles are instead involved in anterograde trafficking; finally, clathrin coated vesicles function both in anterograde transport, from ER to GA and in retrograde trafficking from the PM as well as in endosomal transport (Blackburn et al. 2019). Shortly after budding, the vesicles becomes partially or completely uncoated. Before the completion of the uncoating process, the remnants interact with the tethering complexes such as COG (Zolov and Lupashin 2005) and Dsl1 (Travis et al. 2020).

The last process of vesicle dynamics, is vesicle fusion, that occurs via the interaction of uncoated tehtered vesicles and the target membrane through a SNARE-dependent process. SNAREs are transmembrane molecular machines localized both on the vesicle and on the target membrane (v- and t- SNARES) and work in a bundle formed by four SNARE motifs comprising both v- and t-SNARES (Hong 2005; Jahn and Scheller 2006; Paumet et al. 2004). The tethering step allows vesicle and target membrane to be properly aligned to complete the membrane fusion process. Two different classes of tethering proteins have been described: coiled-coils tethers (CCT) and multisubunit tethering complexes (MTCs) (Lürick et al. 2018; Gillingham and Munro 2003). Most of the known CCT reside in the Golgi and are often referred to as Golgins (Witkos and Lowe 2016). Though CCT differ in size, they are all formed by a long coiled-coil structure often terminating with a noncoiled-coil head domain. Given their elongation CCT are proposed to account for the first contact with the vesicle, allowing to shorten the bridge between the vesicle and the target membrane. CCTs interact with SNAREs, Rabs and other small GTPases to favor the fusion process. On the othe rhand, multisubunit tethering complexes (MTCs) are generally shorter than CCTs and are composed of multiple different subunits (Blackburn et al. 2019). MTCs are further subdivided into CATCHR (complexes associated with tethering containing helical rods), such as COG complex, and non-CATCHR such as TRAPPI (Brunet and Sacher 2014).

As for the CCT, the MTCs interact with Rabs, SNAREs and other CCT to allow the tethering process and membranes fusion to correctly occurr.

The COG Complex

The Conserved Oligomeric Golgi Complex (COG complex) is involved in retrograde trasport-related vesicle tethering between Golgi cisternae and from Golgi to ER.

COG is a bi-lobed complex, formed by Lobe A and Lobe B each composed by 4 subunits, respectively COG1-4 and COG5-8 (Ungar et al. 2002). COG's Lobe A contacts the GA membrane, while Lobe B is attached to the vesicle membrane (Willett et al. 2016). The two lobes communicate by forming an heteroctamer through the interaction of COG1 and COG8 subunits (Willett et al., 2016). Mutations that disrupt COG1/8 interaction are detrimental for the whole complex function, while mutations on other subunits are more likely to affect specifically the other components of the same lobe they reside in (Foulquier et al. 2007). It has been shown that the two lobes can exist alone as tetramers or assembled in the COG complex, cycling between the two states. Consistently with its classification as CATCHR MTC, the COGs subunits are predicted to form alpha-helical bundles, which is crucial for structural stability and flexibility as well as for the dynamic interactions with the trafficking and vesicle machinery (D'Souza et al. 2020; Blackburn et al. 2019).

The COG complex has a high evolutionary conservation with homologous subunits found in al eukaryotes. However, structural information is limited and only available for some subunits in yeast model system.

The different COG subunits exert protein-protein interaction mainly through their N-terminal alpha helical domains, where they specialize in interacting with other classes of trafficking pathway components (for example, COG4, 5 and 6 intercat with several Rab proteins).

Interestingly, prior to Golgi fragmentation, Golgi-derived 60nm vesicles, called COG complex dependent (CCD) vesicles can accumulate as a premature feature underlying COG complex disfunction. These freely diffusible CCDs have made possible some observations on the interactions and functioning of the COG complex during trafficking processes (Shestakova et al. 2006a).

Though still misterious, an assembly/disassembly model has been proposed to explain the dynamics of COG-mediated tethering. According to this model, the two lobes of COG are always engaged in the interaction with COG's Lobe A contacting the GA membrane, while Lobe B is attached to the vesicle membrane. It has been proposed that after the alignment of the two membranes and the formation of the SNARE complex, COG is displaced from the vesicle-cisternae interspace allowing for vesicle fusion to proceed. While the exact mechanism underlying COG recycling is not understood yet, it has been postulated that the specific association with vesiclular factors (coat proteins, Rabs, SNAREs, CCTs) causes the dissociation of the COG complex and the association of the lobe B with the membrane of another vesicle (D'Souza et al. 2020).

One of the major phenotypes associated with COG malfunction is the onset of glycosylation defects (Fotso et al. 2005). Knock down of all individual COG subunits have displayed altered glycosylation of both N- and O- glycan species, due to the destabilization and mislocalization

of multiple components of the Golgi glycosylation machinery (Shestakova et al. 2006b; Oka et al. 2005; Pokrovskaya et al. 2011).
Furthermore, prolonged depletion or complete absence of individual COG subunits, has been reported to cause morphological changes in the Golgi, with fragmentation and dilation of Golgi cisternae (Bailey Blackburn et al. 2016). Intuitively, defects on GA should impair the whole trafficking pathway, from endosomal trafficking, to retrograde trasport and missorting of proteins. It has also been shown that deletion on any of the COG subunits in human cells, renders the whole complex non-functional and results in the degradation of several, but not all, Golgi resident proteins. These proteins, whose stability and function, is sensitive to COG complex changes, are termed COG sensitive proteins (GEARS) (Oka et al., 2004). This group comprehends glycosylation enzymes (MGAT1, MAN2A, B4GALT1, ST6GAL1) and members of the trafficking machinery, as giantin and GOLGA5 (Pokrovskaya et al. 2011).
COGs central role in the trafficking pathway is also shown by the complex' hijacking by multiple infectious pathogens, among which Sars-CoV2, HIV and other pathogenic bacteria and toxins (Stukalov et al. 2021; D'Souza et al. 2020). Given the importance of COG complex in the homeostasis of the secretory pathway and glycosylation, it comes to no surprise that mutations that affect COG subunits were described as causative of CDGs.
Mutations on all the COG subunits have been described, with the only exception of COG3 (D'Souza et al. 2020). The observed mutations, either inherited or *de novo*, differs not only in terms of associated symptoms but also for the nature of the mutation itself and the effect at the mRNA and protein levels. Interestingly, some patients (COG1 and COG6 patients) have been reported to have a 'leaky' phenotype, as, despite the mutation, some wt product is still present (Zeevaert et al. 2008; Shaheen et al. 2013). Furthermore, glycan profiling trough serum transferrin IEF usually provides glycosylation abnormalities, though some interesting exceptions have been described (Shaheen et al. 2013). For example one COG4 patient reported normal serum/plasma and glycosylation status of serum transferrin, however more specific modifications, on the secreted proteoglycan decorin, was found altered (Ferreira et al. 2018).
This hetherogeneity of symptoms as well as of the genetic and glycosylation phenotypes complicated further the diagnosis of CDG in COG patients.

COG5

COG5 is a subunit of COG's lobe B and has been found mutated in several CDG patients. About 18 COG5 patients have been described to date, making COG5-CDG an ultra-rare CDG.
Among the most common symptoms are microcephaly, hypotonia, psychomotor retardation, delayed speech development and cerebral/cerebellar atrophy, though some patients also had skeletal and liver related phenotypes (D'Souza et al. 2020).
In most cases, COG5 mutation causes the reduction of protein levels, also affecting the COG7 protein levels and causing delayed Golgi collapse into the ER upon BFA treatment.
For this project we will describe two new patients with a novel mutation on COG5 that shows a leaky phenotype and no alterations on serum transferrin IEF. Consistently with what

previously reported for COG5 patients, these two siblings show neurological impairments as well as skeletal defects.

Human neurodevelopmental disorders in a dish: the iPSCs revolution

Understanding the complexity of the human brain remains to date a challenge that still need to be tackled. As a result many approaches have been generated to model and recapitulate the human brain, from development to maturation and even pathological conditions such as neurodevelopmental and neurodegenerative diseases.

Though animal models have been proved to be an invaluable tool for studying the brain, one of the main limitation remains the difference in the complexity of mouse brain and human brain. On the other hand post-mortem tissues from human brain have only patially overcome this limitation as they can't fully recapitulate developmental and dynamic processes. Furthermore ethical considerations must be taken into account when working with human derived tissue.

Two dimensional (2D) culture systems have thus historically represented a strategy to model various diseases in vitro, but still 2D cultures cannot recapitulate the tissue complexity of the human brain. 2D cell systems lack the cellular organization that is present in the brain, as they grow in a monolayer format. Furthermore simple 2D systems miss the cell-cell interaction between different cell types that is observed in vivo. To create a 2D system that better mimics the cellular interactions in the brain, co-cutures (i.e. neurons and astrocytes) have been developed (Haenseler et al. 2017; Vahsen et al. 2022). Despite these efforts however, 2D cultures still lack the organization needed to recapitulate the human brain *in vitro*.

The advent of human induced pluripotent stem cells (iPSCs) (Takahashi and Yamanaka 2006) eased this problem by allowing not only to differentiate them in 2D cultures, but also to use iPSCs for growing 3D structures such as neurospheres and organoids. Neurospheres are cell aggregates of multipotent neural stem cells grown in culture that can be further differentiated into varying cell types, such as neurons and glial cells (Soares et al. 2021; Dingle et al. 2015; Zhou et al. 2016). This model allowed for a first simple recapitulation of cell-cell interactions *in vitro*.

Although powerful, neurospheres still lack complete cellular composition and more importantly organization and complexity. Indeed the human brain, especially during development, heavily relies on precise control over the structure and architecture of the nascent brain and the complexity in cell type is fundamental to ensure the correct formation of the tissue. Thus, brain organoids 3D models, represent the optimal system for studying human brain development *in vitro*, as they recapitulate the development process, the functionality and the heterogeneity of the brain.

To generate organoids several protocols have been developed (Sloan et al. 2018; Lancaster and Knoblich 2014; Qian et al. 2020), each with specific conditions such as extracellular matrix (ECM), small molecules and growth factors addition to the culture, but all the protocols available rely on the use of iPSC and embryonic stem cells. These cells are first aggregated and differentiated into embryoid bodies (EBs) that recapitulate the neuroepithelium formation, and then driven towards later stages of differentiationand growth of ventricular like structures

along which all the main cell types (NPCs and neurons) that populate the brain form in a sequential controlled manner. The EBs expansion step comprises their embedding into an ECM-like medium, which ultimately results in organoids growth as differentiation proceeds (Agboola et al. 2021; Lancaster and Knoblich 2014).

Organoids generated without any specific guiding compound are known as unguided organoids, as they freely grow and organize themselves without the addition of molecules that specifically influence the differentiation and growing steps.This allows to obtain a model of the entire brain in a dish, with the different regions of the brain being ricapitulated (e.g. forebrain, midbrain, hindbrain). On the other hand, guided protocols enable researchers to obtain more accurate cell populations and organization of specific brain regions and structures (Swingler et al. 2023).

Furthermore, organoids from different regions can be studied together by forming an assembloid, that is a complex structure with multiple brain regions present at a time (Bagley et al. 2017).

Although very powerful, organoids come with some limitations, as the limited diffusion of oxygen and nutrients in the inner core of their structure, with the formation, as a result, of a necrotic core. To overcome this limitation several protocol variations have been adopted, including, of note, the formation of vascularized organoids (Swingler et al. 2023).

In conclusions, the advent of iPSCs and the subsequent possibility to recapitulate the human brain *in vitro* through the use of human brain organoids, represented a major milestone in the field of neuroscience. Organoids allow studies on brain development and brain functioning as well as tackling neurodevelopmental and neurodegenerative diseases in an unprecedented way, by maintaining the structural, cellular and organizational complexity of the brain tissue.

Pathology, one cell at the time

The study of how single cell dynamics and behavior contribute to brain development in health and disease is a fundamental research area in the field of neuroscience. Neurodevelopmental studies are however limited by the resolution that available labeling techniques can reach to track the history of single cells and their progeny.

The most simple way to label single cells is through dyes and reporters; lipophilic dies, such as DiI have been leveraged to target neural progenitor cells within mouse developing neocortex and used to sort labelled cells out. These dyes freely diffuse along the membranes and create beautiful patches of dye positive cells. However, the lipophilic nature of these compounds can limit their applicability, as the dye diffusion can confound the identification of single cells.

Other non toxic chromogens, such as dextran conjugates are also useful for single cell studies purposes. One example is the combined use of dextran and microinjection, a technique based on the introduction of a needle-like glass capillary into the target cells and that allows to couple the fluorescence properties of a dye with the precise targeting of single cells (Chow et al. 2016). This technique can provide useful insights into cell morphology and dynamics. Of note, delivery into cells via microinjection does not depend on the net charge

of the compund(s), making microinjcetion a very versatile technique for complex molecular manupulations. However, microinjection is a non trivial technique, and requires user experience and a significant amount of training. Several fluorescent proteins and reporters can be microinjected and introduced into single cells, such as GFP and RFP. These dyes can also be targeted to single cells by means of lipofection and electroporation of the correspondant mRNA or DNA.

Electroporation is particularly useful as it extends the use of reporters and single cell labeling to an entire tissue or organ both *in vivo* and *ex vivo*. Electroporation-mediated labeling in the developing brain consists of the insertion of a compound, such as the plasmid encoding a fluorescent protein into the ventricle of the brain. A short pulse of current allows the membrane of the cells lining the ventricle to uptake the nucleic acid. Despite the wide applicability and the relatively easy protocols that have been developed for electroporating tissues and even organoids, the major downfall of this technique is that precise single cell labeling is difficult as several cells internalize and express the plasmid. The complexity and crowdness of a tissue such as brain organoids, renders this technique useful for broad labeling of a big population of cells, rather than of single cells.

More complex techniques have been developed to target single cell types, that rely on the use of selective promoters that only specify the expression of the reporter in the desired cell type. Multicolor lineage tracing techniques have also been implemented to detect and follow the lineage of multiple cells and cell types across a develomental trajectory (Short et al. 2025; Lamprecht et al. 2017). However, despite these techniques are very impressive, full discrimination between single labeled cells remains cumbersome and following morphological and architectural changes following lineage changes is difficult.

To overcome these limitations on currently available techniques, Shull et al. (Shull et al. 2019)developed an automated microinjection robot that efficiently targets single apical progenitor cells lining the ventricle of embryonic mouse brain as well as neurons in both human and mouse tissue. This techniques not only allows to follow the developmental trajectories of single labeled cells, but also to discriminate between the different cells from the complexity of the surrounding tissue. Compared to manual microinjection, automated microinjection proved to be faster and less influenced by the user experience, thus eliminating some pitfalls that limit the use of manual microinjection.

Materials & Methods

Mice

All animal studies were conducted in accordance with the German and Italian animal welfare legislation (for experiments conducted in Germany and Italy, respectively), after approval by the Ministry of Health(project code 75DA4.N.B7F).
Animals for these studies arrived from Charles River and were maintained in standardized hygienic conditions at Cogentech animal house in Milan. All experiments were performed on C57Vl/6J mice. Mouse brains were harvested at E14.5. embryos were transferred into phosphate-buffered saline (PBS). Embryos were decapitated using surgical forceps under a dissectoscope, skulls were open and brains extracted under visual control.

Hemisphere rotating culture (HERO) and pharmacological treatment

After brain collection, the two hemispheres were separated in pre-warmed Tyrode's solution and put in 1mL of Slice Culture Medium (SCM; Neurobasal medium (Thermo Fisher Scientific), 10% rat serum (Charles River, Japan), 2mM L-Glutamine (Thermo Fisher Scientific), N2 supplement (Thermo Fisher Scientific), B27 supplement (Thermo Fisher Scientific) and 10mM Hepes-NaOH pH7.3.
For the pharmacological treatment, 1mL of SCM was supplemented with 1µL of 10µM Golgicide or 10nM BFA, or with 1µL of EtOH or DMSO as vehicle.
Hemispheres were kept in the Hikemoto incubator, in rotation in Hero culture bottles, in a humidified atmosphere with 40% O2, 5% CO2 and 55% N2 at 37° for 6h.
At the end of the treatment hemispheres were transferred in a 12well plate (Corning) in PBS and fixed in 4% PFA overnight. The next day hemispheres were put in PBS, and kept at 4°C until use.

2D cell culture

HeLa

For HeLa maintenance, cells were kept in media containing 10%FBS, 1X P/S, 1X Glutamax (Thermofisher) and DMEM. Media change was done weekly. For HeLa splitting, the media was first removed and cells were washed with PBS. To detach cells, trypsin was added for 5 minutes at 37°C. HeLa medium was then added to detach cells and the cell suspension was centrifuged at 300xg for 5 minutes. The supernatant was discarded and cells were plated in the appropriate volume of culture medium.

HeLa freezing was done in FBS+10% DMSO.

Fibroblasts

Fibroblasts from COG5-CDG patients were obtained from a collaboration with Dr. François Foulquier at the Université of Lille and were used following the patients consent for the collection and usage of biological material for research purposes. Control fibroblasts were obtained from GEDI facility at Human Technopole. Fibroblasts were cultured in DMEM high glucose supplemented with glutamine, 10% FBS and 1X PenStrep. Medium was changed once a week.

For fibroblasts splitting, the medium was removed and cells were washed once in PBS, followed by an incubation with 2mL of 0.5% Trypsin at 37°C for 5 minutes. 10mL of conditioned medium were added to the fibroblasts to detached them from the substrate. Cells were subsequently centrifuged for 5 minutes at 300xg. Fibroblasts were resuspended in culture medium and plated on the appropriate support containing maintenance medium as described above.

For fibroblasts freezing and thawing, the protocol described for iPSCs was followed (see below) with exception of the medium used to maintain fibroblasts.

Fibroblast reprogramming

Patient fibroblasts were reprogrammed at the National Facility for Genome Engineering, Human Technopole (Milan, Italy).Fibroblasts reprogramming into induced pluripotent stem cells (iPSCs) was performed using the Stemgent StemRNA 3rd Generation Reprogramming Kit (REPROCELL #00-0076), following the manufacturer's instructions. Briefly, on Day 0, fibroblasts were harvested and seeded at a density of 40,000–50,000 cells per well on pre-coated 6-well plates (iMatrix-511, Biogems) at a final concentration of 2.4 µg/mL. From Day 1 to Day 3, cells were transfected daily to introduce the reprogramming factors OCT4, SOX2, KLF4, c-MYC, NANOG, and LIN28. From Day 4 to Day 9, cells were cultured in NutriStem™ hPSC XF (REPROCELL) and monitored for the emergence of iPSC colonies. Between Days 9 and 13, primary iPSC colonies were manually picked under phase-contrast microscopy using an EVOS XL imaging system (Thermo Fisher Scientific). A total of 60 colonies per sample were picked and plated into 96-well plates (Passage 0). Starting from passage 1, the clones were transferred into 24-well plates and maintained for 10 passages. At passage 10, the 15 best-performing clones—selected based on proliferation rate and morphology—were cryopreserved. Among these, up to 6 clones were selected for genome integrity analysis to confirm the absence of chromosomal aberrations introduced during reprogramming.

This analysis was performed using low-pass whole-genome sequencing. The 3 best-performing clones, which passed genome integrity screening, were then subjected to a full panel of quality control assays, including: expression of pluripotency markers, differentiation potential into the three germ layers, STR analysis for cell line authentication, amplification and masterbank cryopreservation, post-thaw recovery assessment, mycoplasma testing. For each of the 3 validated clones, a master cell bank consisting of 10 cryovials was generated and delivered to the end-user of the facility.

BFA treatment of HeLa and fibroblasts

Hela cells were treated with 10nM of BFA or with vehicle (EtOH) and fixed at different time points (1h, 2h, 4h or 6h) to assess the time necessary for the drug to fragment the Golgi apparatus. Before fixation (8 minutes in PFA 4% at RT) cells were washed once in PBS. Fixed cells were stored in PBS until further analysis was performed.
BFA treatment on fibroblasts was performed with 10nM BFA and fixed at different timepoints (0, 5min, 10min, 15min, 20min, 25min and 30min) to assess the delayed GA fragmentation in the COG5 mutants.

Organoids and iPSCs

Thawing iPSCs

To thaw iPSCs, the cryogenic vial was quickly put in the waterbath at 37°C for a maximum of 2 minutes. Cells were transferred, with a wet pipet tip, into a falcon already containing 5ml of mTeSR1 (Stemcell). The cell suspension was centrifuged for 5 minutes at 300g. After centrifugation, the supernatant was discarded, and the cell pellet was resuspended into 1ml of mTeSR1 with RI. Then, 1/3 and 2/3 of cells volume were plated into new wells with a final volume of 2ml mTeSR1 supplemented with RI and iMatrix for cell attachment.

iPSCs culture

Control human brain organoids were generated from WTC11 and from HMGU1 iPSCs cell line following the Lancaster protocol (Lancaster et al., 2014). For patients lines, indicated with the code COG52 (female patient) and COG53 (male patient), or KO (COG5 knock out, obtained as described below) iPSC lines the same protocol was followed. iPSCs were cultured on 6 well plates coated with iMatrix (amsbio) and kept in mTeSR1 (Stemcell) at 37°C with 20% O2 and 5% CO2, the culture medium was changed daily. Cells were passaged once a week, when about 80% confluency was reached.

iPSCs maintenance

iPSCs were cultured on 6 well plates coated with iMatrix and kept in mTeSR1 at 37°C and 5% CO2, the culture medium was changed daily. To maintain the iPSCs culture cells were passaged once a week, when about 80% confluency was reached.
To split cells, one wash with Dulbecco's phosphate-buffered saline (DPBS) (Thermofisher), without calcium and magnesium (DPBS -/-) was done before incubation with 1ml ReLeSR (Stemcell) for 30 seconds; ReLeSR was then removed cells were put at 37°C for 5 minutes. A 1ml of fresh mTeSR1 was added and used to detach cells through two to three washings

to maintain intact colonies. Then the appropriate cell suspension was transferred to a new well, in a final volume of 2ml of mTeSR1 with iMatrix to allow cell attachment.

Freezing iPSCs

Cell medium was removed and cells were washed with DPBS -/-, and incubated for 5 minutes at 37°C with 1ml of ReLeSR. Cells were then detached from the plate with 2 ml of mTeSR1 and washed two to four times. The cell suspension was transferred to a falcon and centrifuged for 5 minutes at 200xg. The supernatant was discarded, and the cell pellet was resuspended with 500µl of mFreSR (StemCell), transferred to a cryogenic vial and progressively frozen to -80°C in a freezing box. After 24h cells were transferred in liquid nitrogen for long term storage.

KO line production

COG5 knock-out WTC-11 iPSC lines were generated at the National Facility for Genome Engineering, Human Technopole (Milan, Italy). iPSCs were maintained in StemFlex medium (Thermo Fisher Scientific) and seeded on 0.25 µg/cm^2 iMatrix-511 (Biogems) as previously described (Fiacco et al., 2024), under standard culture conditions (37 °C, 5% CO_2). For genome editing, cells were detached using TrypLE™ Express Enzyme (Gibco) and 2 × 10^5 cells were nucleofected with ribonucleoprotein (RNP) complexes composed of 150 pmol sgRNA (sg5-COG5, 5'-TGTCCAACTGACTGATTCCT) and 122 pmol Cas9 protein (Alt-R® S.p. HiFi Cas9 Nuclease V3, IDT). Nucleofection was performed on a Lonza 4D Nucleofector using P3 Primary Cell Solution and the CA-137 program, supplemented with 4 µM Alt-R Cas9 Electroporation Enhancer (IDT). After nucleofection, cells were transferred to 12-well plates (Corning) containing pre-warmed StemFlex medium supplemented with 0.25 µg/cm^2 iMatrix-511 and CEPT mixture. Three days later, genomic DNA was extracted, and the targeted region was amplified and Sanger sequenced to evaluate the editing efficiency in the bulk population. Single-cell clones were subsequently isolated using the Iota Sciences Cloning Platform, expanded, and screened by Sanger sequencing. Genome integrity of the selected COG5 KO clones was assessed by low-pass whole genome sequencing (1× coverage), confirming the absence of large aneuploidies, chromosomal abnormalities, or clinically relevant deletions/duplications. Cell line authentication was further verified by STR profiling (GenePrint® 10 System, Promega) on a Spectrum Compact CE System (Promega).

Organoids culture

Human brain organoids were generated following Lancaster et al. protocol (2014) with minor modifications (Fig. 4). Briefly, iPSC at 70-80% of confluency were washed once in PBS(-/-) and detached with Accutase (Sigma) for 5 minutes at 37°C; 2 mL of mTeSR1 were added to detach and resuspend in single cells. Cells were centrifuged for 5 minutes at 300xg and

resuspended in 1mL of mTeSR1 supplemented with RI (Tebu-bio srl). Cells were then counted and 9000 cells per well of a U-bottom 96 well plate were added to mTeSR1 with RI medium. Cells were then seeded adding 200µL of suspension to each well of the 96 well plate to form Embryoid bodies (EBs). Media change was done every other day using mTeSR1 without RI. At day 4, medium was changed to Neural induction medium (NIM was prepared with DMEM F12 (Gibco) in ratio 1:1, N2 1:200 (Thermofisher), 1:100 Glutamax (Thermofisher), 1µg/mL of heparin, 0.5% of MEM NEAA (Sigma) and 1:100 P/S) with a volume of 150µL per well. Media change was done every other day. At day 7 the EBs were embedded in Geltrex droplets and put in 6cm petri dishes in Differentiation medium without Vitamin A (DM-VitA was prepared with DMEM F12 and Neurobasal (Gibco) in ratio 1:1, B27 -VitA 1:100 (Thermofisher), N2 1:200, 1:100 Glutamax, 2.5µg/mL insulin (Sigma), 50uM 2-mercaptoethanol (Merck) and 0.5% of MEM NEAA and 1:100 P/S). Media change was done every other day until day 13 when the embedded EBs were transferred in DM+VitA (DM+VitA was prepared with DMEM F12 and Neurobasal in ratio 1:1, B27 +VitA 1:100, N2 1:200, 1:100 Glutamax, 2.5µg/mL insulin, 50µM 2-mercaptoethanol and 0.5% of MEM NEAA and 1:100 P/S).

Organoids were then kept in culture until the desired stage on a shaker set at 70rpm at 37°C with 20%O2 and 5%CO2 levels.

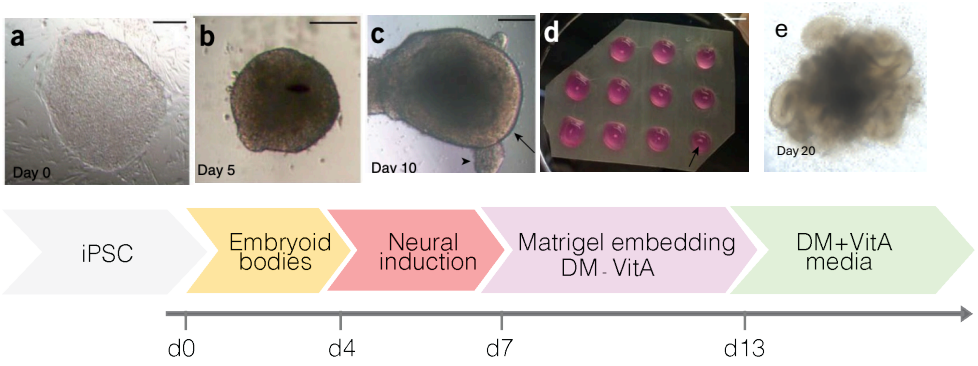


Figure 4. Schematic representation of brain organoid generation protocol. Brain organoids are generated from Lancaster et al. protocol (Lancaster and Knoblich 2014); iPSCs (a) are aggregated to form EBs (b) that undergo neural induction at d4 developing a bright external region corresponding to the neuroepithelium. (d) EBs are embedded in Geltrex at d7 and let grow in Differentiation Medium.

scRNAseq

For scRNAseq GemX technology was used following published protocols from Illumina.

For sample preparation d40 organoids from WTC11, COG52 and COG53 lines were used. 8 organoids from each line were used for scRNAseq experiments. Upon pooling of organoids, the tissue was dissociated using the MACS tissue dissociation kit. Briefly, 200µl of enzyme P resuspended in buffer X was added to the organoids that were then incubated at 37°C in waterbath for 15 to 30 minutes. After incubation 6µL of enzyme A were added to

stop the reaction and full organoids dissociation was achieved through manually pipetting up to 10 times. The suspension was then passed through a 70µm filter and the collected cells were briefly centrifuged at 300g for 2 minutes and finally resuspended in 5% FBS in PBS before being handled to the National facility for Genomics (Human Technopole) for further steps. Briefly, single cells were encapsulated into Gel Emulsion Droplets using the Chromium X instrument (10x Genomics) targeting 5'000 cells for each sample. To optimize costs and efficiency, three or four samples were multiplexed in a well of the 10x chip following the instructions of the GEM-X Universal 3' Gene Expression v4 4-plex Protocol (CG000768, 10x Genomics). From each pool, 3' Gene Expression libraries were generated in accordance with the 10x Genomics Protocols. Libraries were pooled at a ratio dependent on the 10x Genomics indication and loaded on the Novaseq6000 sequencer to achieve a minimum of 50'000 reads/cell for each library.

scRNAseq data analysis

Differential gene expression (DGE) analysis

For the differential expression analysis, a pseudobulk approach was applied, in which raw transcript counts were summed across all cells belonging to each combination of biological sample (*sample_id*) and cell cluster (previously defined by Leiden clustering). This strategy allowed the aggregation of technical replicates, thereby reducing spurious variability. Based on the cell type annotation performed previously, the clusters of interest were selected: cluster 5 (apical progenitors), cluster 7 (basal progenitors), and clusters 6–8–9 (neurons). Differential gene expression (DGE) analysis was then performed using the DESeq2 package (v1.48.2) in R. Only genes expressed in at least 10% of the samples were retained. A DESeq2 object was defined, and the model was fitted using the function DESeq(test = "Wald", fitType = "parametric"). Results were extracted for the contrasts of interest (MUT1+MUT2 vs WT, MUT2 vs WT, MUT1 vs WT, and MUT1 vs MUT2). Significantly regulated genes were identified based on both statistical significance (*padj* < 0.05) and fold-change threshold (|log2FoldChange| > 1.5). Up- and down-regulated genes were then visualized through volcano plots generated with the *ggplot2* package (v4.0.0) in R, highlighting genes with log2FoldChange > 1.5 & padj < 0.05 as upregulated and those with log2FoldChange < -1.5 & padj < 0.05 as downregulated.

Differential abundance (DA) analysis

Differential abundance (DA) analysis was performed using Milopy, a Python implementation of the Milo framework (v0.1.1). The KNN graph was already constructed in the Scanpy workflow using Harmony-corrected principal components (sc.pp.neighbors(mdata["rna"], use_rep="X_pca_harmony", k=100, n_pcs=12)), where k indicates the minimum neighborhood size for DA quantification. Neighborhoods were defined by selecting 10% of

all cells as centers (milo.make_nhoods(mdata["rna"], prop=0.1)), grouping cells into overlapping local regions on the graph. The number of cells in each neighborhood per sample was counted (milo.count_nhoods(mdata, sample_col="sample_id")) and used for differential abundance testing with a generalized linear model. Comparisons included MUT1 vs WT, MUT2 vs WT, MUT1 vs MUT2, and MUT1+MUT2 vs WT. Neighborhoods with SpatialFDR < 0.01 and |logFC| > 2 were considered significantly enriched or depleted. Significant neighborhoods were visualized on the embedding, and beeswarm plots were generated to show DA across clusters. For each cluster and comparison, condition-specific DA neighborhoods (MUT1, MUT2, WT) were reported and visualized using boxplots.

Functional enrichment analysis

Functional analysis of differentially expressed genes (DEGs) was conducted using QIAGEN Ingenuity Pathway Analysis (IPA) (1). A dataset comprising gene identifiers and corresponding expression values from apical progenitors, basal progenitors, and neurons, derived from organoids of two mutated siblings and a wild-type (WT) control, was uploaded into the IPA platform. Each gene identifier was mapped to its corresponding entity within the QIAGEN Knowledge Base. To identify significantly perturbed molecules, an absolute log fold change (logFC) threshold of $\geq$1 was applied. These molecules were then overlaid onto a global molecular network curated from the QIAGEN Knowledge Base. Biological function analysis was performed using a right-tailed Fisher's Exact Test to calculate p-values, estimating the probability that the association between the DEGs and specific biological functions or diseases occurred by chance. A z-score was computed to predict the directionality (activation or inhibition) of each function or disease. Canonical pathway analysis was also carried out to determine the most significantly enriched pathways from the IPA library. Again, a right-tailed Fisher's Exact Test was used to assess statistical significance, and a z-score was calculated to infer the likelihood of pathway activation or inhibition.

Lipid Glycomics

Organoids at d40 were dissociated using the MACS tissue dissociation kit as described before and stored at -80°C before delivery to our collaborators inKU Leuven for lipid glycomics experiments.

The protocol followed for MS on glycosylated lipids has been published in a work from our collaborators (Jáñez Pedrayes et al. 2024). Briefly, cell pellets were thawed and resuspended in 250 µL of 1-butanol/methanol (1:1, v/v) with 1uM deuterated d5-GM3 (Avanti) as internal standard. Samples were sonicated and centrifuged for 15 min at 3,500 g. Pellets were processed for BCA assay. The supernatant was then purified using 0.20µm polytetrafluoroethylene (PTFE) filters (Millipore) and additional 500µL of 1-butanol/methanol (1:1, v/v) were filtered to ensure recovery of the GSLs. GSL solutions were evaporated in a

SpeedVac and resuspended in 100µL of the chromatography starting conditions (methanol/water/isopropanol) and transferred to MS vials.
LC-MS analysis was performed on a Vanquish LC System (Thermo Scientific) equipped with a C18 column (Acquity UPLC- BEH, 130Å, 1. 7 µm; 2.1 mm x 150mm, Waters) coupled to an Orbitrap Fusion Lumos Tribrid mass spectrometer (Thermo Scientific) operating in negative ion mode (m/z range: 690-2000).

Pharmacological treatment on human brain organoids

For drug treatment on organoids, 1uL of 10 µM of Golgicide or 1µL of DMSO were added to organoids medium and kept for 6h at 37°C on a shaker.
At the end of the treatment organoids were transferred to a 12well plate (Corning) in PBS and fixed in 4% PFA for 40 minutes. Organoids were then washed in PBS and infiltrated with sucrose 30% o/n, embedded in OCT and frozen in n-pentane (Carlo Erba) as described below.

EdU labeling on human brain organoids

Organoids were labeled with EdU to assess the presence of cycling cells and in particular cells in S-phase. Organoids were added with EdU 10µM in the culture medium for 1h.
Organoids were then washed twice in PBS and fixed at RT in 4% PFA for 40 minutes.
Labeled organoids were then washed in PBS, infiltrated with 30% sucrose and the next day embedded in OCT and frozen in n-pentane (Carlo Erba).

Preparation of organotypic tissue slices from human brain organoid and mouse embryonic brain tissue

Organotypic slices from the developing mouse brain or from human brain organoids were prepared for microinjection experiments as previously described (Taverna et al. 2012). Briefly, E14.5 mouse brains or human brain organoids were embedded in pre warmed 3% low melt agarose. After complete solidification, the agarose block containing the brain tissue was cut at 250µm of thickness using the vibratome (Leica VT1000S). The slices were collected in pre warmed SCM and transferred to a 3.5cm dish containing warm CO2-independent microinjection medium (CIMM: DMEM-F12 (Sigma), 2mM L-glutamine, P/S, N2, B27, Hepes-NaOH pH 7.3) for microinjection or kept in SCM at 37°C in incubator until microinjection was performed.

Microinjection for lineage tracing

Automated microinjection was performed through a high-throughput robotic platform; Polenghi et al., in preparation). Briefly, organotypic mouse brain slices were placed in CIMM and injected with the microinjection solution containing a fluorescent dye to track the microinjected cells and their progeny (4µg/uL of Dextran A555 10kDa or Dextran A488

10KDa, ThermoFisher). The microinjection needle (Harvard Apparatus, 1.2 O.D.x 0.94x100L mm) was pulled with a Puller (Model P-1000 Sutter Instrument with the following set up: Heat 500, Pull 60, Vel 80, Delay 100 and Pressure 280) and finally mounted on the capillary holder. Microinjection was performed with Autoinjector 2.0 as previously described. Briefly, through the Autoinjector software interface we set the microinjection angle at 45 degrees, then we performed capillary detection and calibration, by clicking on the UI the tip of the pipette until a central position is reached. Tissue edge detection was performed by selecting the apical side and injection parameters set up (Approach: 100µm, Depth: 20µm, spacing: 50µm, speed: 1000µ/s) followed. After injection was performed, microinjected slices were washed in PBS and embedded in collagen matrix (Type Ia collagen (Cellmatrix, Nitta Gelatin Fujifilm Wako/DBA) 1.5mg/mL, ddH2O, 5x DMEM-F12-CO2 independent (Sigma D8900) with phenol red, Reconstitution buffer (2.2g NaHCO3 (262mM) in 100mL of 0.05N NaOH and 200mM HEPES) and let at RT for 5 minutes. The collagen matrix was then allowed solidify at 37°C for 30 minutes; embedded slices were added with 1mL of SCM supplemented with 1µL of 10 µM Golgicide or vehicle DMSO. Slices were then kept in culture at 37°C for 6h. After the treatment slices were washed once in PBS and fixed in 4% PFA o/n. The next day slices were put in PBS and processed.

Fixation, embedding, and sectioning of microinjected organoids and mouse tissue

Organoid and mouse tissue slices were washed twice with PBS to remove culture media, followed by fixation with 4% paraformaldehyde in 120 mM sodium phosphate buffer pH 7.4 at room temperature for 40 min. Fixed samples were stored in 1X PBS at 4°C overnight. Coronal sections of mouse slices (70 µm) were prepared by embedding microinjected slices in pre warmed 3% low melt agarose and cut using a Leica VT1000S vibratome. All slices were collected in PBS and stored at 4°C for subsequent immunofluorescence staining. For cryosectioning, organoid slices were infiltrated with 30% sucrose at 4°C overnight prior to embedding in TissueTek tissue freezing medium (Leica Biosystems, Germany). 20µm-thick sections were cut using a cryostat (Leica Biosystems) and resulting sections were stored at -20°C for further processing.

Brain organoids clearing for whole mount analysis

Microinjection in brain organoids is a powerful tool to achieve single cell resolution analysis, however processing of sliced brain organoids can be cumbersome. We therefore decided to use tissue clearing for this specific purpose and experimental pipeline.

For the slices that were cleared we followed a previously published protocol (Shan et al. 2022). Briefly, for staining of 250µm thick brain organoid slices 30 minutes permeabilization with 0.5% Triton X100 was done, followed by 30 minutes of blocking in IF buffer at room temperature. After blocking slices were incubated with primary antibody diluted in IF buffer at RT for 24h. The next day secondary antibody diluted in IF buffer were added to the slices

for 24h at 80rpm. After washing, slices were incubated with AKS (20% DMSO, 40% TDE, 20% sorbitol, and 6% Tris base dissolved in ddH2O and stirred at RT) for tissue clearing. The clearing solution was kept for 5 minutes at room temperature with shaking of 80rpm. Imaging was done right after clearing.

Immunofluorescence staining

Floating sections were processed for immunofluorescence (IF) staining as previously described (Taverna et al., 2012). In brief, sections were permeabilized with 0.3% Triton-X100 (Carl Roth, Germany) in PBS for 30 min, followed by incubation in blocking solution (10% Gelatin, 0.3% TritonX-100, 5mM NaCl in PBS) for 1h. The sections were incubated with primary antibodies diluted in IF buffer overnight at 4°C. Subsequently, sections were washed 5 times for 5 min each time with IF buffer. Secondary antibodies were diluted (1:500) in IF buffer with DAPI(1:1000) (Carl Roth, Germany) as nuclear counterstain. Sections were incubated at room temperature for 1 h followed by washing (5 times 5 min each) with PBS and one last wash in water. Stained sections were mounted in Mowiol and imaged.

Cryosections were processed for IF staining as follows. Sections were dried for 5 min at RT and then washed once with 1X PBS, followed by permeabilization with 0.5% Triton-X100 (Carl Roth, Germany) in PBS for 40 min. Subsequently, sections were incubated with blocking solution (10% Gelatin, in 0.3% Triton X100/PBS, 5mM NaCl) for 1 h at room temperature. Primary antibodies diluted in blocking solution were incubated with the sections overnight at 4°C, with gentle shaking, followed by washing 5 times for 5 min each time with PBS. Sections were then incubated with secondary antibodies diluted in blocking solution with DAPI as nuclear counterstain for 1 h at room temperature followed by washing for 5 times 5 min each time in PBS and one final wash in water.

For EdU labeling, after the completion of the immunofluorescence protocol, Click-iT™ EdU cell proliferation kit was used following manifacturer's protocol. Briefly, after the last wash in PBS, the slices were fixed in PFA 4% for 15 minutes, following by three washes in BSA 3%. Slices were then incubated with Triton 0.5% for 20 minutes and then washed again in BSA 3%. The 1X Click-iT™ EdU reaction mix (1X Click-iT™ reaction buffer, CuSO4, Alexa Fluor azide and Reaction buffer additive) was then added to the slices for 45 minutes. Following a last incubation with DAPI (1:1000 blocking solution) for 15 minutes samples were washed in PBS and mounted with Mowiol.

For immunofluorescence staining on cells, permeabilization with Triton 0.3% in PBS for 10 minutes was done, followed by 1h incubation with blocking solution at RT. Cells were then added with the AbI solution and kept o/n at 4°C with gentle shaking. The next day cells were washed 3 times for 5 minutes each in PBS and the secondary antibodies were added for 1h at RT. Cells were washed in PBS and, if on coverslips, the sample was mounted with Mowiol.

A complete list of all primary and secondary antibodies used together with corresponding concentrations are listed in the antibodies section in table 1.

Image acquisition

Imaging was performed using a confocal microscope (Zeiss LSM 780 NLO; Zeiss, Germany) or a widefield fluorescence microscope (Zeiss Axio-something; Zeiss, Germany). Images shown here are 0.5 µm-thick single optical sections, unless stated otherwise. Confocal images were taken using either a PlanApo 63X oil or PlanApo40X oil immersion objectives and 405nm, 488nm, 561nm and 639nm laser lines were used. For the acquisition of some patients samples and KO, we also utilized spinning disk confocal microscope, that comprised a Nikon Ti2-E inverted microscope equipped with a CrestOptics V3 Light, which was coupled to Photometrics Prime 95B 25 mm camera, configured with a 50-micron pinhole, and to a Celesta Lumencor as lightsource. The imaging process was conducted using a PlanApo LambdaD FN25 DIC 10X/0.45 and PlanApo LambdaS 40X/1.25 Sil objective, capturing Z-stacks with a 0.5-micron Z-step size to encompass the complete volume of the sample and 405nm, 488nm, 561nm and 639nm laser lines were used.

Image analysis

Immunofluorescence images of single optical sections were quantified using Fiji (Schindelin et al. 2012) and statistical analysis was performed using Prism (GraphPad software). To test for statistical significance, we used Welch's t test, Student's t test and two-way ANOVA for multiple comparisons. For each graph, the number of samples, statistical test and the p value are noted in the corresponding figure legends.

Cell quantifications on fate markers were performed either manually with the CellCounter function, or using StarDist 2D plugin considering all the area corresponding to an organoid ventricle. The percentage of cells was calculated by dividing the number of cell of each fate marker used by the total number of DAPI positive cells. For the quantification of HuCHuD+ cells in the VZ we instead counted the number of cells over the apical length measured with the segment tool.

Organelles and injected cells reconstruction was performed by manually segmenting the organelle or the cell on the single Z-stacks of the channel corresponding to the organelle and then comparing to the areas that were also positive for GFP. Cell reconstruction was then performed and organelles area and number were measured by analyzing their ROI. When calculating the distance from the apical surface, a segment perpendicular to the apical surface was drawn and its length measured.

JaCoP plugin was used quantify the colocalization of two channels, especially for the colocalization of ACBD3 with Golgi or Numb, and SNA with Golgi and Pan Cadherin; spindle

orientations in dividing APs were determined by calculating the angle between the equatorial plate and the ventricular surface (identified by Phalloidin or y tubulin) using the angle tool in Fiji. The percentage of vertical (60°-90°), oblique (30°-60°) and horizontal (0°-30°) cell divisions was calculated and compared between the WT and the other conditions.

Final image panels were processed and assembled using Adobe Illustrator CS5.1 (29.7).

Image analysis for the reconstruction of single cell intracellular architecture

We used a combined panel of cell morphological parameters and marker expression to score labelled cells in mouse tissue and in human brain organoids.

Microinjected cells were identified as cells positive for the microinjection dye upon inspection at the epifluorescence microscope. To assess morphological organization and subcellular architecture, all positive cells in an experiment were imaged at high-resolution using confocal microscopy (see also above).

For all microinjected cells the following parameters were recorded and quantified (i) distance of the microinjected cells from the basal lamina, based on the detection of the cell nucleus using DAPI (ii) cell general morphology, including shape of the cell body, presence and extension of cell's processes (iii) presence, localization and relative distance of the centrosome the Golgi apparatus, detected using specific markers for these two organelles. The centrosome is detected using an antibody against g-tubulin. The Golgi apparatus is detected using an antibody against the Golgi reassembly-stacking protein GRASP-65.

shRNA plasmid preparation

To prepare shRNAs plasmids from delivered glycerol stocks were gently picked with a p200 tip and put in 5mL of LB medium supplemented with 1:1000 ampicillin and put in shaking at 220rpm at 37°C for the rest of the day. The bacterial culture was then let grow overnight in shaking at 220 rpm at 37°C. EndoFree Plasmid Maxi kit (Qiagen) was used to extract the plasmids following manufacturer's instructions. Briefly, the overnight LB culture was harvested by centrifuging at 6000 x g for 15 min at 4°C. The bacterial pellet was then resuspended in 10 mL of Buffer P1 and then added with 10 mL of Buffer P2 and incubated at RT for 5 min. After incubation 10 mL of Buffer P3 were added and the lysate was poured into the barrel of the QIAfilter Cartridge followed by RT incubation for 10 min. The cell lysate was then filtered and added with 3 mL Buffer ER before pouring in the QIAGEN-tip for DNA binding to the column. DNA was finally eluted with 15 mL Buffer QN and precipitated by adding isopropanol and by Centrifugating at ≥15,000xg for 30 min at 4°C. The DNA pellet was finally washed with 70% ethanol and centrifuged at ≥15,000xg for 10 min. The pellet was let air-dry after discarding the supernatant for 5–10 min and the DNA was dissolved in 200µL of water before quantification at Nanodrop.

shRNA validation on HeLa cells

shRNAs were validated in HeLa cells by transfection following Lipofectamine 3000 Reagent protocol (Thermofisher). Briefly, Cells were detached the day before and plated with the desired concentration. Lipofectamine 3000 reagent was diluted in Opti-MeM™ and DNA mix was prepared by diluting DNA in Opti-MeM™ added with P3000™ reagent. The two reaction mix were added together at a ratio of 1:1 and after a 15 minutes incubation, the transfection mix was added to the cells in culture and incubated for 48h at 37°C. After 48h, cells were fixed for 8 minutes in PFA 4% and stored in PBS until immunofluorescence protocol was performed.

Electroporation

We performed electroporation on human brain organoids to knock down COG5 and to reconstitute intracellular architecture and organelles position in single GFP-labeled cells.
Organoids at D40 were collected in DM+VitA without P/S prior to electroporation. To electroporate organoids 1µg/µL of either pCAGGS-GFP plasmid, scramble plasmid (DBA), COG5 shRNA bearing plasmid or combined COG4+COG5 shRNA plasmids were prepared in PBS and 1X Fast Green (Sigma). Scramble and COG5 plasmids were purchased from DBA whereas COG4 plasmid was obtained from Addgene. Plasmids were stored in ice until use.
Borosilicate glass capillaries (O.D. 1.2mm, I.D. 0.94mm. 10cm length, Sutter Instruments) were pulled using a Puller (Model P-1000 Sutter Instrument) with the following set up: Heat 500, Pull 60, Vel 80, Delay 100 and Pressure 280. Organoids were moved to PBS and electroporated with the scramble or with the shRNA plasmid through the injection with a glass pipette in the ventricles identified via visual inspection using a stereomicroscope. For the electroporation 5 pulses were applied at 80V for 50ms each at 500ms intervals using an electroporator (Ecm830, BTX). Electroporated organoids were moved to the differentiation medium without P/S for 4h and then placed back in normal DM.
Electroporated organoids were kept in culture for 48h or 7 days depending on the downstream analysis. 48h were sufficient to assess the effect of the knock down on both apical and basal progenitors as well as for Golgi apparatus reconstruction in apical progenitors, whereas organoids were kept in culture for 7 days after electroporation for neuronal population assessment.

Western Blot

For COG5, COG4 and COG7 quantification in human brain organoids western blots were performed as follows. Organoids were collected and snap frozen in dry ice and stored at -80°C until use. Samples for western blot were prepared by adding SDS protein lysis buffer (2% SDS, 50mM TrisHCl pH8, 10mmM EDTA, 10% Glycerol) to the organoids (10% (w/v) lysate). Samples were boiled at 95°C for 2 minutes. To break all cell clusters the sample was passed through an insulin syringe, followed by ultrasonication (ultrasound time 3s, 10s interval, repeated from 5 to 15 times, ultrasonic power 40kW). Samples were then centrifuged for 10 minutes at 8000x g and the cell pellet was discarded. BCA assay was

performed to determine protein concentration and the lysate was finally aliquoted and stored at -80°C until use.

Lysates corresponding to 20ug of protein were added with1X NuPAGE LDS Sample buffer and NuPAGE™ Reducing Agent (1X final concentration). Samples were put at 70°C for 10 minutes to achieve heat-mediated denaturation.

Samples were loaded on the NuPAGE 3-8% Tris-Acetate gel (Invitrogen) in running buffer, (20X NuPAGE Tris Acetate Running Buffer LA0041 in water) together with the precision Protein Dual Color Standards (BIORAD) ladder. For denaturing electrophoresis the gel was run for 1 hour at 160 V constant. After the electrophoresis, proteins were transferred onto the nitrocellulose membrane using Trans-Blot Turbo Transfer System (BIORAD) with parameters set to: 1.3A-25V for 10 minutes.

The nitrocellulose membrane was washed with TBST (10mM Tris-HCl, pH 8.0, 150 mM NaCl, 0.05% Tween 20) once for 5 min at room temperature. Blocking of non-specific binding was performed on the membrane with freshly prepared 5% non-fat dried milk in TTBS for 1 hour on a shaking platform at room temperature. The membrane was then incubated with the primary antibody prepared in 5% milk with gentle agitation at 4°C overnight. The next day the membrane was washed three times for 5 min each with TBST and then incubated with secondary HRP antibody at 1:5000 in TBST-5% milk for 1h at RT. The membrane was washed three times again for 5 minutes each with TBST. The Clarity Max Western ECL Substrate (BIORAD) was added to the membrane for 5 minutes and finally the membrane was imaged with a digital ChemiDoc imager (BIORAD).

Western blot on lectins

To perform glycan quantifications western blot analysis was done. Samples were first diluted and quantified by BCA with deionized water . Samples were then added with 4X LMSB and reducing agent (10X) (Invitrogen) at 1 µg/µL final concentration.

Samples were heated at 75°C for 10 minutes to achieve protein denaturation and then spinned down at 12 000xg for 1 min. Samples (10-20 µg) were then loaded onto Novex® 4–12 % or 8% Bis-Tris Mini Gel into electrophoresis box and the gel was run at constant voltage of 160V. The gel was placed on the PVDF membrane in the “sandwich” chamber and run for 10 minutes at RT for protein transfer. After the trans-blot the membrane was incubated with blocking solution for at least 1h at RT or o/n at 4°C, on a shaker. The membrane was then washed in TBST and incubated with 3 µg /mL of biotinylated lectin solution in blocking buffer on a shaker for 30 minutes. After TBST washes, a 0.1 µg/mL streptaviding-HRP conjugate in blocking buffer was added to the membrane for 20 min. The membrane was rinsed with TBST and finally incubated with Biorad ECL Western Blotting Substrate solution and acquired with a digital ChemiDoc.

Automatic annotation

The dataset for neural network tissue segmentation consisted of images of pipette tip randomly located at different XYZ locations in the microscope FOV. These images were captured with all combinations of the microscope optovar and objectives. These images were split 80% into the training data set and 20% into the testing dataset. The images in the testing dataset were not exposed to the network during training, so good performance on test images indicated the network may generalize well to novel data. All images were automatically annotated with the pipette tip XYZ position to serve as the "ground truths" for training.

Pipette tip detection error was evaluated by comparing the neural network pipette tip detection results to the annotated "ground truths" in the testing dataset. The neural network was first trained on the images in the training dataset. After training was completed, the trained network was used to detect the pipette tip position in the testing dataset. This detected pipette tip position was compared to the "ground truth" position to compute the positioning error.

The post-calibration positioning error was evaluated by first completing the calibration process (either automatically or manually). Then the computed calibration was used to send the pipette tip position to a random desired position in the microscope FOV. Then the current pipette tip position was marked by clicking on the tip in the video feed to designate the actual pipette position. This actual position was compared with the desired position to compute the positioning error.

The calibration duration was evaluated by performing identical injection experiments on Autoinjector 1.0 and ML-guided Autoinjector and comparing the durations of each process. The injection experiment consisted of injecting a piece of tissue at three different focal planes and repeating this process for three pieces of tissue. The entire experiment (three focal plane injections for three tissue pieces) was timed and the durations of each process were tabulated.

Target annotation and tissue edge detection

The dataset for neural network tissue segmentation consisted of 40 pieces of embryonic mouse brain tissue that was imaged at three different focal heights for a total 120 images for neural network training. These 120 images were split 80% into the training data set (N=96) and 20% into the testing dataset (N=24). The images in the testing dataset were not exposed to the network during training, so good performance on test images indicated the network could generalize well to novel data. All images were manually annotated by a user to identify ground truth pixel values, so all pixels were manually labeled as "background" or "tissue".

Tissue segmentation and edge classification performance were evaluated by comparing the neural network tissue segmentation and the edge classification results to manually annotated "ground truths" in the testing dataset. The neural network was first trained on the images in the training dataset. After training completed, the trained network was used to

segment images in the testing dataset. The results of segmentation on testing dataset were used to count the number pixels corresponding to true positives (TP), true negatives (TN), false positives (FP), and false negatives (FN) in each image. These TP, TN, FP, and FN pixel counts were used to compute the tissue segmentation metrics.

The binary images resulting from tissue segmentation on the testing dataset were then input into the edge classification algorithm. An edge was classified as TP if it had the correct label (apical vs basal) and it coincided with the actual tissue edge. Edges were FP if they had an incorrect label or if it coincided with the background. Edges were FN if tissue segmentation/edge classification failed identify the presence of a tissue edge in the image. (TN were not counted because there are “infinitely” many non-existent edges in an image).

Table 1. Antibodies used and dilutions

Antibodies		
Rabbit anti GRASP65 polyclonal antibody (1:200)	Thermofisher	PA3-910
Rat anti Eomes monoclonal antibody (1:200)	Thermofisher	14-4875-80
Goat anti SOX2 polyclonal antibody (1:200)	BioTechne	AF2018
Rabbit anti Hopx polyclonal antibody (1:200)	Sigma	HPA030180
Rabbit anti COG4 polyclonal antibody (1:200)	Novus Biologicals	NBP2-30718
Rabbit anti COG5 polyclonal antibody (1:200)	Novus Biologicals	NBP2-58968
Rabbit anti Ki67 polyclonal antibody (1:200)	Abcam	ab15580
Mouse anti Dextran monoclonal antibody (1:250)	Stemcell	60026
Rabbit anti COG5 polyclonal antibody (1:200)	Thermofisher	PA5-43586
Rabbit anti COG4 polyclonal antibody (1:200)	Thermofisher	PA5-96810
Rabbit anti TBR2 polyclonal antibody (1:200)	Abcam	ab261913
Mouse anti-ytubulin monoclonal antibody (1:500)	Meck/Sigma	T6557
Rabbit anti COG5 polyclonal antibody (1:200)	Merck/Sigma	HPA041583
Mouse anti GM130 monoclonal antibody (1:200)	BD Biosciences	610823
Mouse anti actin antibody (1:1000)	Merck/Sigma	MAB1501
Rabbit anti HuCHuD polyclonal antibody (1:200)	Abcam	ab184267
Rabbit anti COG5 polyclonal antibody	Abcam	ab229830

Rabbit anti ACBD3 polyclonal antibody (1:200)	Thermofisher	PA5-53331
Rabbit anti Numb polyclonal antibody	Thermofisher	PA1-31840
Rat anti Ctip2 polyclonal antibody (1:400)	Abcam	ab18465
Mouse anti Ki67 monoclonal antibody (1:200)	Cell Signallung/euroclone	9449S
Mouse anti ACBD3 monoclonal antibody (1:500)	Santa Cruz	sc-101277
Mouse anti Pancadherin monoclonal antibody (1:200)	Sigma/Merck	C1821
Rabbit Anti-HOPX (1:200)	SIGMA	HPA030180
Mouse Anti-tubulin b 3 (TUJ1) (1:500)	BioLegend	801202
Rabbit anti Satb2 polyclonal antibody	Abcam	ab34735
Peanut Agglutinin (PNA), Biotinylated	Vector Laboratories/DBA	B-1075-5
Sambucus Nigra (Elderberry Bark) Lectin (SNA, EBL), fluorescein (FITC) (1:400)	Thermofisher/invitrogen	L32479
Sambucus Nigra Lectin (SNA, EBL), Biotinylated	Vector Laboratories/DBA	B-1305-2
Alexa Fluor™ 488 phalloidin (1:500)	Invitrogen	A12379
Donkey anti-Goat IgG (H+L) Highly Cross-Adsorbed Secondary Antibody, Alexa Fluor™ Plus 488	Invitrogen™/Thermofisher	A32814
Donkey anti-Goat IgG (H+L) Highly Cross-Adsorbed Secondary Antibody, Alexa Fluor™ Plus 555	Invitrogen™/Thermofisher	A32816
Donkey anti-Goat IgG (H+L) Highly Cross-Adsorbed Secondary Antibody, Alexa Fluor™ Plus647	Invitrogen™/Thermofisher	A32849
Donkey anti-Rabbit IgG (H+L) Highly Cross-Adsorbed Secondary Antibody, Alexa Fluor™ Plus 647	Invitrogen™/Thermofisher	A32795
Donkey anti-Rabbit IgG (H+L) Highly Cross-Adsorbed Secondary Antibody, Alexa Fluor™ Plus 555	Invitrogen™/Thermofisher	A32794
Donkey anti-Rabbit IgG (H+L) Highly Cross-Adsorbed Secondary Antibody, Alexa Fluor™ Plus 488	Invitrogen™/Thermofisher	A32790
Donkey anti-Mouse IgG (H+L) Highly Cross-Adsorbed Secondary Antibody, Alexa Fluor™ Plus 647	Invitrogen™/Thermofisher	A32787
Donkey anti-Mouse IgG (H+L) Highly Cross-Adsorbed Secondary Antibody, Alexa Fluor™ Plus 555	Invitrogen™/Thermofisher	A32773

Donkey anti-Mouse IgG (H+L) Highly Cross-Adsorbed Secondary Antibody, Alexa Fluor™ Plus 488	Invitrogen™/Thermofisher	A32766
Anti-Rat IgG(H+L) Secondary Antibody	Tissue Processing Facility Human Technopole	

RESULTS

Developing technology for single cell manipulation in tissue

The study of the contribution of single cells to the morphogenesis of a complex tissue as the brain, is a fundamental research area in the context of developmental biology and neuroscience. Neurodevelopmental studies are often limited by the resolution that available techniques can reach to track the history of single cells and their progeny. The challenge of clearly visualizing single neural progenitor cells and neurons from the complexity of the surrounding tissue has been successfully tackled via microinjection, a technique that consists on the insertion into single cells of a fine-tip capillary filled with membrane-impermeable fluorescent tracers. These studies in the human brain remain limited by the availability of the tissue and by ethical limitations. The advent of iPSC derived techniques has revolutionized the field by providing a powerful model system to study in vitro the processes of brain development in human, as lab-grown human brain organoids recapitulate brain development in vitro (Lancaster and Knoblich 2014; Qian et al. 2020; Camp et al. 2015). Applying single cell techniques to human brain organoids would represent a powerful combination of experimental set up to study the dynamics, mechanisms and molecular logic underlying cell fate choices and lineage progression during the brain development.

In previous studies (Taverna et al. 2012) brain organotypic slices have been microinjected and manipulated to study neural progenitor cells in intact tissue from different species. However, manual microinjection comes with limitations in terms of large-scale systematic studies, as it is a high precision and tedious technique that requires skilled users. Thus, efforts have been made to automate this process in murine tissue, with the development of the Autoinjector (Shull et al. 2019), a robotic microinjection platform that overcomes the limitations of manual microinjection and allows to increase the success rate of the experiment while decreasing the difficulties and the user-dependent experimental differences. Automated microinjection allowed to reconstruct the lineage of microinjected apical progenitors and to follow their identity across successive cell divisions.

We now sought (i) to develop a fully automated robot requiring minimal human intervention, ad (ii) to extend the use of automation to human brain organoids. Recently machine learning algorithms have been generalized and widely used for object detection in vision guided robotic microinjection (Alegria et al. 2024).We decided to extend such approaches to perform a fully automated single cell microinjection pipeline in intact tissue, in particular we sought to apply this ML-guided Autoinjector on human brain organoids.

We developed a ML vision guided robot that can automatically (i) image the tissue, either mouse or organoids slices, (ii) detect tissue edges and interfaces and (iii) perform microinjection of into single cells at specific locations within the tissue.

This part of the project was done in collaboration with Jacob O'Brien and Suhasa Kodandaramaiah from the University of Minnesota in Minneapolis, US.

Autoinjector set up

As previously described (Shull et al. 2019) the Autoinjector consists of a motorized pipette micro-manipulator (Sensapex, Finland) that can move in a XYZ directions and that is integrated in a standard inverted epi-fluorescence microscope (Zeiss, DE). A computer-controlled pressure regulator adapted from our collaborators previous work (Kodandaramaiah et al. 2018) is used to regulate the internal pressure of the pipette during microinjection and to unclog the pipette when needed (Fig.5A).

The microscope camera allows to image the tissue and the pipette. The robot utilizes computer vision algorithms to perform real-time detection of the tissue surface and the pipette tip. Automatic pipette calibration allows the program to detect the pipette tip even after successive rounds of microinjection. Once in focus, the tissue can be automatically annotated via a graphic user interface for targeted microinjection. The tip of the micropipette is then sequentially moved to target locations along the annotated tissue edge to execute the microinjection. The robot manipulates the tip of the micropipette to the desired injection location at the tissue interface, briefly inserts the pipette to a specified depth (defined in the graphical user interface, GUI, Fig. 5B) inside the tissue while under controlled internal pressure and retracts the pipette to complete the microinjection process. Notably the movement of the pipette in 3D cartesian space for microinjection results in displacement of the pipette in the microscope field of view (FOV). As the target locations are in the image, the robot automatically performs a calibration process that accurately translates the movement of the pipette in 3D cartesian space via the motorized XYZ stage, to motion in 2D pixel coordinates in camera FOV.



Figure 5. Autoinjector set up.

(A) ML-guided autoinjector set up: the Autoinjector consists of a motorized pipette micro-manipulator that can move in a XYZ directions and that is integrated in a standard inverted epi-fluorescence microscope; a pressure controller allows for the efflux of the injection solution. (B) The user interacts trough a GUI with the robot to perform microinjection.

Calibration automation

Calibration is typically performed by moving an object by a known displacement in cartesian coordinates and detecting the movement with the field of view in pixel coordinates. To automate the process, we trained the YOLOv5 neural network for the X, Y and Z detection of the pipette tip. The output of the neural network is the XY pixel position of the tip in the image and the Z classification of the focal plane the pipette is at (i.e. below, above the current focal

plane). This Z classification is then used to iteratively raise/lower the pipette until it is in focus. Once the pipette was detected, this training process allowed to automatically move to a series of known locations in cartesian coordinate space, and the displacement of the tip of the pipette in pixel coordinates was automatically detected. A transformation matrix related the position of the pipette in cartesian coordinates to displacement in the Field of View (FOV) (Fig. 6A).

We also trained ML models to detect pipettes in focus (Z coordinates). The pipette was manipulated in and out of the plane of focus, with the ML trained to detect the pipette in the best focal plane. The ML model performance was verified manually by a trained experimenter.

The calibration model was trained on mouse tissue and we then extended the application to organoid slices, without additional re-training. highlighting the robustness of the ML-system we developed. The duration of the calibration process was decreased with the ML-based Autoinjector, both in mouse and human organoids tissues, compared to previous values obtained by Autoinjector 1.0 on mouse tissue.

Automated tissue annotation

Automatic target annotation was achieved by a two-step process. First Neural network tissue segmentation drove the categorization of the tissue versus the background (Fig. 6Bi) and then edge classification of the segmented tissue identified the tissue edges as apical or basal based on their curvature (Fig. 6Bii). In neural network tissue segmentation, a U-Net was used to categorize every pixel in an input image as belonging to a piece of tissue or the background, and returned as an output a binary image where each pixel value corresponds to 0 (background) or 1 (tissue). This binary image was then used for edge classification where detected tissue boundaries were extracted and analyzed for their concavity: concave edges (where the edge surrounds/encases background pixels) are classified as apical surfaces (the brain the area surrounding the ventricles) and convex edges (where the edge surrounds encases tissue pixels) are classified as basal (i.e. the edge where neurons reside in the developing brain) (Fig. 6Biii). This further step allowed us to have a fully automated microinjection pipeline -with no human intervention- from the pipette calibration, through tissue edge detection and finally to microinjection into single cells.

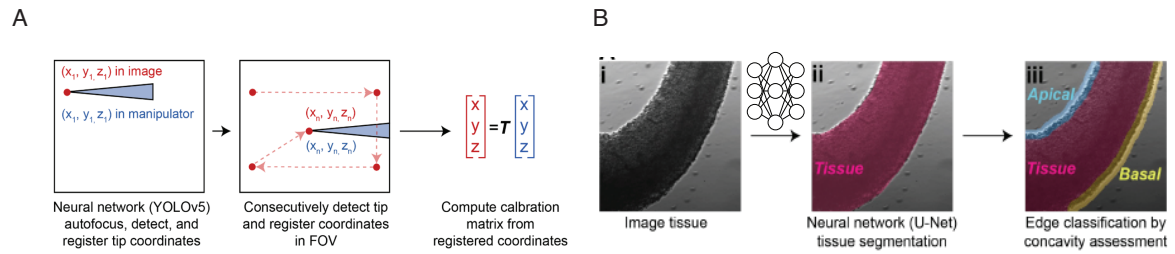


Figure 6. Automated calibration and tissue annotation.

(A) To automate pipette calibration step we trained a YOLOv5 neural network for the X, Y and Z detection of the pipette tip. (B) Automatic tissue edge detection was achieved using a neural network tissue segmentation on embryonic mouse brain tissue that allowed to (i) discriminate tissue from background (ii) segment tissue edges (iii) discriminate between apical-basal tissue edge basing on concavity-convexity parameters.

Robotic microinjection performance in mouse brain slices and human brain organoids

As already discussed, single cell labelling techniques provide useful insights into cellular morphology, intracellular architecture and dynamics during brain morphogenesis. All techniques available to date to label single neurons within the neocortex, do so by labelling neural progenitors first, that will then differentiate into neurons and inherit the label (i.e. a typically a fluorescent reporter). The labelling of neurons is therefore indirect. We thus decided to validate our ML-guided Autoinjector to directly target single neurons in tissue.

We evaluated the robot performance by injecting 250μm-thick E14.5 embryonic mouse brain organotypic slices. The slices edges in the FOV were recognized and classified as apical or basal basing on the tissue concavity/convexity, as previously described. To label neurons, we selected the basal edge and sparsely injected neurons with Dextran A555 dye (Fig. 7A). The fluorescent dye allowed us to then reconstruct labelled neurons morphology (Fig. 7B).

To evaluate the robot performance and efficiency compared with manual microinjection and with the previous semi-automated versions of the robot (Shull et al. 2019), we quantified the number of successful microinjection events by counting the number of injected neurons, observed at the microscope using fluorescence, over the total number of injections performed by the robot (provided by the GUI). We observed an almost two-fold increase in success rate of neuronal microinjection when using our ML-guided autoinjector compared with Autoinjector 1.0 (Fig. 7C). Of note, manual microinjection of neurons within an intact tissue was not feasible because of the lack of fine and fast mechanical control during the procedure.

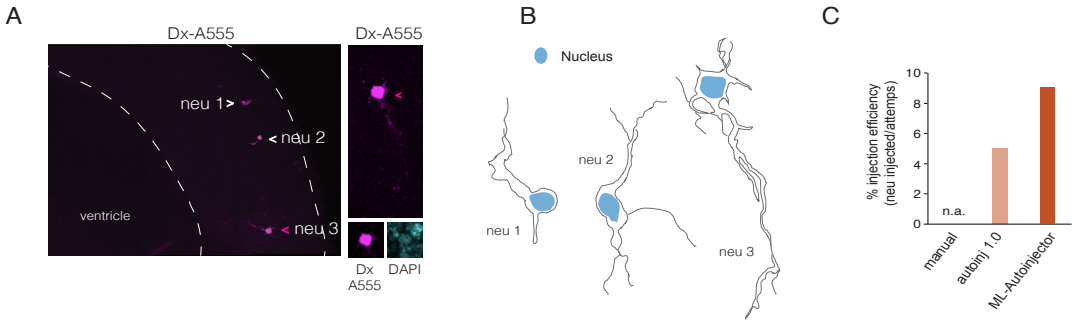


Figure 7. ML-guided microinjection of single neurons in embryonic mouse brain tissue.

(A) Microinjection of E14.5 embryonic mouse brain tissue neurons with Dextran A555 10KDa using the ML-guided autoinjector. (B) Reconstruction of microinjected neurons showing their morphological features. (C) Quantification of microinjection efficiency using manual microinjection, Autoinjector 1.0 or ML-guided autoinjector reveals increased efficiency of injection when targeting neurons.

We next applied the ML-guided autoinjector to human cortical brain organoids slices (see below for a more in depth description of this system). We prepared 250μm thick organotypic organoid slices and we injected Dextran A488 10kDa by approaching the brain organoid slice from the basal side (outer contour) (Fig. 8A-B). Even though organoid slices shape is less homogeneous than mouse tissue, and thus it is more challenging for the algorithm to recognize a concave/convex pattern in its edge structure, the software correctly segmented the edges of the slices by recognizing the outer edge as basal. Also in this case, after microinjection we were able to reconstruct neuronal morphology in human brain organoids (Fig. 8C).

We finally evaluated the microinjection efficiency when targeting neurons of brain organoids, by counting productive injections over the total of injection events, comparing the Autoinjector 1.0 and the ML-guided autoinjector. Also in this case we observed an increase in injection efficiency when using the ML-guided Autoinjector (Fig. 8D).

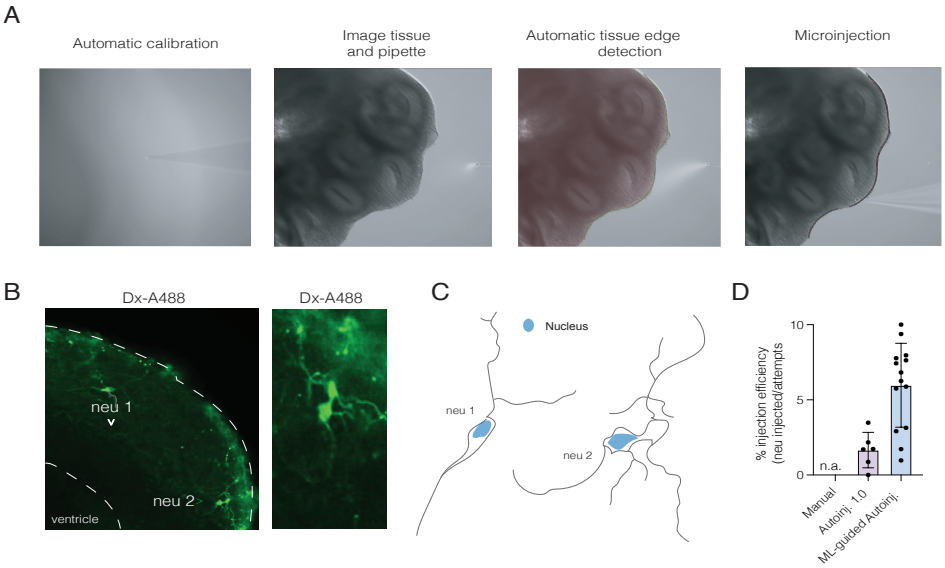


Figure 8. Application of the ML-guided autoinjector on human brain organoids-derived neurons.

(A) ML-guided autoinjector can be extended to human brain organoids. The entire experimental pipeline is reported as frames from recorded movies. (B) Microinjection of neurons in human brain organoids at d40 using Dextran A488 10KDa (C) Reconstruction of injected neurons from human brain organoids. (D) Calculated injection efficiency in human brain organoids using manual injection, Autoinjector 1.0 or ML-guided autoinjector.

Reconstructing intracellular architecture using microinjection

As a single cell labelling technique, microinjection can be combined with downstream high-resolution analysis, such as immunofluorescence to reconstruct intracellular architecture of single neurons in the 3D space. To this end, we optimized a protocol for conventional immunofluorescence on floating sections obtained from brain organoids, and also an alternative protocol for whole-mount immunofluorescence on the entire organoid, based on a custom ultra-fast tissue clearing protocol (see also Materials and Methods).

We focused our attention on the Golgi apparatus (GA) as this organelle is studied by us and other groups for its polarized distribution that is especially relevant in neural progenitor cells and neurons. In apical progenitor cells (APs), the GA is only present in the apical process, but it is absent from the basal process. Upon cell fate switch and differentiation of APs into basal progenitors (BPs), the Golgi is repositioned close to the nucleus. Previous work has established that in mature neurons from mouse and rat the GA is highly polarized, being present in the cell body but absent from dendrites, with the exception of small Golgi outposts (Nakagawa 2024). We employed our microinjection pipeline to gain insight into the organization of the GA in human neurons. By targeting single human neurons via the basal surface of human brain organoids (Fig. 9A), we found that the GA is perinuclear and it is localized in the main process extending from the cell body, most likely the leading process of the migrating neuron. In addition, we observed that the centrosome (as shown by γTubulin

staining) is in close proximity to the GA and to the nucleus (Fig. 9A reconstruction) , similarly to what was previously described in mouse and rat (Nakagawa 2024).
Finally, we decided to extend the use of the ML-guided autoinjector to target human apical progenitors (APs) lining the ventricular zone (VZ) of human brain organoids. We first dissected the organoid to expose the VZ and we microinjected Dextran A555 along the surface of the exposed ventricle (Fig. 9B). Also in this case it was possible to target single APs and to reconstruct their morphology. The possibility to target APs will allow to study not only APs morphology and dynamics but also to track lineage progression during brain development.
In conclusion, we developed an ML-guided automated microinjection that allows to extend the current methodologies for single cell labelling to gain insights into single cells morphology and intracellular architecture, providing a tool to study the cell biology and cellular dynamics of human progenitors and neurons in human brain organoids.

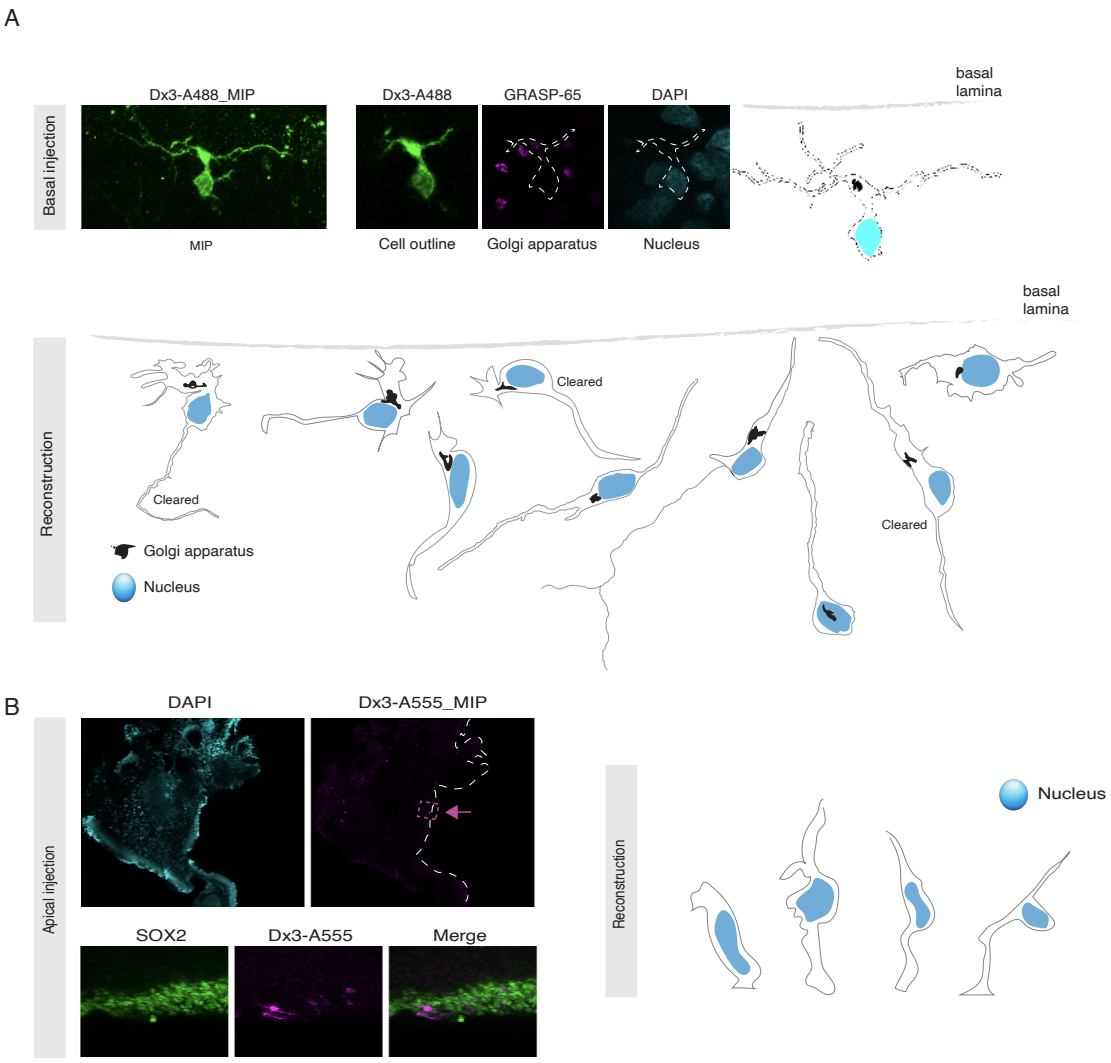


Figure 9. ML-guided Autoinjector allows to reconstruct cellular morphology and intracellular architecture or injected cells in human brain organoids.

(A) Microinjection of single neurons of human brain organoids with dextran A488 (green) and staining with GRASP65 (magenta) allows to reconstruct the morphology of neurons and the localization of Golgi apparatus inside the cell; DAPI is used to stain the nucleus of the injected neurons. (B) Microinjection of apical progenitor cells in human brain organoids with Dextran A555 (magenta) and co-stain with Sox2 (green) extends the use of ML-guided autoinjector to targeting neural progenitor cells and lineage tracing.

Human brain organoids to model brain development in a dish

The advent of iPSC derived model systems, such as human organoids, represented a key conquer in the field of biology and even more so in the context of neurodevelopmental studies. Human brain organoids represent in fact a useful model to recapitulate and study in vitro the cellular and molecular logic of human brain development in physiological and pathological context.

For this project we adapted the Lancaster et al. (Lancaster and Knoblich 2014) protocol to obtain brain organoids from different iPSC lines. We first optimized the protocol using a commercial human iPSC line, WTC11 whose derived brain organoids were examined at different timepoints, day 20 (d20), day 35 (d35), day 40 (d40) and day 60 (d60) to define the dynamics of production of the different cell types of interest, namely apical progenitors and basal progenitors. The identity of neural progenitors (NPCs) and neurons was assessed in all timepoints using fate markers. The VZ contains Sox2-positive apical progenitors (APs; aRGs) and the SVZ mainly contains Tbr2-postive basal progenitors (BPs; IPs and bRG/oRGs)); we used TuJ1 as a general neuronal marker (Fig. 10A). Quantifications showed a gradual but stable increase in the number of Sox2+ progenitors across d20 to d40, reaching a plateau around d60. Tbr2+ basal progenitors started to appear in a consistent number after d20 peaking around d40, though they were still present around d60. Moreover, we measured (i) the cortical thickness as an estimate for the development of the cortical plate (ii) the TuJ1-positive area of the ventricle. We saw a constant increase across all the timepoints in the thickness of the neuronal layer, and a parallel increase of the TuJ1-positive area (Fig. 10B). Finally, we also specifically examined the presence of HopX+ bRGs at later timepoints (d73) and we observed that HopX+ cells were also Sox2+, as previously reported in literature (Penisson et al. 2019) (Fig. 10C).

We figured that d40 was the optimal time to focus our attention on. In fact, d40 organoids show an area of highly organized and densely packed cells forming the ventricular zone (VZ) a less packed region reminiscent of the sub-ventricular zone. Further to investigating the presence of Sox2+ APs and Tbr2+ APs, we investigated which neuronal subtypes were present by staining for NeuN (a broad marker for neurons, Fig. 10D), Tbr1 (marker for layer VI and I neurons, Fig. 10E), Ctip2 (marker for layer V neurons, Fig. 10E, F) and Satb2 (markers for layer IV neurons, Fig. 10F). From a qualitative point of view, irrespective of the neuronal marker used, neurons appear located basal to the VZ and to the SVZ area, suggesting a correct cytoarchitecture of the human brain organoid. The quantifications show that at Day 47 organoids were producing Tbr1- and Ctip2-positive neurons, whereas the population of

Satb2-positive neurons was not very abundant (Fig.10G). We quantified the proportion of neurons double positive for Ctip2 and Tbr1 or for Ctip2 and Satb2 (Fig. 10H) and found that neurons positive for both Ctip2 and Tbr1 are approximately 100% while approximately an 80% of Satb2 neurons are also positive for Ctip2 marker. These data show that human brain organoids contain layer VI, V and VI neurons and suggest that, though simplified in terms of cytoarchitecture, human brain organoids represent a viable option to model human brain development in a dish.

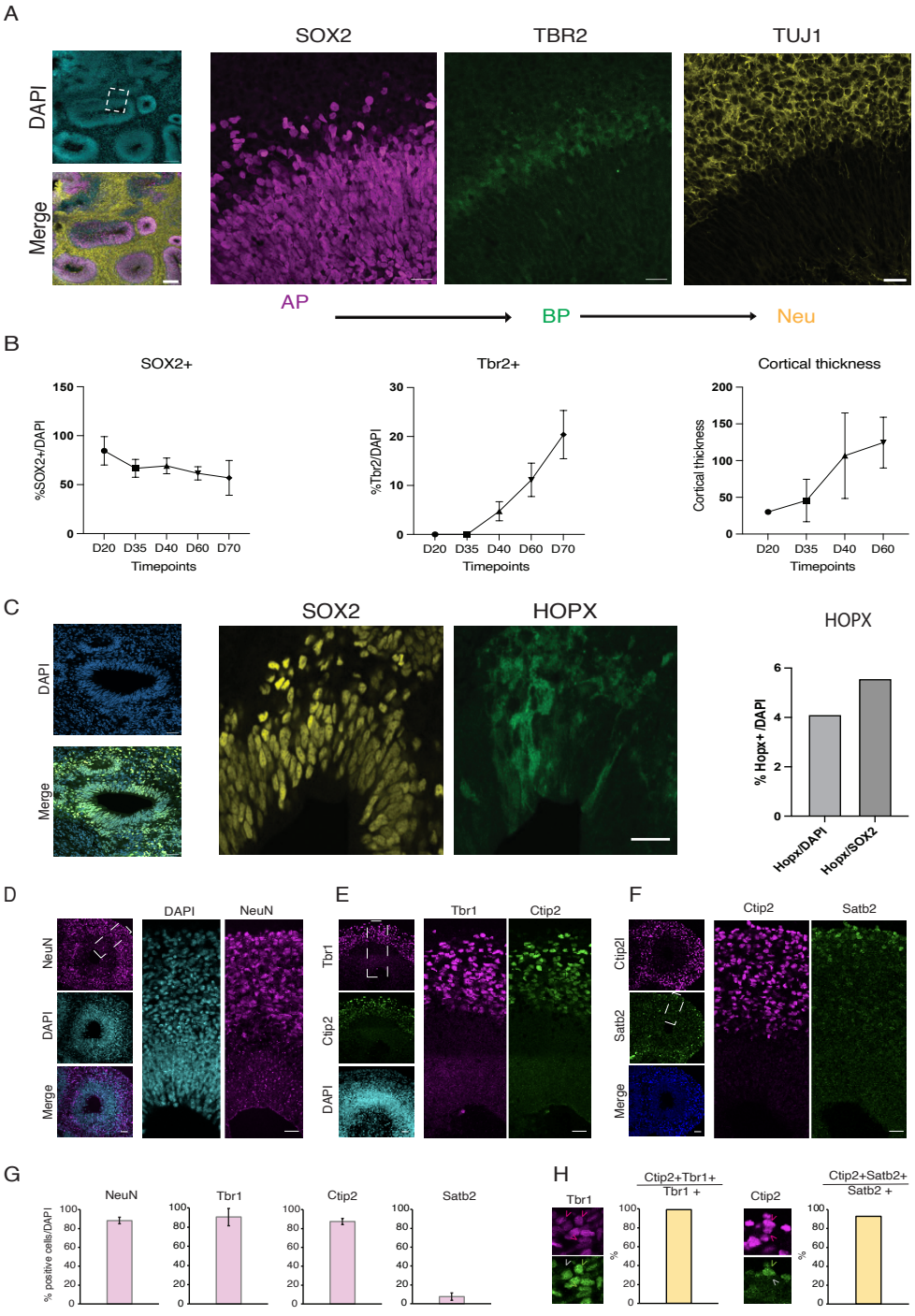


Figure 10. Human brain organoids recapitulate brain development in vitro.

(A) Staining of human brain organoids derived from WTC11 iPSC reveals the presence of ventricular structures containing Sox2+ (magenta), Tbr2+(green) and Tuj1+ (yellow) cells (respectively, APs, BPs and neurons) Scale bar 100μm and 20μm. (B) Quantification of fate markers across timepoints shows that human brain organoids can recapitulate the enrichment in AP, BP and neuronal population following organoid maturation. Scale bar 20μm. (C) HopX+ cells (green) and Sox2+/HopX+ cells are observed in d73 human brain organoids, accounting for the formation of basal radial glia cells (bRGs) at later timepoints of organoid maturation. Scale bar 20μm. (D-F) Neurons develop in the basal-most region of human brain organoids and different neuronal subtypes are present in d40 organoids, as shown by NeuN, Tbr1 and Ctip2 staining; few Satb2 neurons are also present. (G) Quantification of neurons (NeuN) and of the specific neuronal subtypes (Tbr1, Ctip2 and Satb2). (I) Quantification of neurons Ctip2+/Tbr1+ and Ctip2+/Satb2+. Scale bar 20μm.

GA in the human developing brain

Previous work from Taverna et al. (Taverna et al. 2016) demonstrated that the Golgi apparatus is confined to the apical process in mouse APs. In these cells the GA is organized in separated stacks with the cisternae being oriented parallel to the apico-basal axis of the cell.

To understand whether GA is polarized in APs in human developing brain, we electroporated human brain organoids with pCAGGs-GFP plasmid to highlight the cell contour and stained electroporated organoids for GRASP65, a GA marker (Fig. 11A). We identified GFP+ cells along the ventricle and reconstructed single apical progenitor cells, including their apical process. We observed that GA is only restricted to the apical most part of the apical process of APs of human brain organoids, between the nucleus and the apical surface (Fig. 11B). These observations highlight that also in human APs the GA is polarized along the apico-basal axis of the cell, and it is confined in the apical process. Furthermore, and consistently with previous work on mouse tissue, the GA of human apical progenitors was organized in multiple isolated stacks with the cis-to-trans axis oriented perpendicularly to the apico-basal axis of APs (Fig.11, reconstruction).

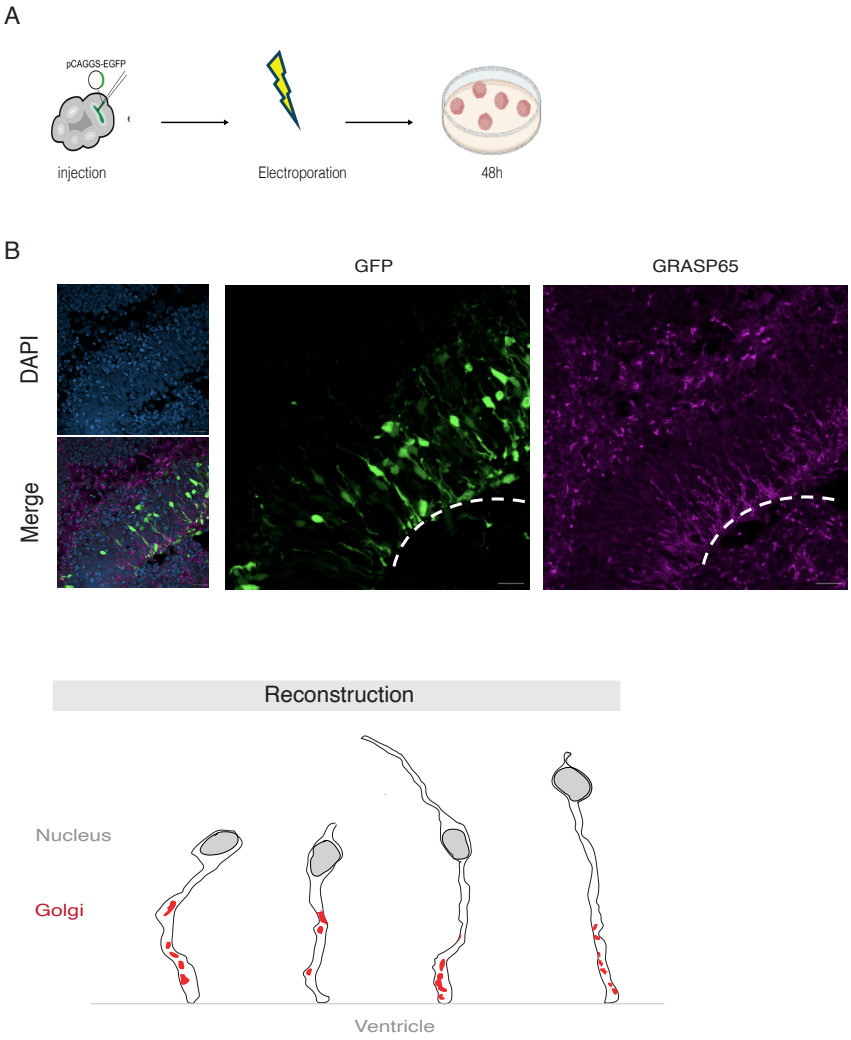


Figure 11. Golgi apparatus is localized in the apical process of apical progenitors in human brain organoids.

(A) Electroporation with GFP plasmid in WTC11-derived d40 human brain organoids ventricles and (B) post processing staining for GRASP65 (magenta, Golgi) allows to reconstruct single apical progenitors (APs, green) and localize the Golgi apparatus in the apical process (Golgi in red, cell nucleus in grey). Scale bar 20µm.

Acute GA disassembly favors AP-to-BP fate transition

It is well assessed that GA undergoes a dynamic process of repositioning upon cell fate switch from apical to basal progenitors, in mouse developing brain as well as in human brain organoids. We wondered whether the specific position of Golgi apparatus could underlie specific functions in maintaining neural progenitor cell identity.

To address this question, we made use of two different Golgi-disassembling drugs: Brefeldin A (BFA) and Golgicide A, whose action induces GA fragmentation by targeting GA at the trans or the cis part, respectively. BFA disrupts protein transport by interfering with the function of ADP-ribosylation factors (ARFs) and their associated proteins, crucial

for COPI vesicles formation. Golgicide A acts on GBF1, an interactor of Arf1, interrupting its activity and ultimately leading to Golgi membranes dispersal and fragmentation.
To assess the amount of time needed by BFA to fragment Golgi apparatus we performed a time course experiment on HeLa cells, by treating HeLa for 1, 2, 4 and 6h. In HeLa cells the Golgi apparatus was fragmented already after 1h treatment (Fig. 12A). For the brain tissue, we run a time course analysis and assessed the Golgi integrity by staining for GRASP65 . These experiments showed that 6h are necessary for Golgi to be fragmented in both the mouse brain and in human brain organoids (Fig.12B-C). We therefore decided to treat the brain organoid and embryonic mouse brain samples with BFA or Golgicide A for 6h to allow for drug penetration and Golgi fragmentation. Of note, after 24h from the treatment the Golgi starts to reassemble (Fig. 12C), consistent with the reversible nature of the two used Golgi disassembling drugs.

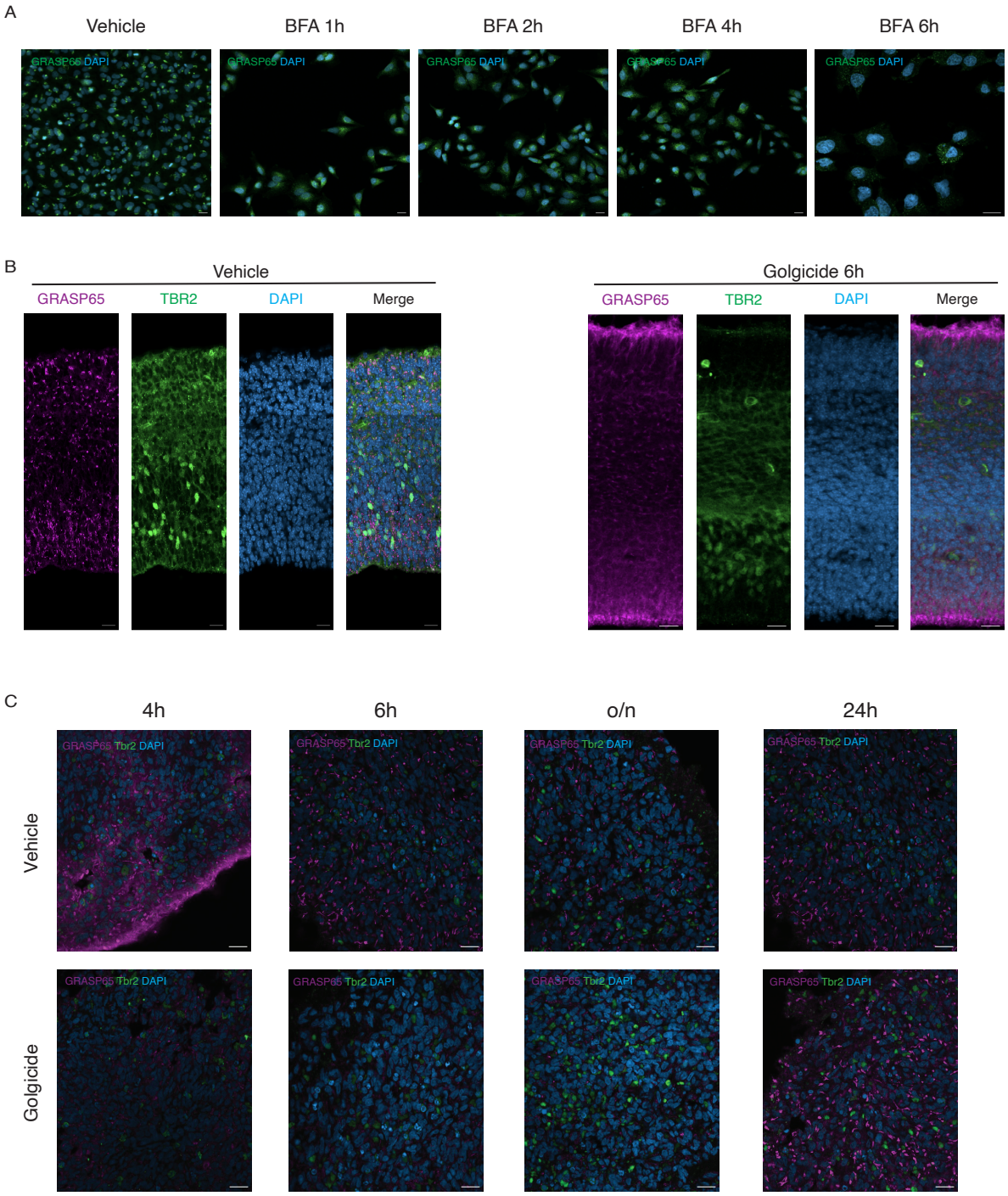


Figure 12. Drug treatment-induced GA fragmentation.

(A) Time-course BFA treatment analysis in HeLa cells; cells were stained for GRASP65 (green) and DAPI (cyan). Scale bar 20μm. (B) 6h Golgicide or DMSO (vehicle) treatment on E14.5 embryonic mouse brain; staining for GRASP65 (Golgi apparatus, magenta), TBR2 (basal progenitors, green), DAPI (cyan). Scale bar 20μm. (C) Golgicide and DMSO (vehicle) time-course analysis in d40 human brain organoids; staining for GRASP65 (GA, magenta), TBR2 (BPs, green) and DAPI (cyan). Scale bar 20μm.

We treated E14.5 embryonic mouse brain hemispheres with BFA or with the vehicle (EtOH), fixed the samples and stained for Tbr2 as marker for intermediate progenitors (IPs), the most enriched population of basal progenitor in mouse developing brain. Upon BFA treatment and Golgi apparatus disassembly we observed a concomitant increase in Tbr2+ cells compared to the control (Fig. 13A). To assess whether the drugs had effects on the neuronal population, we also measured the thickness of the neuronal layers by staining with TuJ1 and by quantifying the area corresponding to the cortical plate within the tissue. Consistent with the short duration of the pharmacological treatment, we did not find any differences in the thickness of the cortical plate in BFA treated samples (Fig.13B). These data suggest that perturbing GA integrity induces a premature fate switch from AP to BP, without affecting the neuronal population. A similar increase in the number of Tbr2-positive IPs was observed by treating E14.5 embryonic mouse brain hemispheres with Golgicide A (Fig, 13C, Golgicide vs vehicle, in this case DMSO).
Human apical progenitors display similar features regarding Golgi apparatus polarization as observed in mouse developing brain, so we wondered whether the increase in intermediate progenitors could also be observed in human brain organoids. We used human brain organoids at day 40 (d40) and we treated them with Golgicide A or with DMSO as a control. We observed that also in human brain organoids upon Golgicide A-induced GA fragmentation there was an increase in Tbr2+ cells (Fig. 13D). We checked whether the treatment could affect the Sox2+ cells population and we observed and increase in the general number of Sox2+ cells both in the VZ and SVZ (Fig. 13E).
Overall, these data suggest that the Golgi apparatus affect NPCs fate both in mouse and human, causing a premature fate switch from apical progenitor to basal progenitor, suggesting an interesting link between GA structural integrity and cell identity during brain development across species.

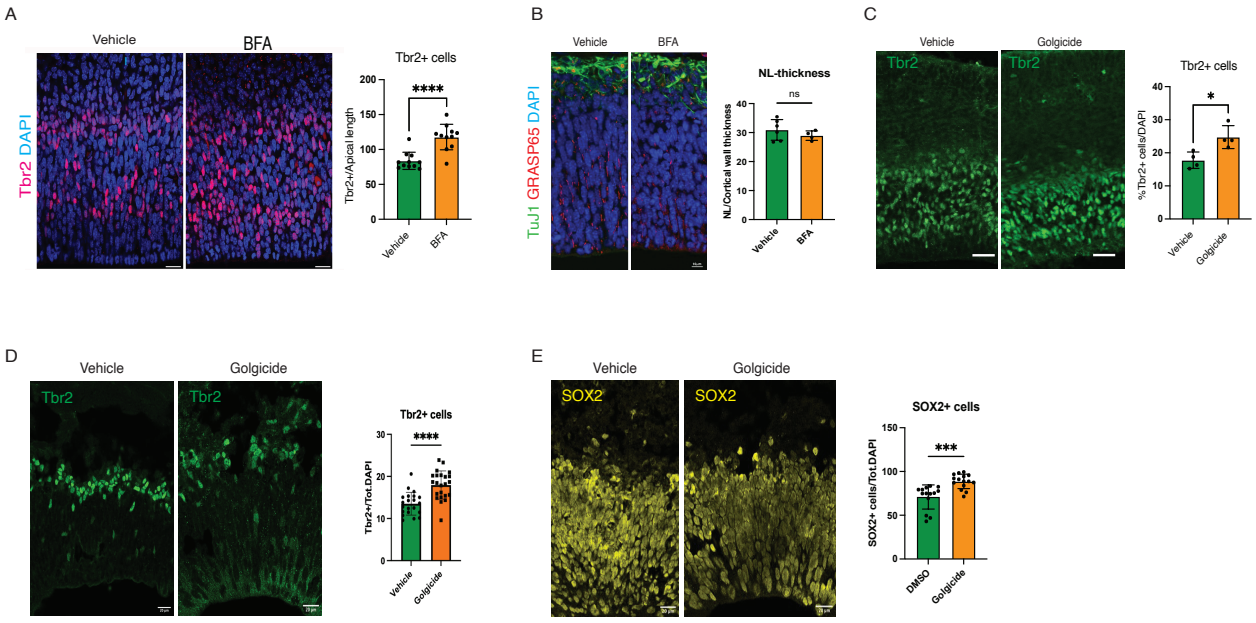


Figure 13. Acute Golgi-disassembling pharmacological treatment increases the number of Tbr2+ BPs in both embryonic mouse brain and human brain organoids.

(A) 6h BFA treatment in E14.5 embryonic mouse brain, stained for Tbr2 (magenta) shows an increase in Tbr2+ intermediate progenitors upon BFA treatment. Scale bar 20μm. (B) Staining of TuJ1 (green) in E14.5 mouse brain reveals that the neuronal layer thickness is unchanged upon BFA treatment (Golgi in red). Scale bar 20μm. (C) 6h Golgicide treatment in mouse E14.5 brain tissue and staining for Tbr2 (green) shows an increase in BPs after treatment. Scale bar 20μm. (D) 6h Golgicide treatment in d40 human brain organoids and staining for Tbr2 (green), shows that also in organoids Golgi fragmentation increases the number of BPs. Scale bar 20μm. (E) SOX2+ population (yellow) is increased after 6h Golgicide treatment in human brain organoids. Scale bar 20μm. Student's t test. ns: not significant p>0,005, *: significant p<0,005. N= 3 and n=3 for E14.5 mouse brain; N=4 n=1 for human brain organoids (N: organoid batches, n: organoids/batch).

GA disassembly affects fate transition by favoring symmetric differentiative division of apical progenitors

The acute (6h) BFA and Golgicide treatments span a short amount of time, not sufficient to allow cells to start and complete a full cell cycle, unless already committed to the division process. Thus, we hypothesized two scenarios to explain how GA disruption affects cell fate choice during brain development. In the first scenario, GA disassembly could induce AP transdifferentiation, a process through which a cell undergoes a change in identity without undergoing mitosis. In the second scenario, GA disassembly could change the mode of cell division and therefore the fate of the daughter cells.

To gain insight into the mechanisms underlying the role of GA on cell fate switch, we used automated microinjection. We first injected Dextran A555 to label single APs lining the apical surface of the embryonic mouse brain organotypic slice (Fig. 14A) through the use of

ML-guided Autoinjector (Polenghi et al., in preparation) and then we treated the injected organotypic slices with Golgicide A, or a vehicle, for 6h to fragment the Golgi.

After fixation, slices were stained with anti-Dextran antibody to highlight microinjected cells and their progeny, along with their identity that was assessed by staining for fate markers such as Sox2 (APs marker) and Tbr2 (BPs marker).

Upon Golgicide treatment, microinjected cells and their progeny were found more distant from the apical surface compared to control (Fig. 14B). In line with that, Golgicide treated cells displayed a decrease in the apical contact with the apical surface (Fig. 14C).
We leveraged the excellent single cell resolution of microinjection and evaluated the percentage of cells found as single cell or in 2-cells clusters, as a proxy for transdifferentiation potential. We found no difference between Golgicide and control in the percentage of microinjected cells found in 2-cells clusters (corresponding to daughter cells) (Fig. 14D). This observation strongly suggests that the treatment does not induce transdifferentation of the injected APs.
We therefore consider more likely that the Golgi fragmentation influences the mode and outcome of cell division. We then measured the degree of symmetry of cell division by assessing the fate asymmetry of the two-daughter cells clusters. There are 3 possible outcome of an AP division: daughter cells are Tbr2-/Tbr2- (symmetric proliferative division), Tbr2-/Tbr2+ (asymmetric self-renewing division) or Tbr2+/Tbr2+ (symmetric differentiative division). Compared to control, we observed that in Golgicide A treated sample there is an increase in Tbr2+/Tbr2+ (symmetric differentiative division) at the expenses of Tbr2-/Tbr2- (symmetric proliferative division). No drastic change in the proportion of Tbr2-/Tbr2+ (asymmetric self-renewing division) was observed (Fig. 14E). These data suggest that the acute perturbation of the Golgi apparatus increases the number of BPs by affecting the mode of cell division, favouring symmetric differentiative division.

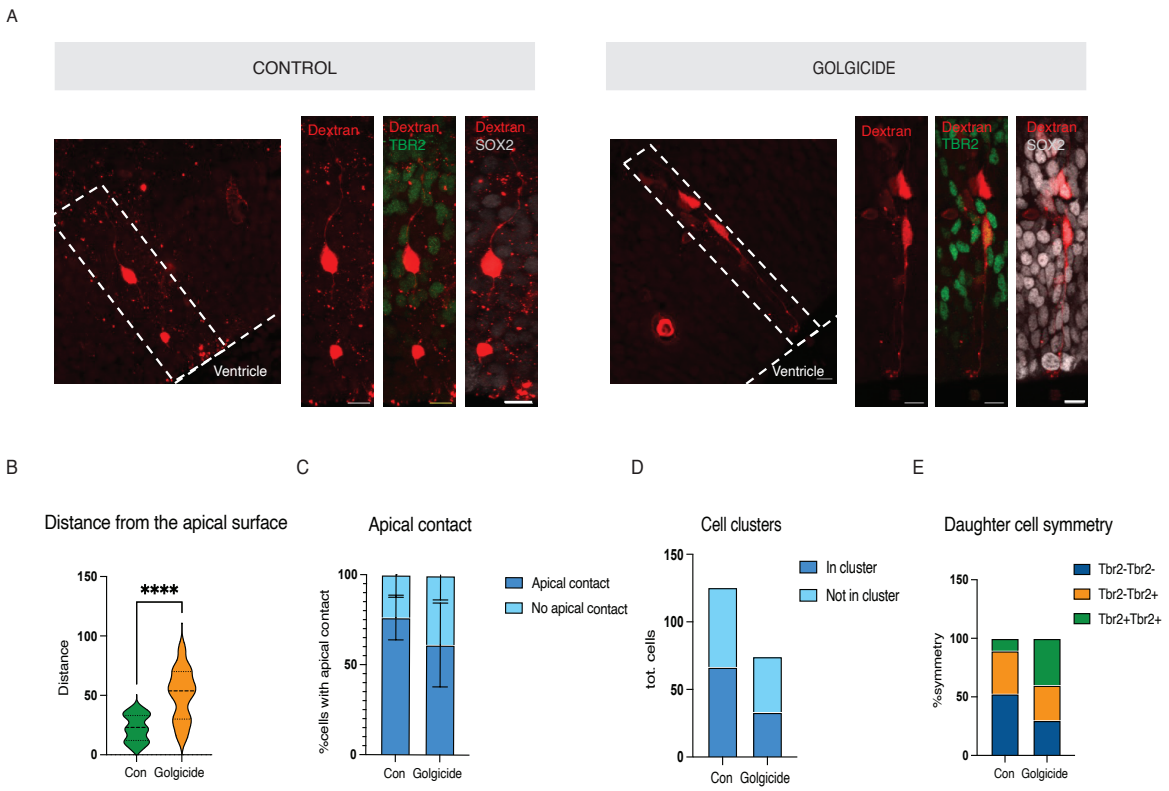


Figure 14. Lineage tracing using the ML-guided autoinjector reveals that drug treatment-induced Golgi apparatus fragmentation favors symmetric differentiative division of apical progenitors.

(A) Injection of apical progenitor cells in E14.5 mouse brain organotypic slices, using Dextran A555 (red) and staining for TBR2 (green) and SOX2 (grey). White dotted line delimiting the ventricle. Scale bar 10µm. (B) Golgicide treatment increases the distance from the apical surface. (C) Apical contacts of injected cells decreases upon Golgicide treatment. (D) The ration between injected cells observed to be part of a cluster does not differ between control and Golgicide conditions. (E) Quantification of daughter cells symmetry reveals an increase in TBR2+/TBR2+ cells in Golgicide treated cells. Student's t test. *: significant p<0,005. N= 3 and n=6 (N: experimental sessions; n: brain slices injected per experimental session).

COG5 knock down affects cell identity and fate of neural progenitor cells

For a more specific analysis on the relationship between cell biology of GA and brain development, we decided to carry on a genetic perturbation and selected COG5 as a candidate for functional manipulation. COG5 is a subunit of lobe B of the COG complex, involved in retrograde vesicle tethering among Golgi membranes and from Golgi to ER. Mutations on COG5 have been found in CDGs and associated with primary microcephaly (Rymen et al. 2012). So, we reasoned that COG5 could be an interesting target to gain insights into the contribution of Golgi Apparatus to brain development.

COG5 is localized at the Golgi apparatus in neural progenitor cells

COG5 is ubiquitously expressed in different cell types, however when checking the mRNAs levels both in human and mouse developing brain, respectively from Florio et al. dataset (Florio et al. 2015)(Fig. 15A-B) and CEREBRA dataset (Fig. 15C), we observed an increased expression of COG5 mRNA in human neurons consistent with their higher secretory activity. We checked COG5 protein localization in human brain organoids, by co staining for COG5 and GM130, a marker of the cis Golgi, and we saw a colocalization of the two proteins with COG5 displaying a similar pattern as that of GM130 (Fig. 15D). Of note COG5, along with GM130, is mainly localized in the apical most part in the ventricular zone, in the apical process of apical progenitors, while it is not detectable in the proximity of the nucleus. COG5 is instead perinuclear in BPs and neurons, occupying the SVZ and the putative cortical plate in the organoids, where it again colocalizes with GM130. These data together support the fact that COG5 colocalizes with the GA and shows a similar pattern of polarization in apical progenitors in the developing brain.

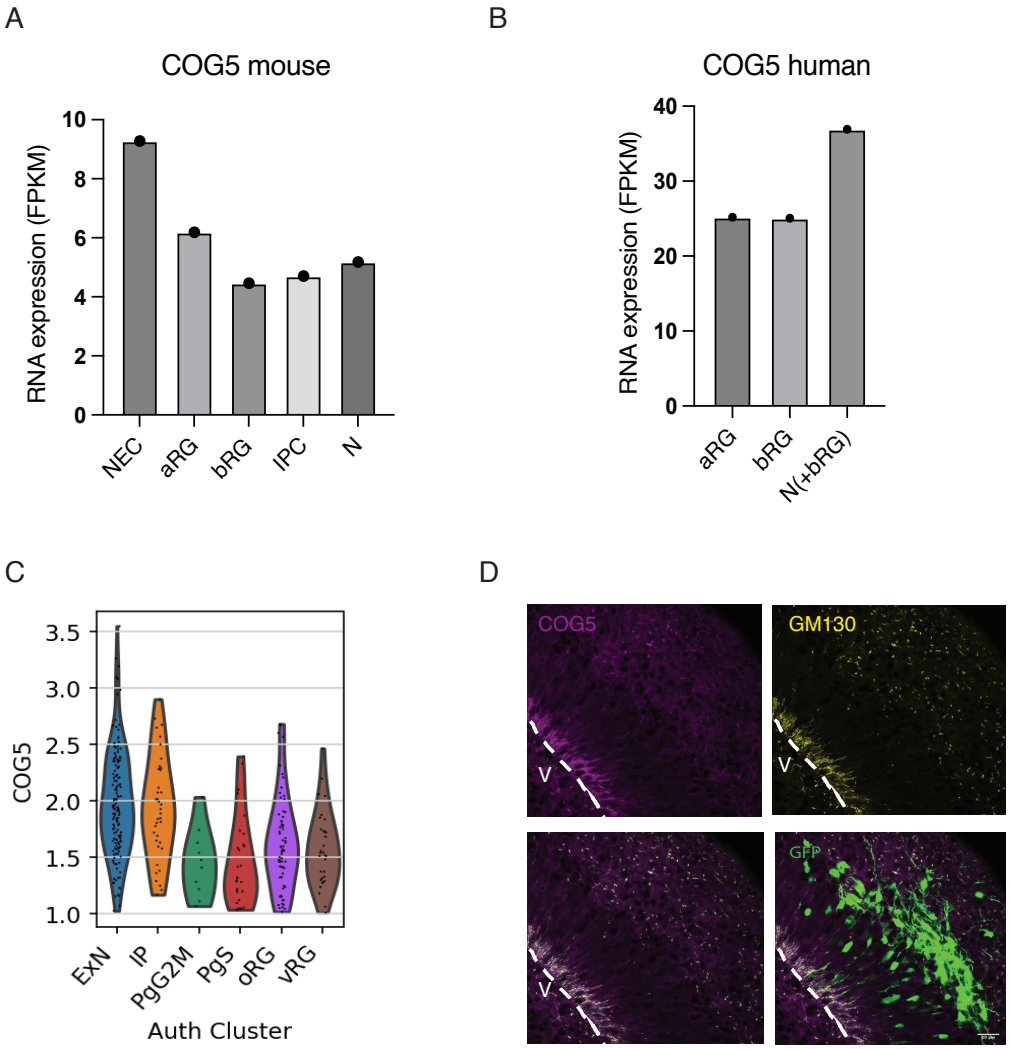


Figure 15. COG5 is expressed across cell types in brain development and colocalizes with Golgi apparatus.

(A-B) RNA expression analysis from Florio e al. bulk RNAseq dataset. In panel A E15.5 embryonic mouse brain tissue show COG5 RNA expression across NPCs (NEC, aRG, bRG, IPC) and neurons (N); panel B shows COG5 RNA expression from human brain tissue. (C) COG5 RNA expression in human foetal brain from CEREBRA atlas across NPCs and neuronal cell types. The dataset considered was extracted from (Polioudakis et al. 2019). (D) Staining for COG5 (magenta) and GM130 (GA, yellow) in d40 electroporated (GFP in green) human brain organoid; white dotted line highlights the ventricular surface (V). Scale bar 20μm.

Genetic perturbation of COG5 in human brain organoids using shRNA electroporation results in the disassembly of the Golgi apparatus

Next, we wondered whether a specific perturbation of COG5 could have similar consequences as those observed through drug-mediated Golgi fragmentation. To do so we decided to knock down COG5 (or COG4 and COG5 together) in human brain organoids by electroporating the plasmid encoding either for an shRNA targeting COG5 or COG4, or a scramble, that also expressed GFP for the identification of the electroporated apical progenitors.

We validated the plasmid for shRNA mediated silencing of COG5 and COG4 by transfecting the plasmid encoding for the shRNA in HeLa cells. 48h after transfection cells were fixed and stained for COG5 and for GM130 as a Golgi marker (Fig. 16A). HeLa cells transfected with COG5 shRNA showed a decreased intensity for COG5 immunofluorescence signal, calculated as the difference between the mean signal of COG5 and the mean signal of the background (Fig. 16B), suggesting that the mRNA was correctly knocked down. A less sharp, but still significant decrease in the signal was observed for the double KD of COG4 and COG5 that could be explained by the different expression of the COG5 shRNA plasmid when co transfected with COG4 shRNA. We also assessed whether the KD had an impact on Golgi structure by calculating the number of Golgi units per cell and the area of each unit (Fig. 16C). Interestingly, for both knock down conditions (COG KD and COG4+5 KD) the number of Golgi units was increased compared to the Scramble control and the GFP control, suggesting a fragmentation of the GA, a feature supported also by the fact that a concomitant decrease in each Golgi units area was observed in the KD conditions (Fig. 16D).

The validated plasmids were electroporated in human brain organoids. 48h after electroporation organoids were fixed and stained for GM130 to assess GA integrity. We observed the KD of COG5 alone or a combination of COG4shRNA and COG5shRNA lead to an increase in the number of Golgi units observed along the apical process of apical progenitors and a concomitant decrease in their area, suggesting a that the knock down of COGs induces GA fragmentation (Fig. 17A).

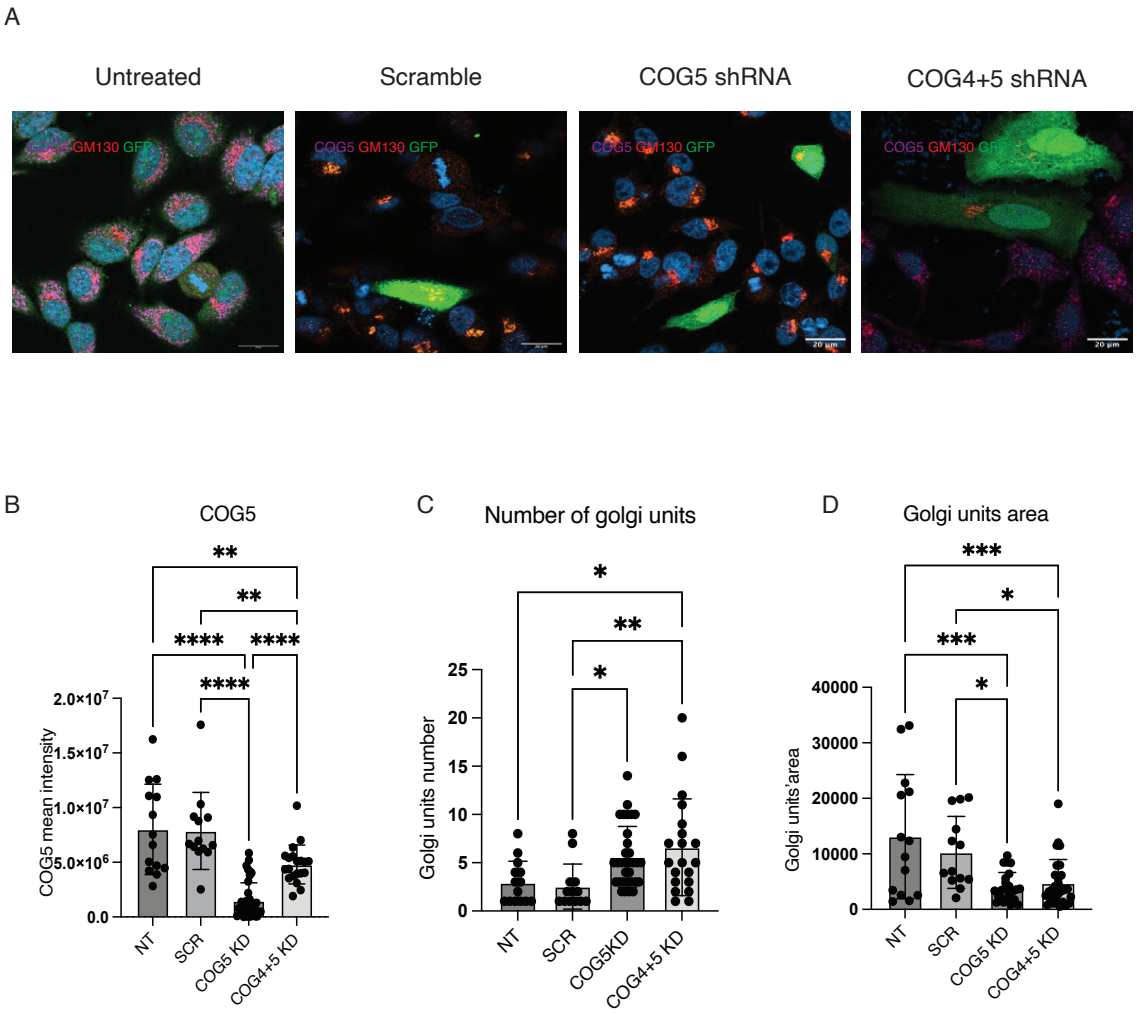


Figure 16. COG5 KD in HeLa cells compromises Golgi integrity.

(A) Validation of shRNA for COG5 and for COG4; the plasmid also contains a GFP cassette thereby transfected cells are GFP+ (green); staining for COG5 (magenta) and GM130 (red) as a Golgi markers was performed. (B) COG5 levels were decreased upon COG5 shRNA-encoding plasmid transfection of HeLa. (B-C) Quantification of Golgi units and Golgi units area performed on GM130 immunofluorescence signal reveals an increase in the number of Golgi units in KD conditions and a decrease in each units area in COG5 and COG4+5 KD HeLa. Scale bar 20μm. One-way ANOVA multiple comparison test. If no comparison shown the test provided not significant value (p>0,005), *: significant p<0,005. N=2, n Control=20, n COG5sh= 44, n COG4+5sh= 8 (N: experimental sessions, n= analyzed cells).

The acute knock-down of COG5 in human brain organoids favours the generation of BPs

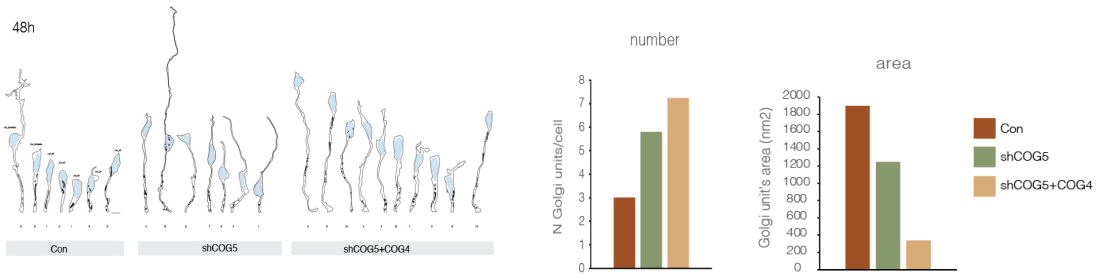
We next examined whether there was an effect of the KD on cell positioning and cell identity. First, 48h after electroporation no significant difference was found in the number of GFP+ cells in the ventricular zone and in the subventricular zone when comparing between the two conditions (Fig. 17B). However, we observed an increase in the distance from the apical surface of electroporated KD cells compared to the scramble 48h (Fig. 17C). These data are compatible with the idea that the GA perturbation can influence the identity and positioning of neural progenitors.

In line with that, Tbr2 staining revealed an increase in the number of Tbr2+/GFP+ cells in the KD condition compared to the control. We also observed an increase in the COG5 KD in Sox2+/ GFP+ cells, but only in the SVZ, while the number of Sox2+/ GFP+ cells in the VZ was not significantly different between control and KD (Fig. 17D).

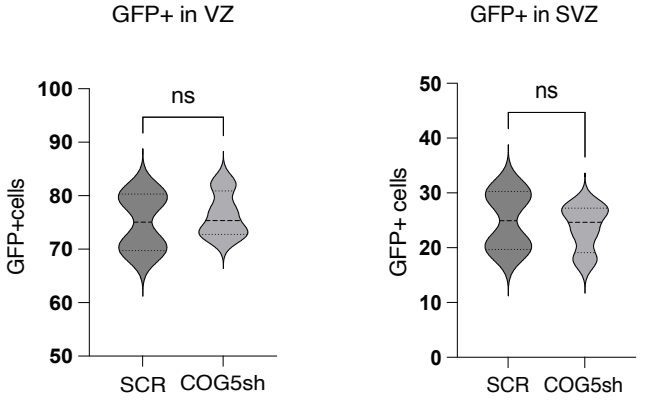
These results suggest that the acute KD of COG5 leads to an increase in IPs and in Sox2+ BPs. The quantification of double positive for Tbr2 and Sox2 revealed a general increase in this double positive population in the COG5 KD, and this trend was observed with no distinctions both in the VZ and in the SVZ.

We then checked the neuronal population 7 days after electroporation by looking at the neuronal population using HuCHuD+ and we observed no difference in the KD compared to the control, suggesting the overall the neuronal population is not affected in terms of number of cells. However, when checking with subtype-specific neuronal markers such as Ctip2, -which stains for layer VI neurons- we found a slight increase in the Ctip2 population in the KD compared to the control (Fig. 17D).

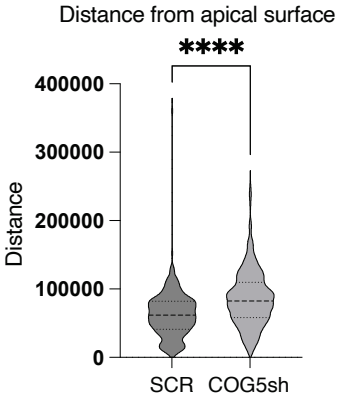
A


48h
Con
shCOG5
shCOG5+COG4
number
N Golgi units/cell
area
Golgi unit's area (nm2)
Con
shCOG5
shCOG5+COG4

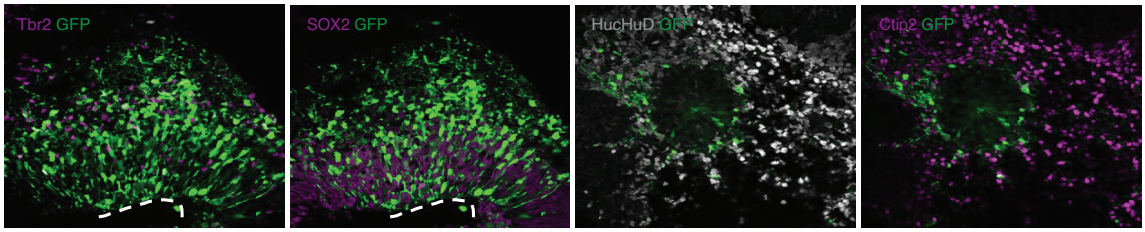
B


GFP+ in VZ
GFP+cells
ns
SCR
COG5sh
GFP+ in SVZ
GFP+ cells
ns
SCR
COG5sh

C


Distance from apical surface
****
Distance
SCR
COG5sh

D


Tbr2 GFP
SOX2 GFP
HucHuD GFP
Ctip2 GFP

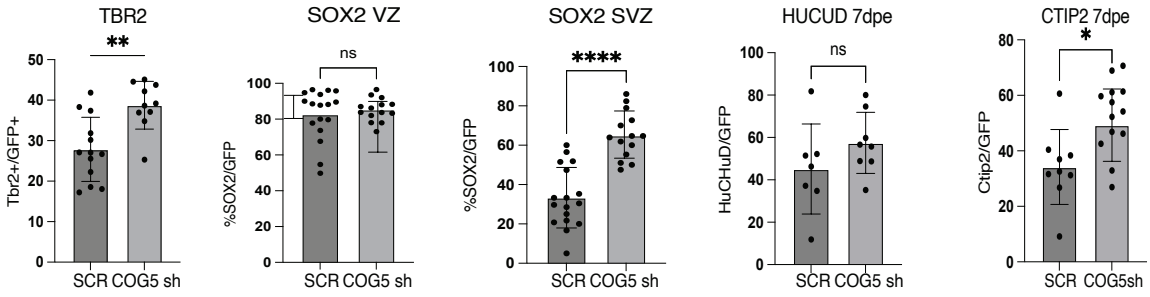

TBR2
**
Tbr2+/GFP+
SCR COG5 sh
SOX2 VZ
ns
%SOX2/GFP
SCR COG5 sh
SOX2 SVZ
****
%SOX2/GFP
SCR COG5 sh
HUCUD 7dpe
ns
HuCHuD/GFP
SCR COG5 sh
CTIP2 7dpe
*
Ctip2/GFP
SCR COG5sh

Figure 17. Knock down of COG5 in human brain organoids affects the integrity of Golgi apparatus and affects developmental trajectories.

(A) COG5 and COG4 shRNA-encoding plasmids were electroporated in ventricles of human brain organoids at d40. Reconstruction of electroporated APs and their GA in human brain organoids was done by co staining GFP+ cells with GM130; quantification of Goli units number and area. Test one-way ANOVA. (B) Quantification of GFP+ electroporated cells partitioning between VZ and SVZ. (C) Quantification of electroporated GFP+ cells distance from the apical surface. (D) Staining for Sox2 (magenta), Tbr2 (magenta), HuCHuD (grey) and Ctip2 (magenta) (respectively APs, BPs and neurons) shows an increase in BPs and Ctip2+ neurons in COG5 KD compared to the control. SOX2+ cells were quantified distinguishing between VZ and SVZ. Scale bar 20μm. Student's t test. ns: not significant p>0,005, *: significant p<0,005. N= 3 and n=3 (N= organoids batches, n= organoids/batch/condition

Finally, we also checked whether the number of cycling cells was affected by the COG5 knock down by staining for Ki67, which marked cycling cells, and EdU labeling to mark cells in S phase. We did not observe any difference between the KD and the control (Fig. 18). This observation is in line with our hypothesis that the perturbation of COG5 and of the Golgi Apparatus integrity, affects the cell identity and cell fate possible by influencing cells that are already committed to cell division, as observed previously for the lineage progression experiment after the acute disassembly of the Golgi apparatus.

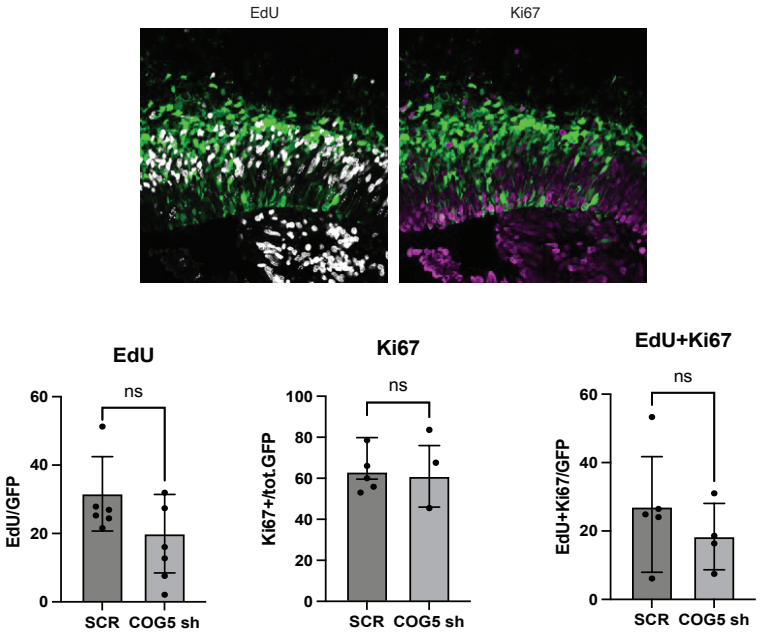


Figure 18. COG5 KD does not affect the number of cycling cells.

Electroporation of COG5 shRNA (green cells) and staining for cells in S-phase (EdU, grey) and cycling cells (Ki67, magenta) reveals that COG5 KD does not affect cycling cells across all phases of cell cycle. Scale bar 20μm. Student's t test. ns: not significant p>0,005, *: significant p<0,005. N= 3 and n=3 (N= organoids batches; n= organoids/batch/condition.

Modeling the neurodevelopmental manifestations of COG5-CDG using human brain organoids

Few CDG patients with COG5 mutation have been previously described in literature to date, making COG5-CDG an ultra-rare CDG. These patients harbor one or multiple homozygous mutations that ultimately cause impairments in COG5 function. The clinical manifestations are heterogeneous as the severity of the disease depends on the effect of the mutation on the protein structure and function. Despite this heterogeneity, most of the reported patients display clinical defects on the brain, both on the organ development and functionality, with a plethora of pathological manifestations spanning from microcephaly, to brain atrophy and intellectual disabilities.

Identification of two COG5-CDG patients harboring new COG5 mutations

In collaboration with the group of Prof. François Foulquier at the University of Lille we obtained fibroblasts from two siblings, a male and a female, with a novel mutation on COG5 that has not been previously described. The mutation was discovered by WGS by clinicians in the CHU of Montpellier and the two patients have been diagnosed with multiple multi organ symptoms associated with microcephaly, deafness, cerebellar atrophy, optic atrophy, intellectual impairments and liver, spleen and bones related diseases.

The homozygous mutation as been described as NM_006348.3:c.632-33909T>A p. ? (hg38), and an RT-PCR on the two patients lymphocytes revealed the presence of a frameshift mutation (NM_006348.3(COG5):p.(Asp211Valfs*12) caused by a complete or partial retention of intron 6 between exon 6 and exon 7, ultimately leading to a premature stop codon (Fig. 19A).

As a first experimental assessment our collaborators performed a BFA assay on patients' fibroblasts (Fig. 19B). BFA assay is widely used to reveal Golgi-related defects, as it amplifies any impairment in the dynamics of Golgi fragmentation and reassembly. Indeed, as observed in Fig. 19C the Golgi apparatus took longer to get fragmented in the two siblings fibroblasts compared to the fibroblasts obtained from the healthy heterozygous mother, with the female fibroblasts showing an even more prominent delay compared to the brother cells.

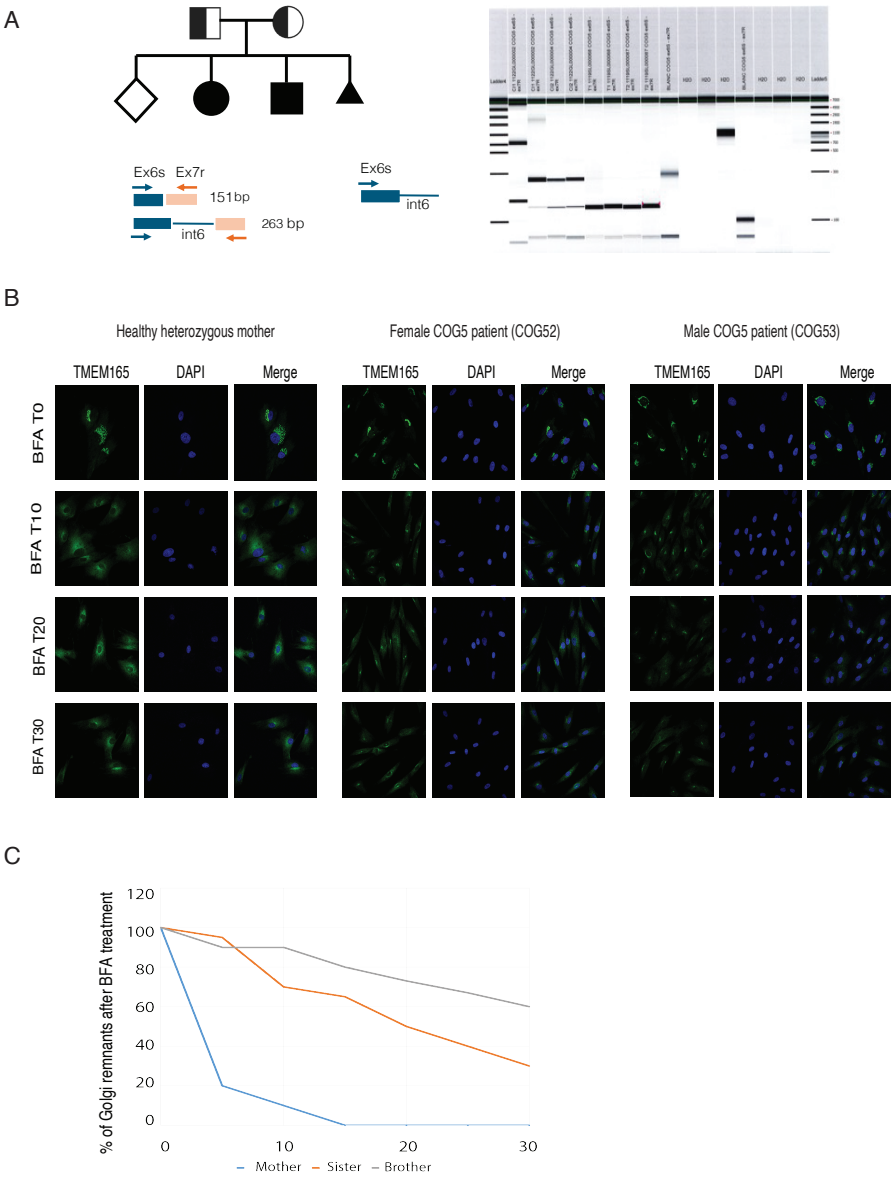


Figure 19. Characterization of a novel COG5 mutation in two CDG patients.

(A) Pedigree diagram describing the COG5 CDG patients two siblings, a male and a female, harboring COG5 mutation in homozygosity, and two healthy heterozygous parents. Electrophoresis gel of COG5 RNA product showing that the mutation causes the retention of intron 6 between exon 6 and exon 7 of COG5 gene. (B) BFA treatment on the two patients fibroblasts and on the fibroblasts of their healthy mother reveal a delayed Golgi fragmentation in the two siblings. TMEM165 (green) stains Golgi apparatus, DAPI (blue) stains fibroblasts nucleus. Data obtained from our collaborators from the University of Lille.

We compared the structure of Golgi apparatus in patients fibroblasts (COG2: female patient, COG53: male patient) and in commercial control fibroblasts by staining for GM130 (Fig. 20A). Interestingly, although the number of Golgi units is the same in control and the patients samples (Fig. 20B), the area of each Golgi unit was slightly decreased in the male patient compared to the control (Fig. 20C), suggesting that at the steady state the mutation does not cause a massive fragmentation of the GA. However, when checking the overall structure of the Golgi apparatus some changes can be observed, with Golgi apparatus appearing more compacted, especially in the male patient. Further studies by electron microscopy could be useful to dissect subtle structural differences in the patients Golgi compared to a control line or even with their healthy mother fibroblasts.
The fibroblasts were reprogrammed to iPSCs by the GEDI facility at Human Technopole. The iPSCs were subjected to extensive quality check, including genome stability and the ability to generate all three germ layers, and only those that pass all quality controls were used for experiments.
The iPSCs identifiers were labeled as COG52 for the female patient and COG53 for the male patient and they were used to obtain human brain organoids.

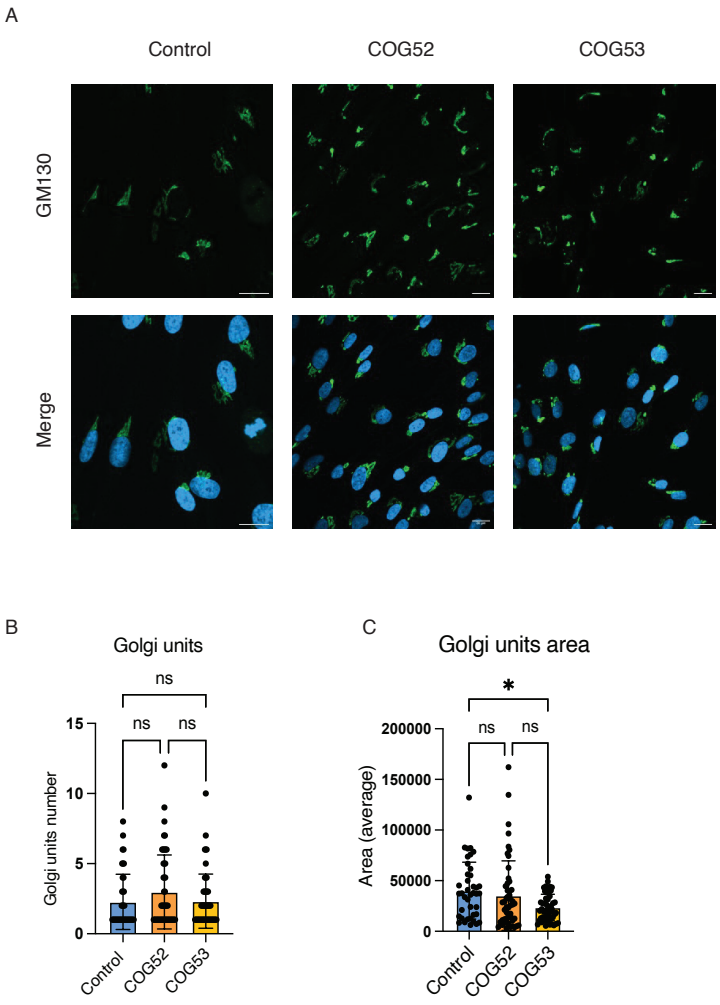


Figure 20. COG5 mutation affects the structure of Golgi apparatus.

(A) GM130 staining (green) of fibroblasts from the two patients and from a control line reveal structural alterations on Golgi apparatus. (B-C) Golgi units and area quantifications reveal only minor differences between the patients and the control. Scale bar 20μm. One-way ANOVA test. ns: not significant p>0,005; *: significant p<0,005. N= 2, n control =40, n COG52= 51, n COG53= 50 (N: fibroblasts preparations, n: cells analyzed/condition). COG52: female patient. COG53: male patient. Control: human commercial fibroblasts.

COG5-CDG human brain organoids reveal defects in the COG complex

We grew brain organoids and performed a western blot analysis on the total lysate to check whether the mutation affected the protein levels beside the observed effect on the mRNA (Fig. 21). Indeed, we observed a strong reduction of COG5 protein in the brain organoids grown from the two patients. Interestingly small levels of the COG5 protein are still present, possibly due to the fact that some mRNA is still correctly spliced. Instead in our COG5 knock out brain organoid model the protein is completely absent as expected.
We next wondered whether the mutation could affect a site of interaction with other COG subunits, leading to an effect on other COGs. Notably COG4 and COG7 have been described to interact with COG5, so we performed a western blot on the brain organoids lysate and compared controls, the two patients and the KO. Though no massive difference in the amount of COG4 proteins was detected, COG7 protein levels were strongly reduced in the two patients and in the COG5 KO. Of note, COG5 and COG7 belong to the LobeB COG complex, while COG4 belongs to LobeA. Our data suggest that the mutation influences the interaction between the Lobe B COG5 and COG7 and when COG5 is mutated or completely absent, as in the case of the KO, COG7 dynamics are also affected, possibly by increased degradation of the subunit (or of the Lobe) that is not correctly bound to its COG5 interactor.

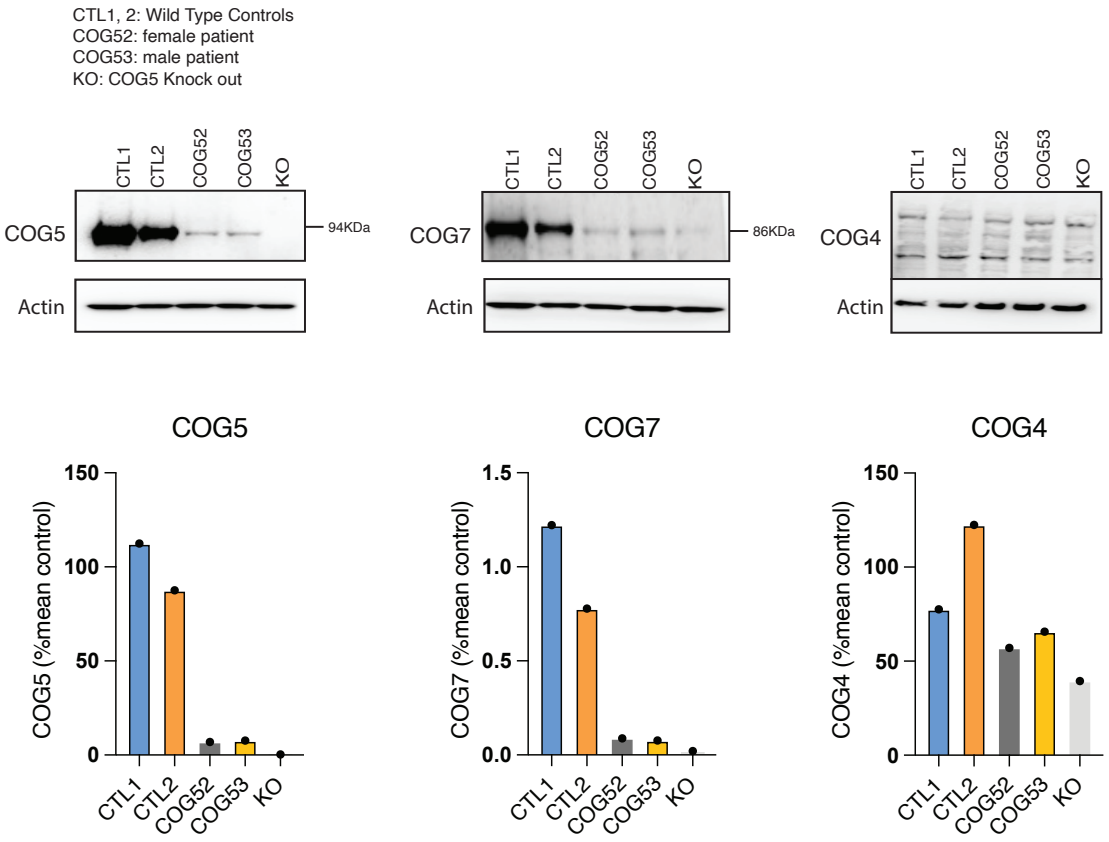


Figure 21. COG5 mutation decreases COG5 and COG7 protein levels.

Western blot on human brain organoids and band volume quantification reveal lower levels of COG5 protein in both COG52 and COG53 and complete absence of the protein on the KO condition compared to the two controls (WTC11 and HMGU1). Lower levels of COG7 protein are also observed to be decreased in the patients and in the KO. COG4 protein levels are only slightly decreased in the KO. Band volumes were normalized over actin. N=1, n= 3/condition (N: organoids batch, n: organoids/condition). COG52: female patient; COG53: male patient; KO: Knock out WTC11 line; WTC11, HMGU1: wt controls.

COG5-CDG mutations affect GA architecture in apical progenitors

To gain insights into the effects of the COG5 mutation on brain development, we grew human brain organoids from patients iPSCs (COG52 and COG53) and COG5 KO iPSC line and we determined the structure of GA in apical progenitors. To do so we electroporated the organoids at d40 with pCAGGS-GFP plasmid, we stained for GM130 and we reconstructed single apical progenitor cells using an image analysis program (Fig. 22A). We observed an increase in the number of Golgi units in both patients and in the KO (Fig. 22B). Consistently, in both patients and in the KO condition there was a remarkable decrease in the area of each Golgi unit (Fig. 22C). These results suggest that the mutation as well as the complete lack of COG5 impairs the structure of the Golgi Apparatus of apical progenitors by inducing GA fragmentation and/or by affecting the integrity and structure of Golgi stacks in the apical process of apical progenitors.

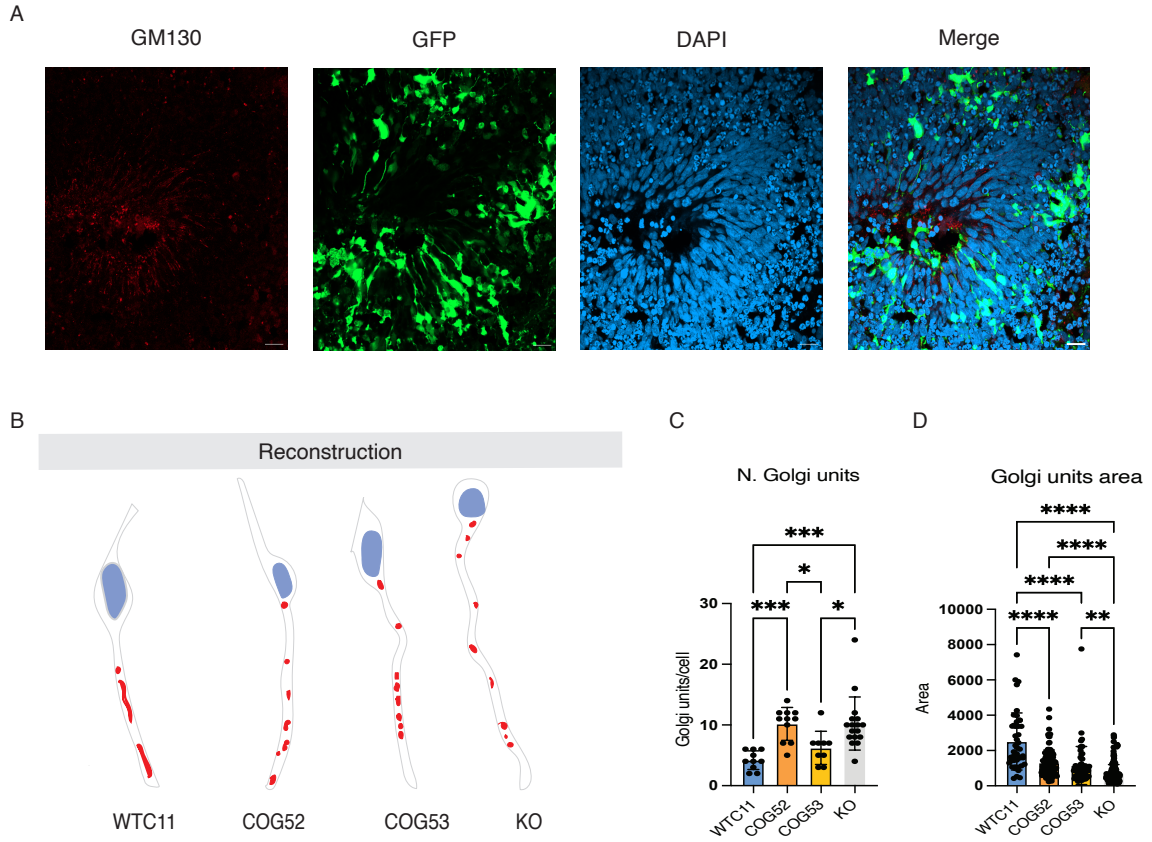


Figure 22. Golgi apparatus structural integrity is affected by COG5 mutation and COG5 KO.

(A-B) d40 Human brain organoids were electroporated (A) and staining for GM130 (red) was done to reconstruct single apical progenitor cells and their GA (red), nucleus (blue), cell contour (grey). (C) Quantification of the number of Golgi units and (D) the Golgi area. N=3 n=3. One-way ANOVA test, if no line was shown: not significant p>0,005; *: significant p<0,005. N= 2 and n=41 (N: organoid batches, n: total analyzed apical progenitor cells across conditions). COG52: female patient; COG53: male patient; KO: Knock out WTC11 line; WTC11: wt controls.

Brain organoids from COG5-CDG patients show impaired growth and general architecture

Then we examined how and if this impairment in Golgi apparatus structure affects brain organoid development. It has been reported by clinicians that the two patients have a microcephaly phenotype, caused by the COG5 mutation. Furthermore, several reports in literature show that patients with COG5 mutations or Golgi apparatus related diseases (Golgipathies), have severe clinical neurological defects, with primary and secondary microcephaly. Primary Microcephaly (PM) refers to a smaller brain at birth, and is typically caused by impairments in the correct sequence and timing of appearance of NPCs or by increased neuronal cell death. To understand whether the microcephaly observed in the patients could be recapitulated with our model system, we quantified the size of the

organoids by measuring their area at d40 and we observed a decrease in the area of the brain organoids in both patients (COG52 and COG53) compared to the two control lines WTC11 and HMGU1, and also when comparing between the KO and the controls (Fig. 23A, B). The smaller organoids size in COG5-CDG and COG5 KO suggest that indeed partial or complete lack of COG5 protein affects the correct development of the brain organoids.
We then assessed whether the structural composition of the brain organoids was affected, by measuring the number of ventricles within each organoid; also in this case we observed a decreased number of ventricles in the two patients and in the KO line in respect to the controls (Fig. 23C). Of note, the area of the ventricles and the apical length show no differences between the patients and the controls, while KO organoids have an increased area and ventricular apical length compared to all the other conditions (Fig. 23D, E). In general, our data show that the size of the organoid and the number of ventricles per each organoid differs between the controls and the mutated conditions. In addition, the analysis of COG5 KO suggests an interesting role of the COG5 protein in determining brain development and organoid growth, with different effects caused by differences in the protein levels.

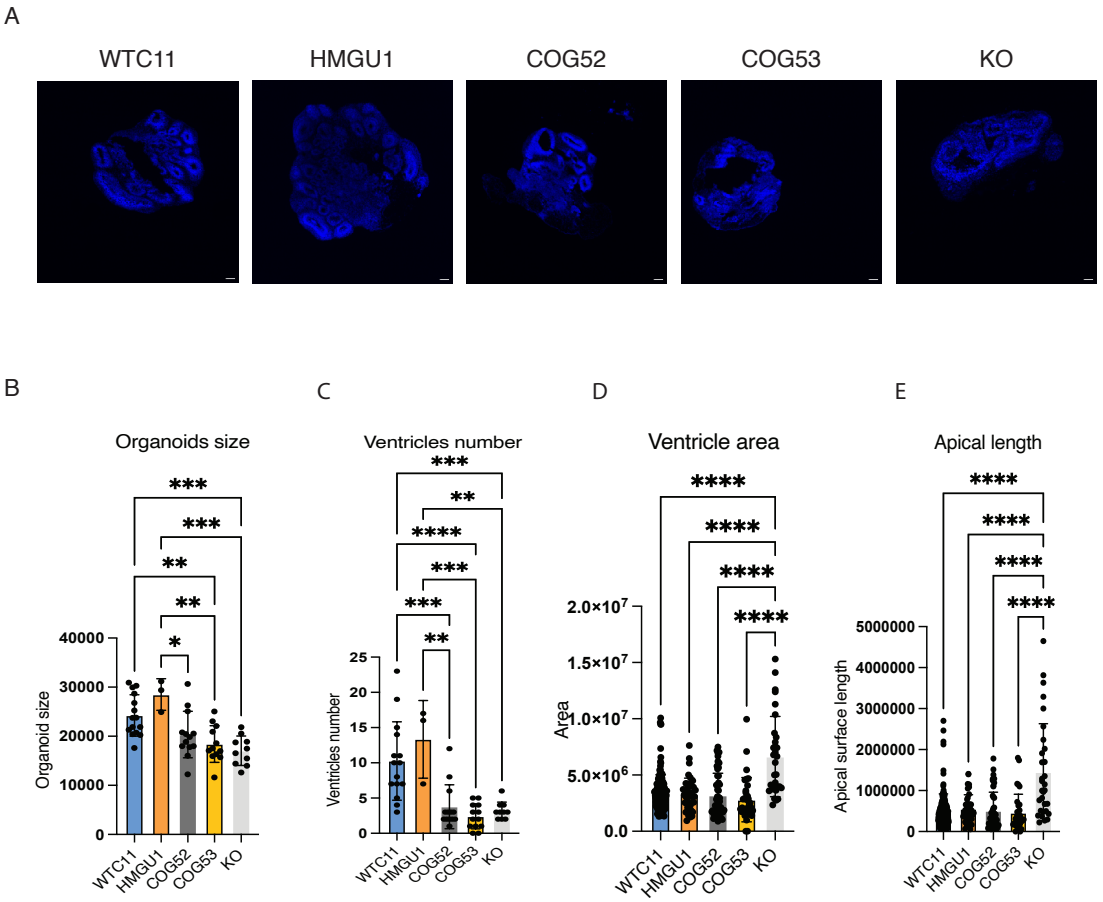


Figure 23. Human brain organoids recapitulate the microcephalic phenotype of the two patients.

(A) DAPI staining (blue) on d40 human brain organoids. Scale bar 200μm. (B-C) Quantification of organoid area, ventricles number, area and apical length. (N=3, n=39) (D-E) The ventricle area and the apical length were increased in the KO organoids. One-way ANOVA test. if no line was shown: not significant p>0,005; *: significant p<0,005.N: organoids batches, n: total organoids across conditions. COG52: female patient; COG53: male patient; KO: Knock out WTC11 line; WTC11, HMGU1: wt controls.

Brain organoids from COG5-CDG patients show altered progenitors' composition

We then sought to define progenitors' composition in human brain organoids (Fig. 24A). We focused on d40 and we observed that though the number of Sox2+ cells was not affected in the two patients nor in the KO compared to the control, there were differences in the intermediate progenitor population: whereas in the two patients the number of Tbr2+ cells were decreased, in the KO a significant increase in Tbr2+ intermediate progenitors was observed. (Fig. 24B)

We then examined the effect on the neuronal population by staining for HuCHuD and we observed a small decrease in neurons only in the male patient (Fig. 24B). This was also reflected by the decrease in the cortical plate (CP) thickness (Fig. 24C). When we stained for the layer VI-specific marker Ctip2 +, we observed a huge drop in this neuronal population especially in the male patient (COG53), but not in the other conditions (Fig. 24B).

We next wondered whether these differences in IPs and Ctip2+ neurons abundance could be explained by differences in timing of maturation of the organoids, and we performed the immunostaining at three different timepoints d20, d40 and d60. Whereas for Sox2+ cells and HuCHuD neurons the trend was similar across the four conditions, for Tbr2 and Ctip2 cells we observed a lower slope indicating a delayed appearance of these NPCs and neurons in the two patients compared to the control (Fig. 24C).

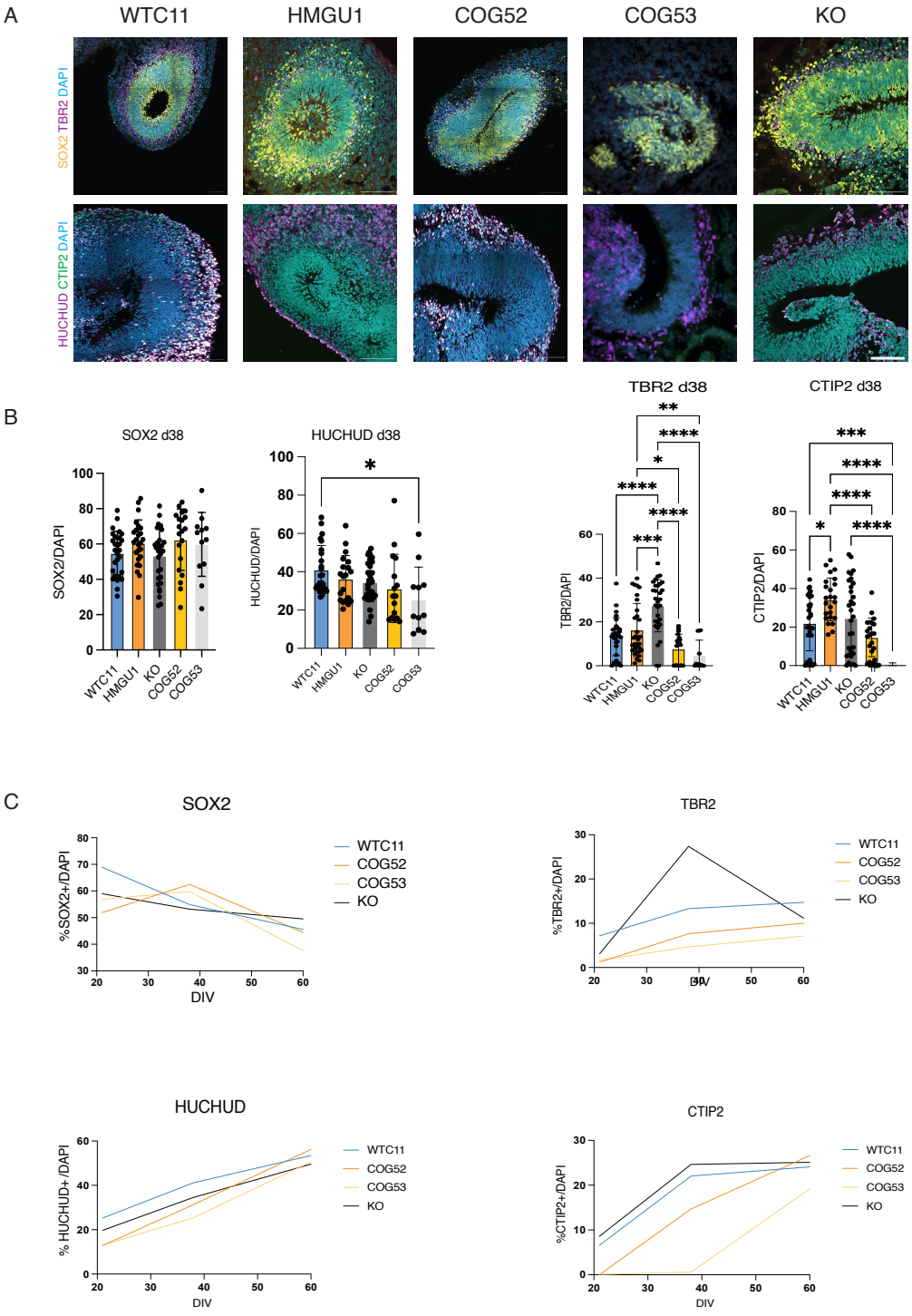


Figure 24. COG5 mutation and KO differentially impair brain development by altering progenitors and neurons composition.

(A) d38 brain organoids were stained for Sox2 (yellow), Tbr2 (magenta), HuCHuD (magenta) and CTIP2 (green) as fate markers. Scale bar 20µm. (B) Quantification of SOX2+ cells and HuCHuD+ cells in d38 brain organoids. (C) Quantification of Tbr2+ BPs and Ctip2+ neurons in d38 brain organoids. (C) Time-course analysis of fate markers in d21, d38 and d60 brain organoids. One-way ANOVA test, if no line was shown: not significant p>0,005; *: significant p<0,005. N=3, n=3(N= organoids batch, n= organoids/batch/condition). COG52: female patient; COG53: male patient; KO: Knock out WTC11 line; WTC11, HMGU1: wt controls.

To understand if the architecture of the ventricles was changed, along with changes in the populating cell types we measured the total thickness of the ventricle, from the apical surface to the basal lamina, and we also quantified the thickness of the neuronal layer and of the ventricular zone across timepoints. We observed that the total thickness of the ventricle was decreased at d38 (Fig. 25A), corresponding to the mid neurogenesis stage in our organoid model, paralleled by a decrease in the thickness of the ventricular zone between the WTC11 wt and the COG53 patient, but not the COG52 (Fig. 25B). The fact that Sox2+ cells don't reflect this change in the thickness is not surprising, as Sox2 is not specific marker for APs as it is also expressed in bRGs populating the SVZ. These data further suggest that patient organoids display a slower maturation compared to the control counterpart and that d38 is a critical timepoint for GA to have an influence on brain development. On the other hand, by analyzing specifically the neuronal layer (NL), we saw a global decrease in the NL thickness across all timepoints (Fig. 25C). This quantification reflects the global effect of the mutation on the neuronal population, that can't be efficiently recapitulated by the HuCHuD staining alone. It is possible that the mutation, by influencing the switch from AP to BP also, directly or indirectly, impairs the differentiation of neurons. However, when quantifying the direct neurogenesis, by measuring the number of HuCHuD+ cells in the VZ, we didn't observe any differences among all the conditions, suggesting that the effect of the mutation is strongly affecting the indirect neuronal developmental trajectory. The decreased NL thickness could be linked to increased cell death of neurons. However, when looking at the DAPI staining to identify pycnotic nuclei, we did not observe a massive increase in apoptotic cells within the putative cortical plate.

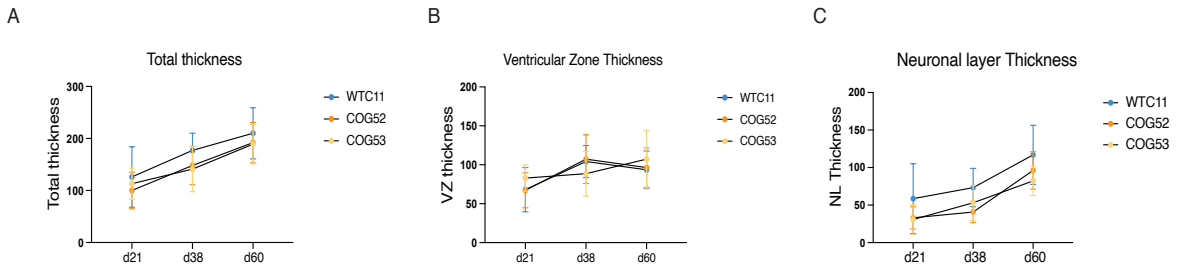


Figure 25. COG5 mutation decreases the thickness of the ventricular area and of the neuronal layer in brain organoids.

(A-B) In both patients a decreased overall thickness and a decreased thickness of the ventricular zone was observed at d38. (C) The neuronal layer thickness was decreased in the two patients across all the timepoints. One-way ANOVA test, significant differences($p<0,005$) were observed at d38 for the total thickness and Ventricular zone thickness, in a comparison between COG52, 53 and WT. $p<0.005$ was also observed across all timepoints for the neuronal layer thickness comparing between patients and wt control. N=3, n=3(N= organoids batch, n= organoids/batch/condition. N=3, n=3 (N: organoid batches, n: organoids stained/batch/condition/timepoint). COG52: female patient; COG53: male patient; WTC11: wt control.

We finally checked if the mutation on COG5 could affect cell cycle by staining for Ki67 and EdU and interestingly we observed a significant effect only in the KO, where more cells were observed in the cell cycle especially in S phase (Fig. 26).
Overall these data suggest that in the two patients, impairments in Golgi apparatus structure, caused by COG5 mutation, change the way the brain organoids mature, in particular causing a strong delay in the male patients who, showed a strong decrease in the area of each Golgi unit, though not accompanied by an increase or decrease in their number.
The female patient (COG52) instead showed a less severe phenotype in terms of brain organoid growth and development, though a stronger effect was observed on the structure of Golgi apparatus of apical progenitors. Interestingly the complete lack of COG5 protein in the KO lead to specific effect on the intermediate progenitor population, without affecting any other cell type, despite the strongest disruption of Golgi apparatus. Of note, these data specifically point to the idea that the effects of COG5-CDG mutations and the one of the full KO are principally different, adding more complexity to the overall brain phenotype linked to dysregulation of COG5 protein function.

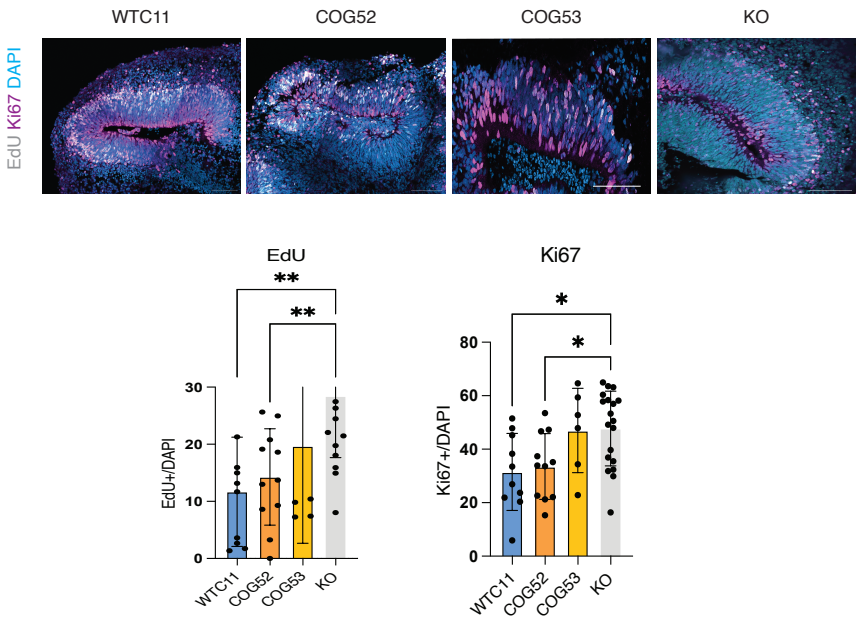


Figure 26. COG5 KO alters the number of cycling cells.

EdU and Ki67 staining revealed an increase in the number of cycling cells (Ki67+, magenta) and of cells in S-phase (EdU+, grey) at d38. One-way ANOVA test, if no line was shown: not significant p>0,005; *: significant p<0,005. N=3, n=3 (N= organoids batch, n= organoids/batch/condition). COG52: female patient; COG53: male patient; KO: Knock out WTC11 line; WTC11: wt control.

COG5-CDG alters the mode of division of apical progenitors

In a first attempt to find a mechanistic explanation underlying the obtained results on the role of COG5 in brain development, we wondered whether COG5 protein impairment, and as such Golgi apparatus defects, could influence cell division mode. Indeed, division plane of mitotic cells influence the fate of the two daughter cells, by allowing a symmetric/asymmetric partitioning of cell fate determinants and also of the organelles inherited from the mother cell (Kosodo et al. 2011; Ayala and Colanzi 2017). We wondered whether the observations we obtained on the influence of COG5 mutation on cell fate could be explained by how daughter cells were dividing and inheriting determinants from the mother cell.

We stained for phalloidin, pan cadherin and DAPI to be able to reconstruct single mitotic cells at the apical surface. We reconstructed the division plane using a horizontal, vertical or diagonal cleavage angle by measuring the angle of division of mitotic cells in respect to the apical surface. We found that whereas in the WTC11 control organoids there was a more homogeneous distribution among all the possible division planes (27% horizontal, 31% diagonal, 41% vertical) in the two patients and in the KO most of the divisions show a vertical or diagonal angle, while a smaller percentage of cells were dividing horizontally (10% for the COG52, 11% for COG53 and 12% for the KO line). Though COG52 and the KO displayed more similar proportionality between vertical and diagonal division plane, in the male COG53 patient half of the divisions were happening through a diagonal division plane (Fig. 27). Furthermore in both mutants and in the KO condition there is an increase in the usage of diagonal cleavage plane, when comparing with the WTC11 control organoids. These observations could partially explain why in the male COG53 patients the overall number of SOX2+ cells is not changed compared to the control and why less Tbr2+ IPs and Ctip2+ neurons are produced. However, it is interesting to notice that in the KO line the trend in Tbr2+ intermediate progenitors is the opposite compared to the COG53 patient, despite the similarity in the differences in cell division mode. This could suggest that the dosage-dependent role of COG5 in brain development goes beyond the simple influence on cell division mode of apical progenitors. Finally, diagonal cleavage plane has been described to lead to different potential division outcomes, producing either symmetric divisions or asymmetric divisions, explaining the diversified effects on cellular identities that we observed across all of the conditions.

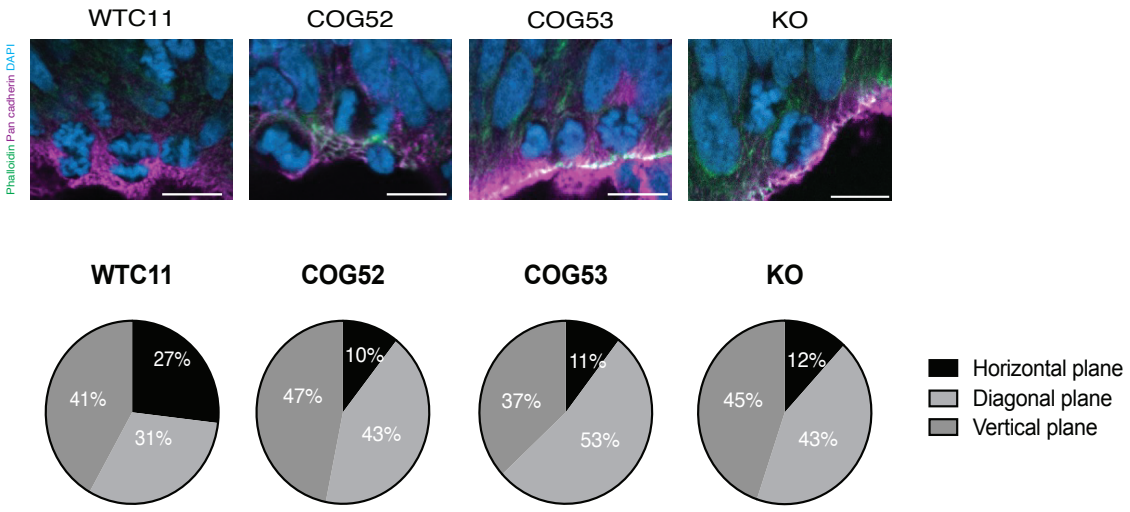


Figure 27. COG5 mutation affects the cell division plane in apical progenitor cells.

Quantification of the angle of division of mitotic apical progenitor cells at the apical surface reveals a decrease in horizontal cleavage plane (black) and an increase in vertical plane of division (dark grey) in both patients and in the KO condition. Diagonal division planes are represented in grey. Percentages of division for each angle are indicated. N= 3, n WTC11= 67, n COG52= 47, n COG53= 38, n KO= 67. (N: organoid batches, n: mitotic cells quantified). COG52: female patient; COG53: male patient; KO: Knock out WTC11 line; WTC11: wt control.

The analysis of scRNAseq transcriptional make up reveals premature switch to neuron generation

To gain insight into the transcriptomic signature of the cellular alterations underlying the changes in fate markers that we observe in COG5 mutant patients, we performed single cell RNA sequencing (scRNA-seq) on d38 cortical organoids. We sequenced 24 WTC11 (WT), 24 COG52 and 24 COG53 organoids from 3 different batches and obtained respectively 13185,13549 and 11330 cells (calculated as the average value considering the three biological replicates for each condition), that passed all the quality control steps. Leiden clustering revealed 5 principal clusters pertinent to human mid neurogenesis (cluster 5 for APs, cluster 7 for BPs and clusters 6,8,9 for neurons) and few minor clusters of other cell types.

Cluster 5 was enriched of SOX2 and PAX6 cells indicative of apical radial glia cells, whereas cluster 7 was enriched of both basal progenitors described by EOMES and interestingly also BCL11B (or CTIP2) and Tbr1 neurons, suggesting that in our organoids this cluster groups both BPs and their immediate neuronal progeny. Clusters 6, 8 and 9 instead, more specifically grouped most of the neuronal subtypes observed by expression of markers such as migrating DCX neurons and upper layer CUX1 and Satb2 neurons (Figure 28).

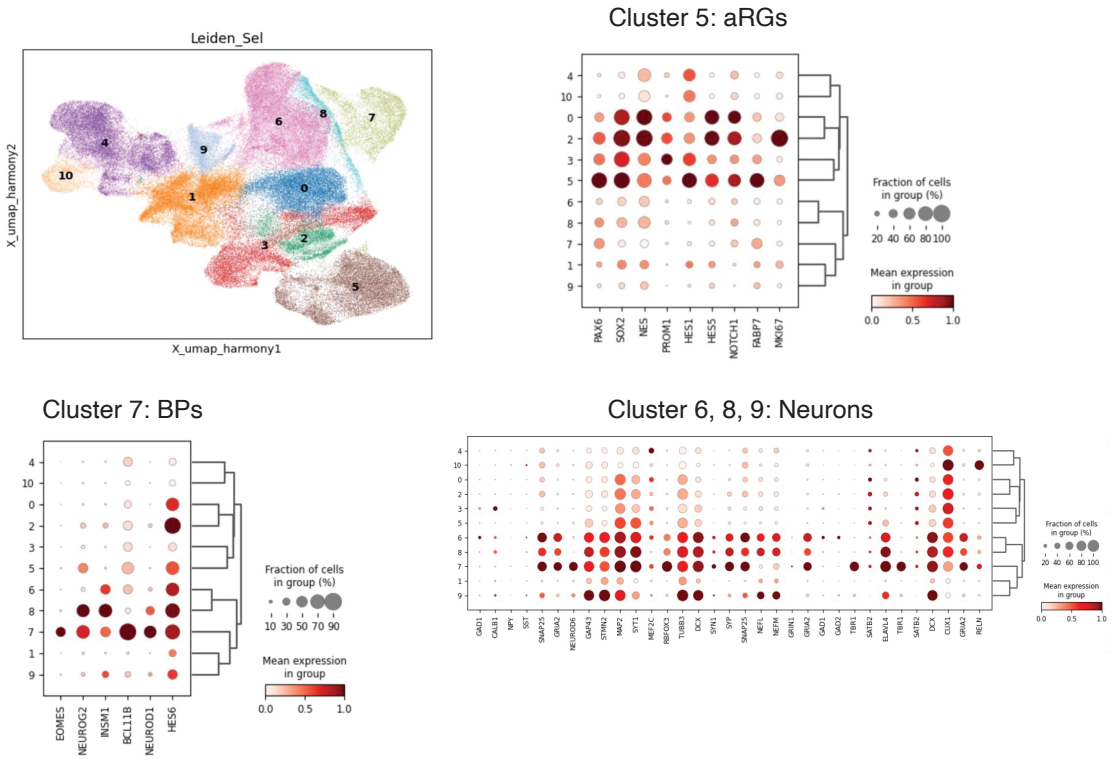


Figure 28. Identification of NPCs and neuronal clusters with scRNA seq analysis of patient derived human brain organoids.

Leiden clustering reveals clusters of APs, BPs and neurons (respectively cluster 5, 7 and 6-8-9).

To quantify consistent changes in cell composition across all biological replicates sample, differential abundance analysis was performed and revealed specific neighbourhood patterns that differed between the two patients. A total of 6487 neighbourhoods were identified, and Milo method was used to compute the variation in cell numbers between replicated for the same experimental condition to test for differential abundance. Comparison between COG53 and WT revealed a low log-Fold change (logFC<2) corresponding to the clusters of aRGs (cluster 5, Fig. 29A,B, C) and BPs (cluster 7, Fig. 29A, B, D); while for neuronal clusters most of the neighbourhoods were depleted suggesting a general reduction in neuronal abundance, in cluster 6 and 9, 34 and 2 neighbourhoods respectively had a logFC>2 showing an enrichment compared to the WT (Fig.29A, B, E).

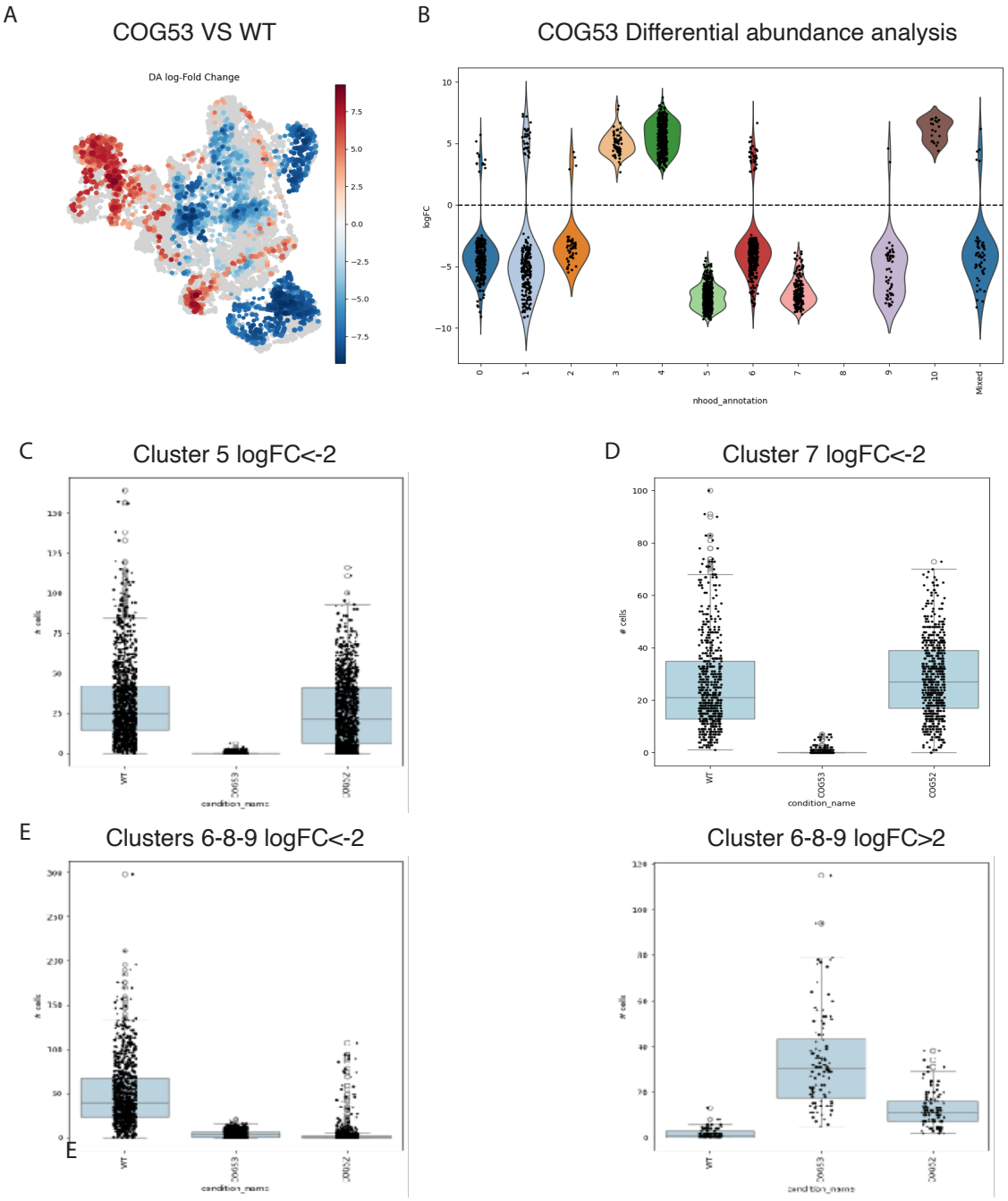
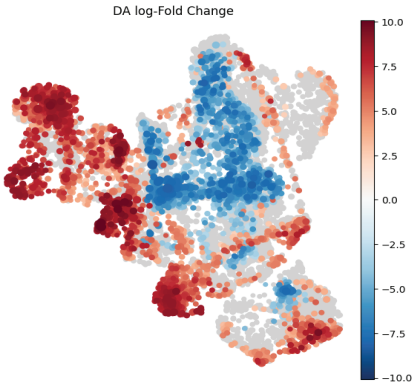


Figure 29. COG5 mutation reduces NPCs in the COG53 patient.

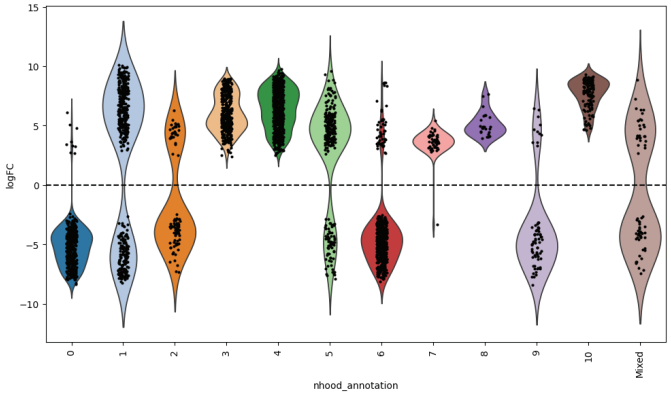
(A) Differential abundance analysis on scRNAseq brain organoids grown from COG53 male patient iPSCs reveals depletion on almost all cell types (APs, BPs, neurons) compared to the WT. (B-D) A decrease in both cluster 5 and cluster 7 related neighbourhoods. A negative logFC was observed for both cluster indicating a depletion of these cell types. (B,E) Neuronal clusters 6-8-9 show a dual feature whereby some neighbourhoods are depleted (logFC<-2) and few are enriched compared to the control. A positive log Fold change (LogFC>2) indicates enrichment of neighbourhoods and negative logFC (logFC<-2) indicates a depletion of neighbourhoods. Adjusted p value < 0.05. COG53: male patient; WT: WTC11 wild type control.

Considering COG52 patient in respect to the WT a partial enrichment of neighbourhoods corresponding to cluster 5 (207 neighbourhoods, Fig. 30A,B, C) and 7 (50 neighbourhoods, Fig. 30A,B,D) was observed, with few neighbourhoods being still depleted for cluster 5. The neuronal clusters mostly showed mixed behaviour, with cluster 6 and 9 showing both enriched and depleted neighbourhoods and cluster 8 only showing an enrichment (Fig. 30A,B, E).

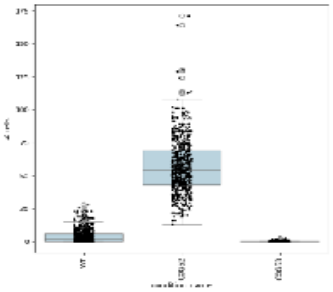
A

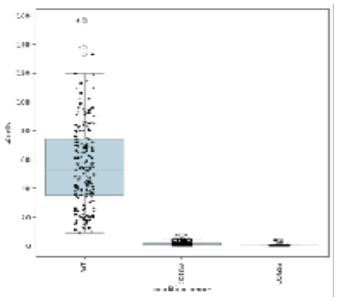

COG52 VS WT
DA log-Fold Change
10.0
7.5
5.0
2.5
0.0
−2.5
−5.0
−7.5
−10.0

B

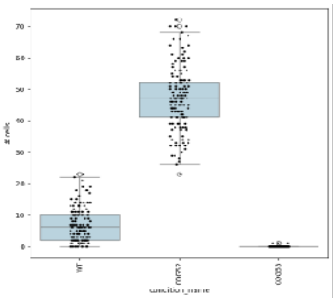

COG52 Differential abundance analysis
logFC
nhood_annotation
Mixed

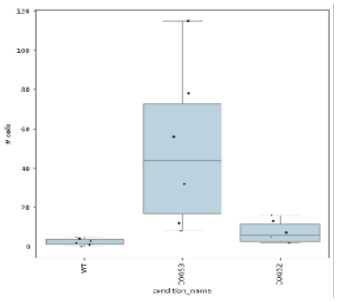
C


Cluster 5 logFC>2

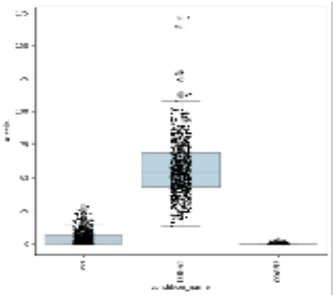

Cluster 5 logFC<-2

D


Cluster 7 logFC>2


Cluster 7 logFC<-2

E


Cluster 6-8-9 logFC>2

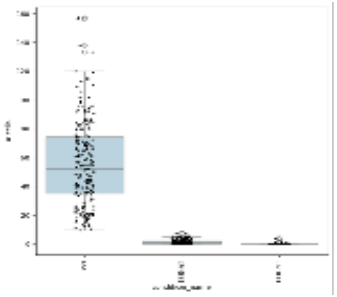

Cluster 6-8-9 logFC<-2

Figure 30. COG5 mutation affects both NPCs and neurons in COG52 female patient.

(A) Differential abundance analysis on scRNAseq brain organoids grown from COG52 female patient iPSCs reveals an enrichment in some neighbourhoods within cluster 5 and cluster 7, while neuronal clusters (6-8-9) are overall depleted (B-C) An enrichment in AP cluster 5, compared to the WT control, was observed, along with a depletion on some of the neighbourhoods within the same cluster. (B-D) Cluster 7 neighbourhoods were found to be mostly enriched in COG52 patient compared to the WT control. (B-E) Neuronal clusters 6-8-9 show a dual feature whereby some neighbourhoods are depleted (logFC<-2) and few are enriched compared to the control. A positive log Fold change (LogFC>2) indicates enrichment of neighbourhoods and negative logFC (logFC<-2) indicates a depletion of neighbourhoods. Adjusted p value < 0.05. COG52: female patient; WT: WTC11 wild type control.

Inter patient comparison revealed an overall lower abundance of all cluster types in the male COG53 patient compared to the female COG52, in line with our experimental data on fate markers and overall structure of the organoids (Fig. 31A-E).

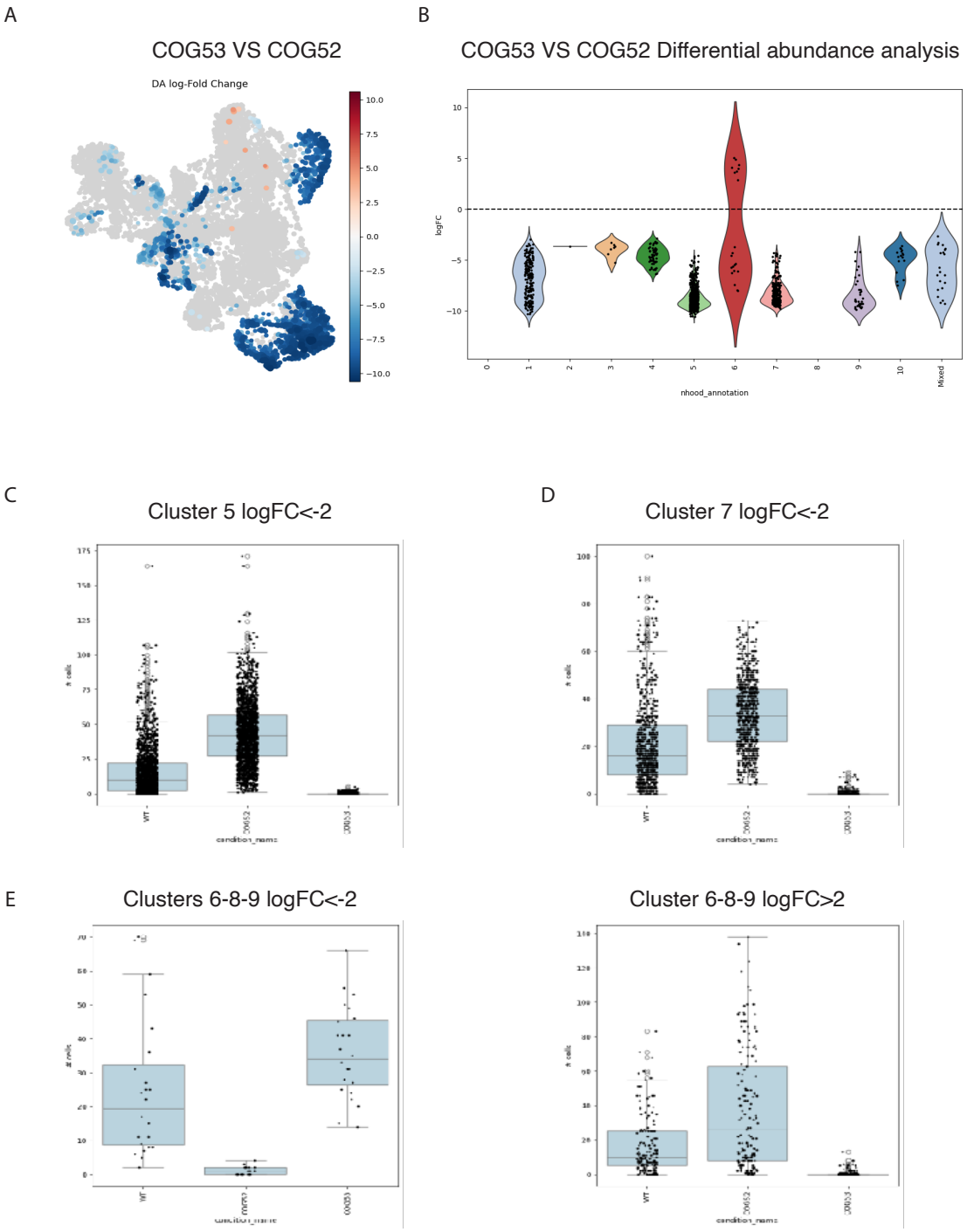


Figure 31. Differential abundance analysis reveals an overall depletion of all NPCs related cell clusters in a comparison between COG53 and COG52.

(A-D) Cluster 5 and 7 neighbourhoods are depleted in the male COG53 patient compared to the sister COG52. (A, E) Few neuronal-related neighbourhoods are enriched in the neuronal clusters. A positive log Fold change (LogFC>2) indicates enrichment of neighbourhoods and negative logFC (logFC<-2) indicates a depletion of neighbourhoods. Adjusted p value < 0.05. COG52: female patient; COG53: male patient; WT: WTC11 wild type control.

To gain transcriptomic insights into the cellular mechanisms and pathways underlying the effects of COG5 mutation, we performed differential gene expression analysis and pathway analysis. We found respectively 570, 604 and 1064 differentially expressed genes (DEGs) when comparing between the two mutant conditions and the WT. We also found significant number of DEGs when comparing between the two mutants for each cell cluster, that was more pronounced for genes expressed in APs and BPs (531 and 1059 respectively) further prompting to inter patient variability, despite COG52 and COG53 harbouring the same mutation.

Pathways analysis in APs reveals alterations in Notch pathways

In APs 672 genes were differentially expressed between COG52 and WT and 595 DEGs were found for COG53 and WT comparison. Among the two patients common upregulated genes were found involved in the orchestration of neural stem cell differentiation in the developing brain, as H3C3. Genes involved in ECM regulation were also observed to be enriched in both patients compared to the control. PRKAR1B, a regulator of the PKA signaling was found to be overexpressed in COG52 compared to the WT, suggesting a role for this pathway in the development of COG52 brain organoids; on the other hand SFRP1, an antagonist of Wnt pathway was found to be depleted in the male COG53, further propting to the relevance of COG5 mutation in affecting signaling pathways. Furthermore, in both patients enrichment or depletion of proteins related to the trafficking pathway and dynamics were observed. For example PLEKHA5, an adapter involved in membrane dynamics and signaling, was upregulated in the COG53 patient compared to the WT, while CD82, a tetraspaning membrane protein involved in signaling, cell adhesion and migration, was depleted (Fig. 32A-B).

Pathway analysis revealed specific pathways enriched or downregulated in the different cell types (AP, BP and neurons) comparing across patients and WT. Specifically, cell differentiation vs proliferation decision and neuronal development pathways were observed in APs populations. Signalling molecules such as BMP, FGF, TGF and IGF have been described to be present in the CSF underlying APs and to interact with receptors on the apical plasma membrane of these cells to influence developmental trajectories (Ferent et al. 2020). Interestingly these pathways have been found to be activated in the two patients' samples, compared to the control. More specifically, these molecules showed an increased levels in the patients APs, suggesting that COG5 mutation could affect the balance between signals received from the extracellular environment (Fig. 32C-D). Another relevant pathway for determining the correct sequence and timing of NPCs occurrence is the Notch signalling pathway. Indeed, we observed a global predicted inhibition of Notch pathway and a predicted activation of its antagonist Numb in all cell types. Further supporting these data, we found Hes5, a canonical Notch effector, to be downregulated in APs. Hes5 has been previously described for its role in preventing premature neuronal differentiation. Its downregulation in our patient brain organoids could be linked to a loss in the correct program of self-renewal vs neurogenesis (Fig. 32E-F).

Finally, cell polarity pathway regulators such as alpha catenin and SLIT3 were also found to be differentially expressed (respectively down and upregulated) between the patients and the control.
Taken together these results suggest that COG5 mutation affects the way APs respond to signals coming from the extracellular environment and that rearrangements in cell polarity could parallel the defects on the Golgi apparatus.

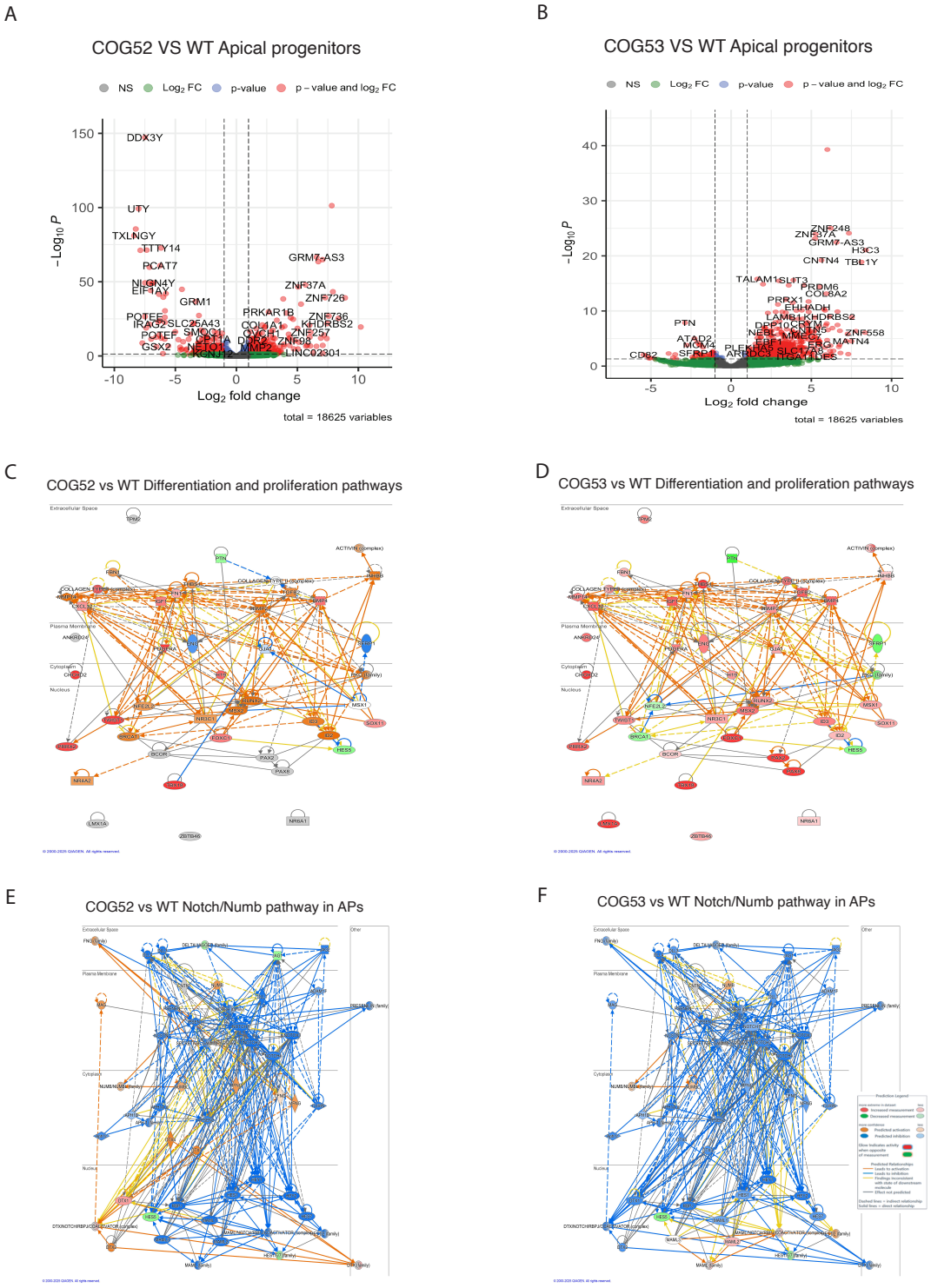


Figure 32. Pathways analysis in APs reveals alterations in cell differentiation vs proliferation decision and neuronal development pathways.

(A) Volcano plot showing differential gene expression (DEG) in a comparison between COG52 and WT and (B) COG53 and WT in apical progenitor cell-related cluster 5. (C-D) Differentiation vs proliferation-related pathway analysis in APs cluster 5. (E-F) Notch pathway predicted inhibition in cluster 5 cells in COG52 and COG53 compared to WT. Adjusted p value < 0.05. COG52: female patient; COG53: male patient; WT: WTC11 wild type control.

COG5-CDG shows a change in the subcellular distribution of Numb/Notch upstream regulators

scRNAseq data points to a possible dysregulation of Numb and Notch pathway. To investigate in details whether alterations in pathways related to these fate determinants could explain the phenotypes that we observed, we stained the organoids for ACBD3, Golgi and Numb. Our interest in ACBD3 stems from the observation that ACBD3 is associated with the Golgi Apparatus of interphase cells and it is released in the cytoplasm when Golgi gets fragmented during mitosis; in the cytoplasm ACBD3 interacts with Numb, a known antagonist of Notch, and influences cell fate of the dividing cells (Zhou et al. 2007). We thus wondered whether ACBD3 could be differentially partitioned between Golgi and cytoplasm in apical progenitors of our patients and KO organoids, given the fragmentation-like phenotype of the Golgi in our mutated conditions. The hypothesis was that being the Golgi more fragmented in the patients and in the KO, ACBD3 could be found released in the cytoplasm throughout the cell cycle and therefore more associated with Numb compared with the control.
Immunofluorescence staining revealed that less ACBD3 was colocalizing with Golgi apparatus (Fig. 33A). No differences were found in the degree of overall colocalization between ACBD3 and Numb, besides a small decrease in their colocalization only in the male COG53 patient compared to the female counterpart and with the KO (Fig. 33B).
Of note, when we evaluated by western blotting the level of ACBD3 in the total homogenate we found no change between controls and COG5 mutants (Fig. 33C). Furthermore, when we measured the partitioning of ABCD3 between membrane and cytosol, we observed an increase in the fraction of membrane-bound ABCD3 in both patients and the KO organoids (Fig. 33D). These data suggest that in patients there is a re-localization of ACBD3, that is released from the Golgi and now associates with another membrane-bound compartment. Additional studies are necessary to define the compartment ACBD3 associates with in patients and KO cells. Taken together, these data suggest the interesting possibility that COG5 affects the trafficking of morphogen receptors and accessory proteins, how they are processed and delivered to the target compartment and how they are retained in the GA.

Our current working hypothesis that though ACBD3 is less colocalized at the Golgi, is not extensively released in the cytosol, consistently with our observations that the Golgi fragmentation is not massive. Very interestingly, in the patients' membrane fractions we observed a higher band recognized by ACBD3 antibody. We hypothesize that this band could correspond to a post translational modification, possibly ubiquitylation, of ACBD3. Further analysis to better dissect the identity of this ACBD3 corresponding band could shed light into the contribution of COG5 mutation, but not complete KO, to the formation of specific post translational modifications on proteins in general, and more specifically how post translational modifications of ACBD3 differentially influence cell fate by modulating its interaction with Numb.

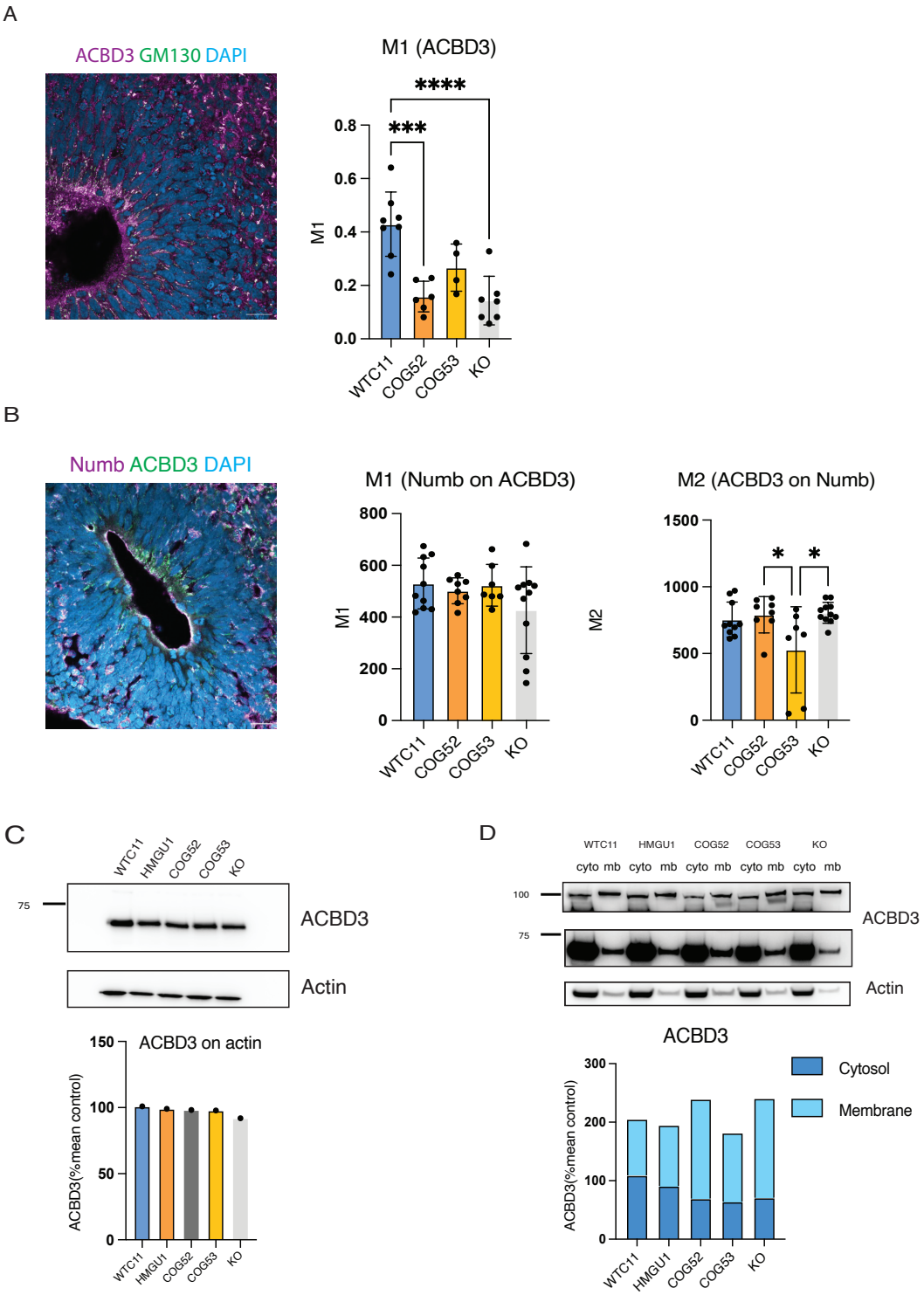


Figure 33. ACBD3 protein trafficking in COG5 patients and in KO organoids.

(A) ACBD3 (magenta) co-staining with GM130 (green) in human brain organoids reveal a lower colocalization of ACBD3 to the Golgi indicated as M1 value from JacoP plugin in ImageJ. Scale bar 20µm. N=3 n=3. (B) ACBD3 (green) colocalization with Numb (magenta) shows a lower M2 value for the COG53 patient compared to the COG52 and to the KO, but not with the WT. Scale bar 20µm. N=3, n=3 (C) ACBD3 protein levels measured as

percentage of ACBD3 on the control, from total homogenate of human brain organoids for each condition, (D) Western blot of cytosol-membranes fractionation of human brain organoids reveal an increased localization of ACBD3 at the membranes in both patients and in the KO compared to the controls. For western blot analysis 1 organoid batch was used. For each batch, 3 organoids per condition were pooled together. For immunofluorescence staining N= organoid batches, n= organoids/batch/condition. One-way ANOVA test was performed for quantification analysis of immunofluorescence stainings; if no line was shown: not significant p>0,005; *: significant p<0,005. COG52: female patient; COG53: male patient; KO: Knock out; WTC11 line; WTC11, HMGU1: wt controls.

Pathways analysis in BPs

From our previous experimental results, we found that cluster 7, including both IPs and Ctip2 neurons, is the most affected by the mutation in terms of cell abundance. To gain insight into the transcriptomic profile of these cells we performed a DEG analysis to detect differentially expressed genes that could explain the differences observed between the patients and the WT. We found that in the female patient most enriched genes, compared to the WT, were related to axon associated cell adhesion (CNTN4), factors involved in microtubule, cilia, cytoskeletal interactions (SAXO2) and ITGA2, an integrin that has been reported to influence migration and adhesion. Also, among the downregulated counterpart, genes involved in actin cytoskeleton dynamics, cell motility and migration were found, such as TMSB4Y. This suggest that COG5 mutation can affects BPs by regulating the intracellular architecture and the migration property of the cells (Fig. 34A).
In the COG53 patient most enriched genes were involved in axon guidance, synapse formation and functioning and cell cycle regulators (GMNC), though also ARL17B, key for vesicle trafficking, was found to be enriched. As for the downregulated genes, cell cycle progression, cholesterol biosynthesis (FDFT1) and activators of the Wnt pathway were observed. Cholesterol plays key roles in membrane structure, myelination and synaptogenesis. It would be interesting to understand whether the decrease in FDFT1 expression levels lead to decreased levels of cholesterol, thus impacting on the correct maturation of synapses (Fig. 34B).
In BPs the most enriched pathways in COG patients compared to the control were pertinent to differentiation of CNS cells, and those related to neuronal formation and maturation, consistently with the more differentiated state of BPs that will give rise to neurons and with the presence in the examined cluster of neurons (Ctip2 and Tbr1). In addition, BMP was one of the most relevant pathways to be differentially regulated between patients and control. In particular, BMP2 was activated in the two patients while its inhibitor SOSTDC1 showed a decrease (Fig. 34C-D).
Interestingly, BPs from the two patients showed differentially activated/inhibited signalling molecules related to the differentiation of the CNS. For example, while IGF1 is strongly activated in COG53, in COG52 it shows a predicted reduction. This was not the case however for POU3F2 gene -a transcription factor crucial for brain development- that was reduced in both patients compared to the control. Loss of POU3F2 can lead to

developmental delay, intellectual disability and cognitive impairments, similarly to what observed in our two patients.
Consistent with the fact that neurons also cluster with IPs, the axonal guidance pathway is represented in cluster 7 (Fig. 34E-F). Interestingly a global inhibition of ADAMS family of proteases operating in the extracellular milieu is observed, consistent with the observation on DEGs that implicate the ECM among the differences between the patients and the WT. Semaphorins, crucial for neuronal guidance and synaptogenesis, are also activated in the male patient, but not in the female patient. Furthermore, while ITGA2, involved in NPC adhesion and migration, is activated in the female patient, an inhibition is observed in the male patient.

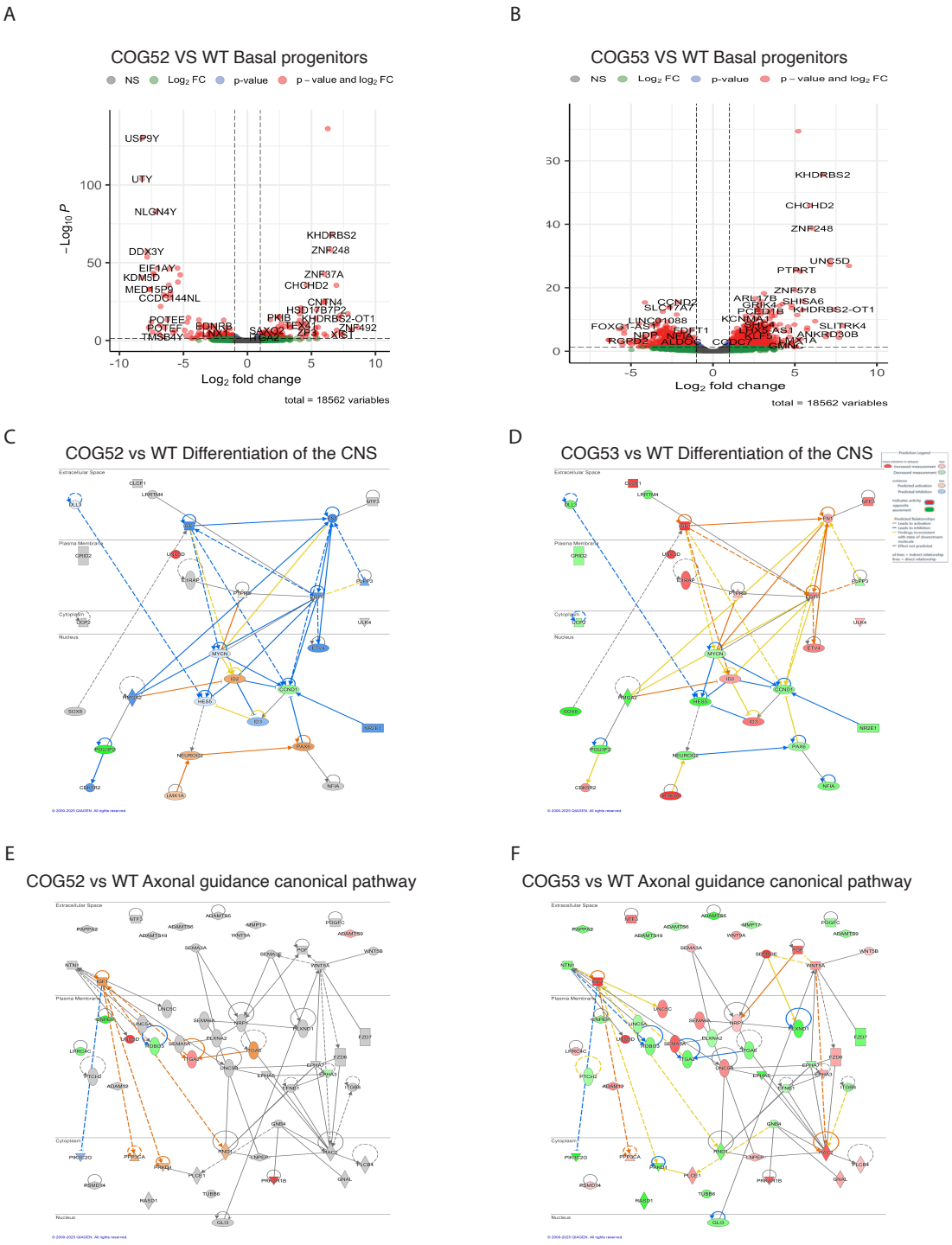


Figure 34. Pathways analysis in BPs reveals alterations in CNS differentiation and axonal guidance pathways.

(A) Volcano plot showing differential gene expression (DEG) in a comparison between COG52 and WT and (B) COG53 and WT in basal progenitor cell-related cluster 7. (C-D) CNS differentiation and development pathway analysis in BPs and neurons in cluster 7. (E-F) Axonal guidance related pathway in basal progenitor cluster 7. Adjusted p value < 0.05. COG52: female patient; COG53: male patient; KO: Knock out WTC11 line; WTC11: wt control.

Other significant pathways that emerged from the comparison between patients and WT BPs are related to the branching of neurons and to the synapse development. Of note, the activation of CUX2 in the COG53 male patient cluster 7 could suggest an enrichment on CUX2+ neurons, that need to be further confirmed by immunofluorescence analysis.

Interestingly, among the genes involved in the synapse development, SV2C, that encodes a synaptic vesicle glycoprotein crucial for the dopaminergic system, is activated in both patients compared to the control. On the other hand, LRRC4C gene, that plays a role in the development of excitatory synapses and regulates axon guidance, is inhibited in the COG52 female patient and activated in the COG53 male sibling. These counteracting pathways of activation/inhibition could explain why the two patients show partially different phenotypes.

Finally, we also examined Notch pathway and, as we observed in the APs, there is a general predicted inhibition of the pathway, with a predicted activation for Numb signalling molecule (Fig. 35A-B). However, in this case no activation or inhibition-related predictions were possible for the female patient. Nevertheless, the DEG analysis showed that LNX1, a Numb interactor, is inhibited also in the COG52 BPs, suggesting that still this pathway could be relevant in COG52 BPs.

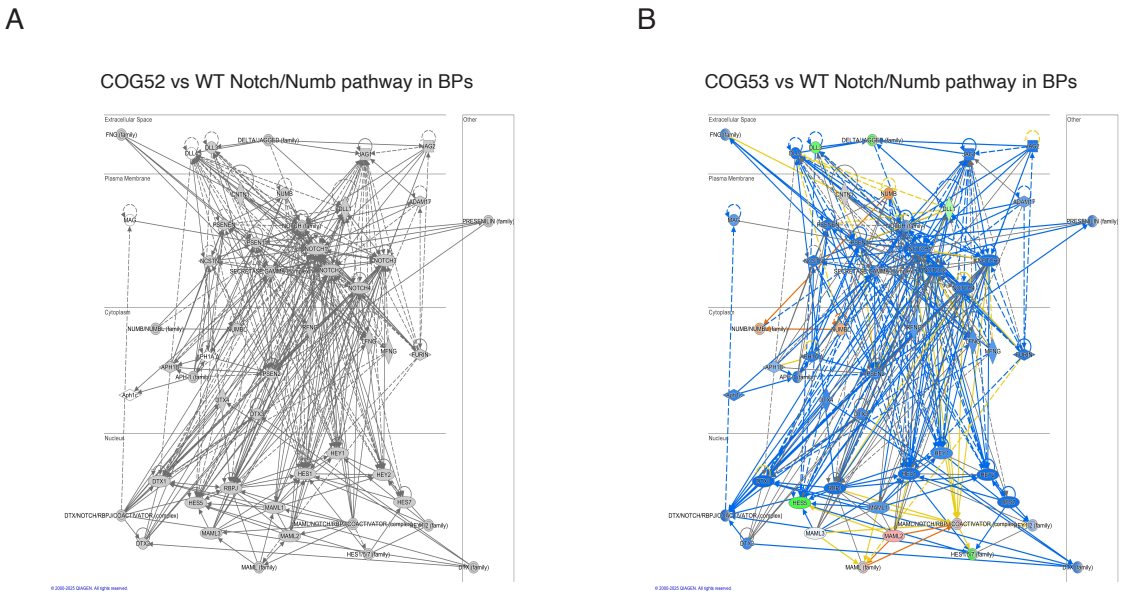


Figure 35.Notch pathway is inhibited in cluster 7 cells from COG53 patient organoids.

(A) Pathway analysis of cluster 7 in COG52 patient didn't reveal any significant activation or depletion. (B) Notch pathway predicted inhibition in cluster 5 cells in COG52 and COG53 compared to WT. Adjusted p value < 0.05. COG52: female patient; COG53: male patient; KO: Knock out WTC11 line; WTC11: wt control.

Pathways analysis in neurons

The neuronal clusters were the most heterogeneous in terms of relative abundance, as some clusters (6, 9) show both depletion and few neighbourhoods show enrichment. To account for these differences more immunofluorescence analysis will be needed to understand which neuronal types are enriched and which one, further to Ctip2 neurons are depleted instead.

We also analysed DEGs to get a better picture on the transcriptomic profile of neurons in patients vs the control. For the COG52 female patient we found an upregulation of GRM7-AS3, which transcriptionally represses the metabotropic glutamate receptor 7 modulating neurotransmitter release and synaptic plasticity at post synaptic terminals. Furthermore, we observed an enrichment of neuronal migration-related factors such as COL1A, LAMB1 and axonal guidance (CHDC2). Downregulated genes were instead related to cytoskeleton dynamics and vesicle trafficking between ER and Golgi as well as TUBB3, which is critical for neuronal structure (Fig. 36A).

Similarly, in the COG53 male patient while cell adhesion, axonal guidance and synaptic signalling related genes were upregulated, transcription factor and chromatin remodelling related genes were depleted (PIR, RGPD2, EN1) (Fig. 36B).

When computed the neuronal related pathways we found that COG5 mutation impact on the differentiation and maturation of neurons with downregulated pathway effectors being related to decreasing the number of specific neuronal types (Fig. 36C-D).

As for APs and BPs, IGF1 growth factor was activated in neurons from the two patients; IGF1 is crucial for radial glia cells development, but it has also been described to be important for synaptogenesis, synaptic connectivity and plasticity. In the two patients BMP4 remains among the activated genes. Interestingly some of the inhibited genes, such as GSX2 and EN1, relate to the production of fewer neurons (interneurons and dopaminergic neurons respectively). Collectively these data suggest that COG5 mutation affects the production and degree of maturation of different neuronal populations, selectively affecting the development of some neuronal types, and that the neuronal migration and synaptogenic process are highly influenced by impairments in GA structure and function.

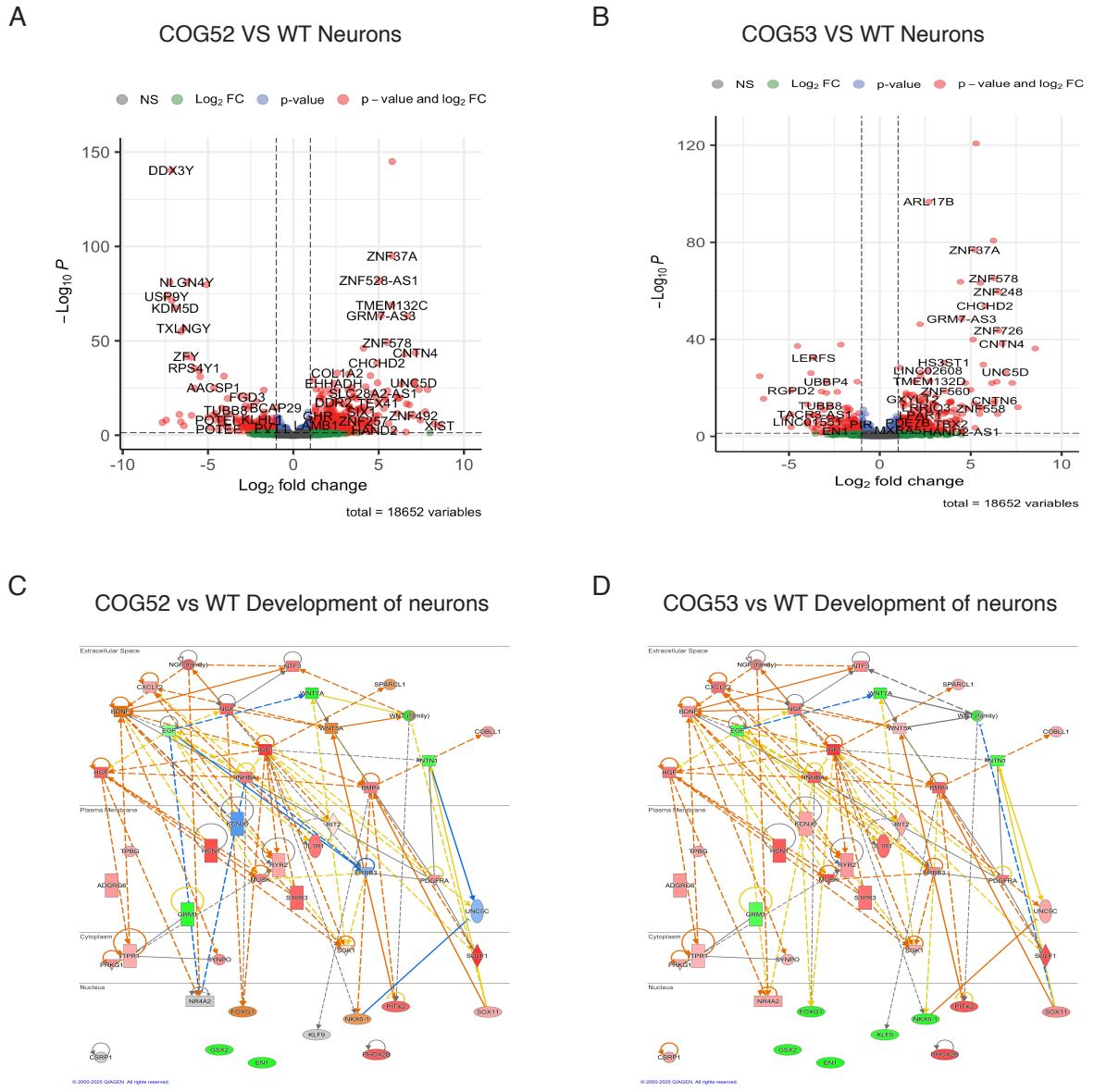


Figure 36. Analysis of neuronal clusters reveal activation of neuronal developmental related pathway.

(A) Volcano plots showing differential gene expression (DEG) in a comparison between COG52 and WT and (B) COG53 and WT in neurons clusters 6-8-9. (C) Neuronal development pathway analysis of clusters 6-8-9 in patients. Adjusted p value < 0.05. COG52: female patient; COG53: male patient; KO: Knock out WTC11 line; WTC11: wt control.

Glycans profiles in COG5-CDG human brain organoids

The diagnostic test used by clinicians for the CDG diagnosis consists in the assessment of glycosylation, and in particular sialylation, defects of plasma proteins such as transferrin. However, it has been reported that the two COG5-CDG patients we are studying don't show any difference in serum N- and O-glycosylation profile. So, we wanted to investigate whether specific differences in glycosylation and sialic acid derived modifications were tissue specific, and found specifically in the brain. We performed a western blot analysis of whole organoid homogenate and we stained for *Sambucus Nigra* lectin (SNA), which binds sialic acid (Fig. 37A). We normalized the signal of the SNA on the Ponceau and we observed that in the two patients SNA intensity was strongly decreased compared to the WTC11 control, and only slightly decreased compared to our other control, HMGU1. However, the SNA levels of the KO were comparable with those of the WTC11 control. This poses interesting questions as of whether and why there are specific mutations on COG5 that implies defects in sialylation, when the lack of COG5 protein, as shown in the KO condition, is not relevant for this glycosylation type, at least in brain organoids.

We next wondered whether there could be other glycans affected by COG5 mutation. We specifically focused on O-glycans, as they are produced in the Golgi apparatus. We performed a western blot staining for *Peanut Agglutinin* (PNA) lectin, that recognizes O-linked core disaccharide galactose (Fig. 37B). Interestingly we observed that different control organoids, grown from different cell lines, showed different basal levels of PNA, however when comparing between the WTC11 and the patients' lines, only the female patient showed reduced levels of PNA, while the male patient showed increased O-galactosylation. Once more, the complete lack of the protein, as shown in the KO condition, doesn't affect O-glycosylation neither. We cannot exclude that since this assay captures the global glycosylation profile of the brain organoids, more subtle and protein-specific effects could be found with a technique with higher sensitivity.

We then wondered whether rather than being differentially expressed, sialylated proteins could be differentially localized within cells. To address this point we performed an immunostaining for SNA and GM130 and colocalization analysis didn't show any difference between the control and the mutated conditions (Fig. 37C), suggesting that sialylated glycans may not be differentially retained in the Golgi in the mutated lines. Preliminary experiments suggest however that the colocalization of SNA with pan cadherin is reduced in the male patient compared to control (Fig. 37D). Though further investigations are needed, this could be explained by a differential trafficking of sialylated glycans due to the mutation on COG5, rather than on their impaired production.

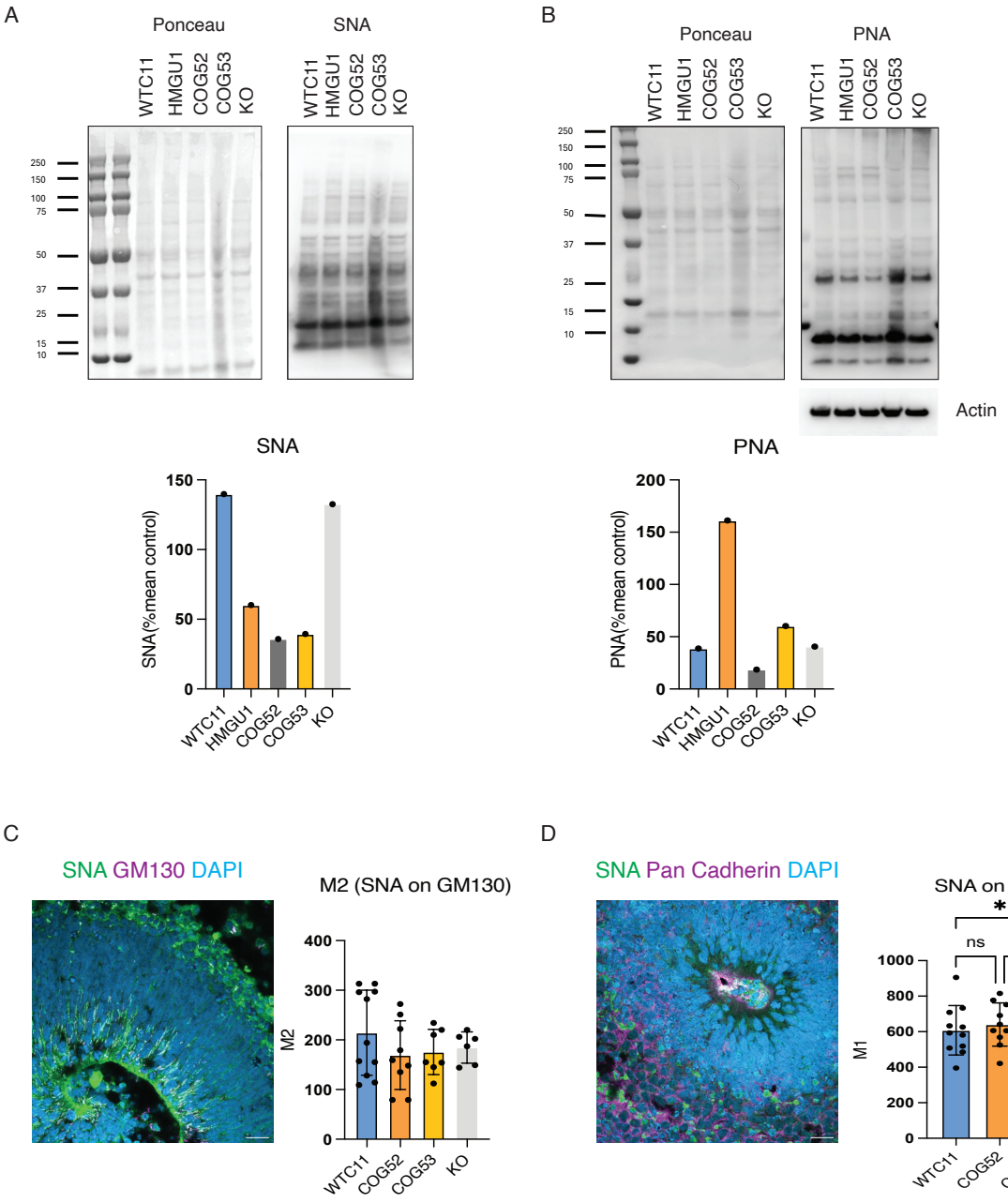


Figure 37. SNA distribution is impaired in COG5-CDG patients brain organoids.

(A) Western blot for SNA on total homogenate of human brain organoids reveal decreased levels of SNA in both patients compared to the control. (B) PNA western blot on total homogenate of human brain organoids show no significant differences between patients and control organoids. (C) Colocalization analysis of SNA with Golgi (GM130) calculated as M1 value from JaCoP plugin in ImageJ. (D) Colocalization analysis of SNA with Pan cadherin in human brain organoids ventricles calculated as M1 value. Scale bar 20µm. For western blot analysis 1 organoid batch was used. For each batch, 3 organoids per condition were pooled together. For immunofluorescence staining N= 3 organoid batches, n= 3 organoids/batch/condition. One-way ANOVA test was performed for quantification analysis of immunofluorescence stainings; if no line was shown: not significant p>0,005; *: significant p<0,005. COG52: female patient; COG53: male patient; KO: Knock out WTC11 line; WTC11, HMGU1: wt controls.

Glyco-lipidomics in COG5-CDG human brain organoids

The secretory pathway is responsible not only for protein glycosylation but also for lipid glycosylation. Indeed, it has been observed that contrary to the whole human body situation, most of the glycosylation in the brain is on lipids. Interestingly, lipid composition is known to affect the structure and function of several receptors, including Notch receptors. To get a broader picture on the effects of partial or complete lack of COG5 in human brain development, we collaborated with the group of Peter Witters in KU Leuven to obtain the profile of glycosylated lipids in COG5 patients brain organoids.

Gliycosphingolipids (GSLs) are widely present on the plasma membrane of cells in the brain, specifically enriched in lipid rafts where they contribute to membrane organization, signal transduction and cellular communication. GSLs are first synthetized starting from a ceramide moiety in the ER, with subsequent processing through the addition of Glucose, GlcNAc, Galactose, GalNAc, and sialic acids units. The first processing event occurs in the ER with the addition of a galactose unit to the lipid and further processing happens in the Golgi apparatus where the combination of different sugar units provides the formation of different lipids with specific glycan signature. In particular distinct series can be found, including the globo-series, lacto(neolacto)-series, and ganglio-series, each derived from lactosylceramide (LacCer) through the action of specific glycosyltransferases (Fig. 38A).

GSLs analysi on control organoids showed that the most abundant population is represented by ganglio series GSLs, in particular GD3, GD2 and GD1ab, with specific differences in their abundance comparing between the ceramide with palmitic acid fatty acid (16:0 carbon backbone) and the stearic acid fatty acid component (18:0 carbon backbone) (Fig. 38B). In lower percentages also HexCer and LacCer are found.

Considering the most abundant glycosylated GSLs present in the control, our collaborators investigated whether differences could be observed in the two patients lines (Fig. 38C). It has been observed that for all the globo series that imply sialylation as lipid post translational modification are reduced in the two patient lines compared to the control (Fig. 38C). In contrast, HexCer the precursors for the glycosphingolipid pathway, and the Lac series lipids are enriched in the two patients compared to the control (Fig. 38C). Overall, these data suggest that in the two patients the lipid glycosylation pathway is affected by the COG5 mutation leading to an increased presence of GSLs precursors and a decreased production of more mature series-specific glycosylation of lipids, especially when glycosylation involves the addition of sialic acid. Possibly this is due to mislocalization of specific glycosyltransferases within the Golgi apparatus because of the mutation on COG5.

Finally it is interesting to notice that also GD3 and GM3 series with fatty acid backbone 24:1 are enriched in the patient organoids compared to the control. d18:1/24:1 describes a ceramide with a sphingosine base and a nervonic acid as the N-linked fatty acid and it is common in brain and nerve tissue, particularly in myelin.

Taken together these observations could open interesting possibilities of investigation connecting the glycosylated lipid phenotype with the clinical phenotype of the two patients considering the impact that COG5 mutation could have on neural development, membrane stability and synaptic signaling.



Figure 38. . Lipid glycosylation analysis of patient derived human brain organoids.

(A) Cartoon representing GSL synthesis adapted from Janez Pedrayes et al. (2025). (B) Quantification of GSL subtypes in WTC11 WT human brain organoids. (C) Characterization of GSL subtypes in human brain organoids in comparison between WT (grey) and patients (pink). Quantifications were performed by Andrea Janez Pedrayes from the group of Peter Witter in KU Leuven.

DISCUSSION

A machine learning-guided microinjection robot to target and study single cells in the developing brain

Single-cell analysis techniques are at the forefront of neurodevelopmental studies as they allow to reconstruct single cell trajectories and cellular history. This is extremely relevant to understand how single cells contribute to tissue morphogenesis in contexts such as brain development where the timing of appearance of neural progenitors and neurons has a great impact on the overall neocortex formation.

Some challenges however underlie the techniques available to date, such as the fact that during tissue preparation and dissociation for e.g. scRNAseq, the cell is completely taken out of its tissue context, loosing not only connections with neighbours, but also its own morphology and overall architecture, features that are crucial in determining its proliferation/differentiation potential. To circumvent these limitations, we previously developed a microinjection into single neural stem cells as a way to target single neural stem cells in tissue, and that allows to disentangle and visualize single cells from the complexity of the surrounding tissue. Microinjection is based on the insertion of a fine-tip capillary filled with fluorescent dye into single cells within a tissue with high spatial precision. This type of single cell labelling allows not only to manipulate single cells in tissue, but also to reconstruct lineages and cellular history, and can also be coupled with scRNAseq. However, also this technique comes with some side aspects such as the time of the experimental procedure and the tight dependency on user's technical skills that can limit the success rate of the process.

To overcome this issue, we developed the Autoinjector to allow for an automatic, high resolution and precision microinjection with minimal human intervention, and therefore little need for user experience. Recently machine learning algorithms have been generalized and used for object detection in vision-guided microinjection; in a combined effort with Jacob O'Brien and Suhasa Kodandaramaiah from the University of Minnesota we leveraging these concepts to developed a machine learing-guided (ML-guided) Autoinjector to automatize the entire pipeline of this experimental procedure, from pipette calibration to tissue edge detection and finally to serial microinjection into single cells.

One of the most time-consuming steps during microinjection is to get the tissue and pipette tip in the same focal plane, without unwanted collisions between all objects involved (pipette, plate, tissue). Calibration is a necessary step to localize the pipette in space, and it is typically performed by moving the object, in this case the pipette, and by detecting the movement with the field of view in pixel coordinates. To automate this process, we trained a YOLO5 neural network and provided an XYZ detection of the pipet tip. We calculated that this model allowed to decrease the duration of the calibration procedure compared to previous versions of the Autoinjector.

We first trained our tissue detection model on mouse tissue slices for lack of tissue edges complexity and then extended the application on human brain organoids. Automatic annotation was achieved through a first neural network-based segmentation that allowed to distinguish the tissue from the background and then the edges were classified as apical or

basal considering their curvature (concave vs convex). This process allowed to correctly detect the apical part and the basal side of mouse brain tissue and be later extended to human brain organoids, that present fewer neat edges, but that could still be recognized correctly as basal or apical by our system. Of note, our system did not need any re-training on human brain organoids, highlighting its robustness and generalizability.
We applied our ML-guided Autoinjector to microinject single neurons within the basal side of the organoids and we then also tested its ability to target single apical progenitor cells from the apical side of the tissue. The injection efficiency (neurons injected over the total attempts) revealed an increase with the ML-guided Autoinjector compared to the previous version of the robotic platform, both in mouse and human tissue. Furthermore, we could successfully reconstruct the morphology and intracellular architecture of all microinjected cells in their native environment.
Overall, we believe that the ML-guided Autoinjector could be extended in future to single cell manipulation via injection of compounds to selectively impact cell behaviour, allowing to extend current methods for single cell tracking and manipulation. This would be particularly relevant to gain insights into cell biology and cellular dynamics of neural progenitors and neurons in different tissue types, among which human brain organoids to tackle cell biological questions in the context of development.

Polarized localization of the GA in human apical progenitors

GA is commonly located in a perinuclear position, in proximity to the endoplasmic reticulum. However, GA can acquire specific localization in polarized cells, coherently with their compartmentalization of functions. In the context of brain development, the most well know polarized cell type are APs, that own two different compartments, an apical process and an elongated basal process. In the APs from the mouse developing neocortex the GA is restricted to the apical process and absent from the basal compartment. The polarized distribution of the GA is reflected by the glycan composition of the apical and basal process, with GA-derived glycans being confined in the apical process.
Considering the evolutionary similarities between mouse and human developing brain, we hypothesized that Golgi polarization in APs could be a shared feature. We thus characterized GA localization in human APs and observed Golgi stacks along the apical process of apical progenitors in human brain organoids. Finally, towards the basal most part of the ventricle single compact Golgi structures were observed close to the nuclei of basal progenitor and neurons. These results extend the current knowledge regarding GA polarization in apical progenitors to human brain development and confirm that also in human tissue GA is polarized and non-pericentrosomal in APs, while being perinuclear in other NPCs subtypes and in neurons.

Acute GA fragmentation induces a cell fate switch

Human disorders that entail defects in the secretory pathway (such as Congenital Disorders of glycosylation, CDGs) are often associated with severe neurodevelopmental manifestations, suggesting a link between trafficking pathways and neural stem cell behaviour. The cellular and molecular mechanisms linking traffic and fate choice during brain development are largely unexplored.

We wondered whether the specific perturbation of GA structure and function in apical progenitors could impair cells' identity and affect cell fate switch. We used a pharmacological treatment to fragment the GA and we found that both in mouse brain tissue and human brain organoids the Golgi fragmentation induces a premature fate switch from APs to BPs, We think that the effect on the BP population is due to a change in the program cell fate switch of apical progenitors, as the treatment (only 6h) was not long enough to exert an effect on the whole trajectory AP→BP→Neurons. Since the treatment was too short to allow cells to complete a full cell cycle division, we envisaged two possible hypothesis to explain our observations. In the first scenario GA disassembly could induce transdifferentiation of AP into BP, a process of cell fate change that excludes the cell cycle entry. The second hypothesis instead postulates that the mode of division of APs is influenced by Golgi fragmentation and in turn this affects the downstream progeny of a dividing APs. Indeed, it has been previously observed (Polenghi and Taverna 2023) that symmetric vs asymmetric partitioning of cell fate determinants and subcellular compartments in the two daughter cells influences the outcome of cell division.

Using the robotic platform we developed for single cell microinjection, we tracked the progeny of single APs and observed that Golgicide treated cells acquire a more basal fate, as shown by an increase in Tbr2+ cells. We then leveraged the excellent single cell resolution of microinjection and analysed the symmetry of daughter cells clusters, a proxy for the symmetry of the mother cells division. We found that Golgicide treatment increases the percentage of symmetric Tbr2+/Tbr2+ daughter cells clusters, strongly suggesting that the fragmentation of the GA induces AP→BP fate switch by influencing the mode of division of apical progenitors, favouring their symmetric BP-genic divisions.

Leveraging the genetics of CDGs to understand the mechanisms linking GA function to neural stem cell identity

To define the mechanism linking GA function to fate transition, we decided to focus on congenital disorders of glycosylation (CDGs), a class of rare diseases associated with severe neurological manifestations. Of all CDGs we got particularly interested in the analysis of COG5-CDG: COG5 is localized at the GA, providing us with a genetic tool to perturb the GA function.

COG5 is a protein subunit of the Conserved Oligomeric Golgi complex (COG). COG complex is formed by two lobes, A and B, each composed of 4 subunits, interacting through the COG1-COG8 bond. COG5 is located on lobe B and has been described to interact with COG7, within lobe B. Several mutations on COG5 have been described to cause CDGs and in most cases COG5 mutations are associated with alterations in brain development,

including primary microcephaly (PM) a condition that refers to a brain smaller at birth. At the cellular level PM is typically caused by impairments in the correct sequence and timing of appearance of NPCs during brain development.
COG5 KD in apical progenitors affects Golgi apparatus structural integrity as observed by an increase in Golgi units and a concomitant decrease in their area. This phenotype was even more pronounced when silencing both COG5 and COG4, which is a subunit of lobe A on the COG complex. Furthermore, KD-mediated perturbation of GA was paralleled by an increase in Tbr2+ IPs and SOX2+ cells in the SVZ. Moreover, no change was observed in the number of EdU- and Ki67-positive cells, suggesting that GA fragmentation doesn't affect cell cycle progression *per se*.
Taken together, these results suggested that acute perturbations of GA-related proteins, either *via* pharmacological treatment or genetic manipulation, impact lineage progression during brain development and favours the generation of basal progenitors.
Pathological conditions affecting brain development often time arise because of impairments in the correct timing and sequence of NPCs appearance. We here suggest a link between GA perturbation and its effect on the program of cell differentiation, possibly by affecting the cell division mode.

COG5 mutations affect cell fate and identity during brain organoid development

From clinical observations we knew that the two patients showed a phenotype of microcephaly. We make use of human brain organoids from COG5-CDG patients to verify if also in pathological conditions the GA compromission is paralleled by a change in neural stem cell behaviour. In addition, we reasoned that the use of patients derived organoids might help us gaining insight into the mechanisms linking defective GA function and altered brain development. Of note, the patients' cells we are using are unique, as the two COG5-CDG patients are, to the best of our knowledge, the first COG5-CDG patients without noticeable defects in N-glycosylation (assessed at the level of the plasma glycosylation and in fibroblasts). We think this might put us in the privileged position to disentangle -at least in part- the effects of COG5 mutations on the structural integrity of the GA from the one on glycosylation *per se*.
When preparing human brain organoids from patients' cells we observed that the area of the two patients' organoids -and of the KO- as well as their internal ventricle number was decreased compared to control. Furthermore, the overall thickness of the cortical wall (VZ and NL) was reduced in COG5-CDG mutation, suggesting that the clinical phenotype of microcephaly can be recapitulated in our brain organoid model. This suggested that human brain organoids could be efficiently used to model brain development in vivo. We also observed a decrease in the number of Tbr2+ intermediate progenitors and in Ctip2+ neurons in both patients, while SOX2+ cells were not overall affected and the general neuronal population HuCHuD+ was only slightly reduced in the male patient. The time-course experiments show that d38, corresponding to mid-neurogenesis in vivo, is a key moment for cell determination as the biggest alterations on NPCs and neurons cell types are observed at this timepoint. These differences smoothen with proceeding development, suggesting that

GA structural and functional integrity is particularly crucial during the first waves of generation of BPs from APs to BPs. Of note, and in line with this idea, it has been shown that AP-to-BP transition entails a profound reorganization of the intracellular compartments, in particular along the Golgi-centrosome axis.
Proving further evidence on the link between COG5 mutation and its effect on brain development, scRNAseq analysis showed a global depletion of clusters corresponding to all cell types considered (APs, BPs and neurons) for the COG53 male patient, while the COG52 female patient, showed an overall enrichment of APs and BPs clusters and a global depletion (with few exceptions) of neurons. Moreover, the cluster 7 identified as basal progenitor population, also contains neurons possibly explaining why, despite the decreased Tbr2 population in the COG52, the global cluster is enriched in the COG52 patient. Another tempting speculation could hypothesize a Golgi-mediated control on the translation of fate marker-related transcript, by affecting the fate decision pathways and in turn cell identity by mediating the translation of specific fate markers. The overall number of neurons when analysing HuCHuD post mitotic neurons was not significantly affected, although a thinner neuronal layer was observed, consistently with scRNAseq data that prompt to a general depletion of most neuronal-related clusters. It would be interesting to define the identity of the neuronal subtypes that are, conversely, upregulated in the mutants compared to the WT, as an imbalance of neuronal subtypes has been correlated to brain development impairments, such as intellectual disability.

COG5 mutations affect the mode of division of APs

To gain insights into the mechanisms underlying COG5-CDG, we performed a pathway enrichment analysis on the scRNAseq dataset we generated. We observed that pathways related to cell differentiation vs proliferation decision were overrepresented and differentially regulated in the patients compared to the control, suggesting that the cell identity maintenance vs cell differentiation decision is crucially affected in the COG5 mutants. Symmetric vs asymmetric division is accompanied by a change in cell division plane or angle, with a differential segregation of determinants ultimately influencing the fate of the daughter cells, We thus investigated whether the cell division plane was changed in APs. We observed an increased in vertical and diagonal division planes in COG5 mutants and a concomitant decrease in the horizontal cleavages (typically associated with direct neurogenesis). Finally, it is worth noticing that despite similar percentages of cells in vertical and diagonal division mode, in the KO line the trend in Tbr2+ intermediate progenitors is the opposite compared to the COG53 patient. This could suggest that the dosage-dependent role of COG5 in brain development and the dosage-dependent effect of Golgi apparatus structure and functionality goes beyond the simple influence on cell division mode of apical progenitors.

ACBD3 distribution in COG5 mutant brain organoids

scRNAseq dataset also shows that signalling pathways affecting fate decision, such as Wnt, BMP, FGF, IGF and Notch, were differently up or down regulated in COG5-CDG patients,
For example, Hes5, a canonical Notch effector that prevents premature neuronal differentiation, is downregulated in the two patients compared to the control, and consistently the Notch pathway is predicted to be downregulated, while Numb, a Notch antagonist is has a predicted upregulation, suggesting that COG5 mutation affects the balance between pathways effectors and their antagonists. Reports (Zhou et al. 2007) show a link between GA function and Notch pathway: ACBD3, an interactor of Numb, is released from the GA in the cytoplasm upon Golgi apparatus fragmentation during mitosis. In the cytoplasm ACBD3 interacts with Numb and influences cell identity and the fate of the daughter cells by counteracting with Notch pathway.
In COG5 mutants we observed a strong decrease of the fraction of ACBD3 associated with the GA, possibly due to the tonic GA fragmentation. In parallel, we also observed a reduced colocalizing between ACBD3 and Numb. scrNAseq, immunofluorescence and biochemistry data all suggest an ACBD3-mediated impairment of Notch pathway in COG5 mutants and link that impairment to structural changes of the GA.
On a general note, our observations suggest defects in the trafficking of proteins, as ACBD3, and possibly also lipids, from GA to target compartments. This is in line the main role for COG complex is the tethering of vesicles to their target compartments within the GA or at the level of the ER. By affecting the COG5 subunit of the complex, the Golgi architecture changes along with the capability of functioning thus exerting a broad effect on the secretory pathway. APs are highly susceptible to extracellular signals, such as those coming from the CSF. Missorting of receptors and polarity determinants could broadly affect how APs sense and respond to signals, leading to an impairment in cell fate switch. Finally, these receptors are heavily glycosylated, hence defects in the GA machinery could impair receptors' function by affecting their glycosylation signature. Further investigations on the effect of the mutation on the trafficking dynamics will be needed to explore this possibility.

Divergent cellular and molecular phenotypes in COG5-CDG patients

Interestingly, though the two patients harbour the same COG5 mutation and have similar clinical phenotypes, they display different cellular and molecular phenotypes when comparing their brain organoid. Of note, the female patient (COG52) was diagnosed later than her brother (COG53). A possible explanation on the higher severity of her symptoms could be that treatments to counteract the pathological effects of the mutation started earlier in the brother, thus leading to less severe symptoms. However, our results suggest that the differences between the two siblings have deeper connection with the cellular responses to COG5 mutation, which are not equal within the two patients. While the Golgi apparatus structure was altered in both patients, in the apical progenitor cells population the GA of the COG52 appeared to be more fragmented than that of the male patient, suggesting that the same mutation could differentially alter the integrity of the Golgi and as such influence the trafficking pathways. In fact, we have previously hypothesized that alterations on the

secretory pathway could explain the observed impairments in the lineage trajectories during brain development. We showed that, opposite to the more severe GA-related phenotype, the male patient shows a stronger depletion of all cell types: apical and basal progenitors were found to be strongly depleted, and the neuronal population was found to be highly affected in the COG53 male patient compared to the COG52 female patient. Collectively these results suggest that there is a differential regulation of the cell fate switch between the sister and her brother.

Interestingly, both patients show less APs dividing with a horizontal cleavage plane, with the COG53 male patients showing a more pronounced increase in diagonal division. Diagonal divisions are typically associated with an asymmetric division that generates one AP and one BP, suggesting an earlier switch to asymmetric division and a premature depletion of the AP pool in the male patient, influencing the overall cell populations within the developing brain. This hypothesis could also explain the lower number of neurons that we observed in the male patient. Hence, it could be possible that the same COG5 mutation differentially influences the cell division mode, ultimately impairing the cell trajectories of brain development. To tackle this hypothesis lineage tracing experiments will be needed to dissect at the single cell level the identity of the two daughter cells.

The differences between the two patients were also reflected in their transcriptomic analysis. The general reduction of ECM-related components and signalling pathway, and the depletion of integrin signalling in the COG52 NPCs, compared to the COG53, suggest polarity defects in the COG52 NPCs, possibly leading to premature differentiation and neurogenesis as well as disrupted cortical layering and organization. O-glycans are essential components of the ECM and we showed a reduction in this class of glycosylated proteins in the COG52 female patient but not in COG53 male patient; these observations further corroborate the relevance of the ECM as a mechanism for altering cell fate switch in the COG52 female, but, possibly, not in the COG53 patient. The enrichment of these pathways in the COG53 male patient could imply that different mechanisms affect brain development between the two siblings. This possibility is also supported by the observation that in the comparison within COG52 and COG53 neurons, the same pathway that were depleted in APs are now enriched in the neurons of the female patient only, strongly suggesting that apical progenitors are losing their maintenance programs too early, exiting stem cell state and over activating neuronal programs upon differentiation. Of note, the enrichment of some neighbourhoods of aRGs and of BPs observed in the female patient, could be explained by the fact that the cluster that we identified as APs contain other radial glia cells, as the markers that we used to define the clusters are not specific for apical progenitors only.

In conclusion, both patients share an alteration in the timing of NPCs occurrence, but we hypothesize that the mechanisms underlying these alterations are different, with ECM composition possibly playing a crucial role in the COG52 female patient but not in the COG53 male patient.

Considerations on the effects of COG5-KO on neural stem cells

We make use of COG5-KO organoids to study the effects of a complete lack of COG5. COG5-KO organoids exhibit a reduced size and a lower number of ventricular structures along with an increase in ventricle area, reflecting the role of Golgi apparatus in influencing the correct sequence and timing of progenitor cells during brain development.

The complete lack of COG5 protein implicated a structural impairment, as demonstrated by the concomitant increase in the number of Golgi units and a decrease in each units' area. Our findings are in line with previous experiments on the relevance of COG5 for proper structural maintenance and functioning of Golgi apparatus (Bailey Blackburn et al. 2016), with morphological changes being observed in partial or complete absence of individual COG subunits. Furthermore, it has been shown that deletion on any of the COG subunits in human cells, results in the degradation of several, but not all, of the Golgi resident protein. This could explain why in COG5-CDG cells the COG7 protein is absent, possibly because of an degradation.

Our data show that the complete absence of KO of COG5 affects the cell trajectories in brain development by altering the production of intermediate progenitors, that are shown to be increased upon COG5-KO and when the Golgi is fragmented. The observed peak in the production of TBR+ cells is consistent with our previous observations on both mouse and brain organoids treated with Golgicide as well as with the results obtained with the shRNA-mediate knock down of COG5. In COG5 KO organoids, apical progenitors divide through both diagonal and vertical division planes. While vertical divisions produce two daughter cells with the same fate, asymmetric divisions lead to divergent identity of the daughter cells. We therefore hypothesize that, while causing Golgi fragmentation, COG5 alters the production of BPs, possibly by influencing cell division. To address this question lineage tracing experiments will be performed to track lineage progression of single labelled apical progenitor cells. Of note, it would be interesting to understand whether GA fragmentation also affects the outcome of cell division of intermediate progenitors. Further to influencing the outcome of cell division, by affecting the partitioning of polarity determinants, GA fragmentation is a major checkpoint for the cells to enter mitosis. It is in principle possible that a constitutive fragmentation favours the entering of apical progenitor cells in mitosis.

To conclude, we have here showed that COG5 KO alters brain development, by specifically affecting the AP to BP differentiation program. We have also provided proofs that this happens because of changes in cell division mode and we hypothesize that COG5 KO causes alterations in the trafficking pathway, impairing the APs response to signalling pathways.

Are glycolipids a main molecular target in COG5-CDG?

GSLs are essential lipids in the outer leaflet of cell membranes, forming specialized membrane domains called lipid rafts. Lipid rafts contain cholesterol and act as signalling platforms by clustering proteins and receptors to enhance signal transduction and membrane trafficking. Interestingly, Notch ligand activity is modulated by GSLs membrane composition in *Drosophila*. Furthermore, studies in mammals demonstrated that suppression

of glucosylceramide synthase, a key enzyme in GSL production, lead to reduced Notch activation. Linking the observations from our scRNAseq experiments, as well as the proposed role of ACBD3 in influencing brain development in COG5 patients, we hypothesize that Notch signalling pathway is also affected by the decrease in the ganglioseries GSL.
Interestingly, the signalling pathways that we observed to be altered from our scRNAseq data (BMP, FGF, EGF, Wnt, IGF and Notch) have been reported to be influenced by lipid rafts and GSL, with alterations in the lipid rafts composition being associated with changes in growth-factor receptor behaviour and differentiation outcomes. We can thus hypothesize a convergent regulation of several signalling pathways linked to their trafficking defects, their sorting, and decreased levels in ganglioseries GSLs that in turn impair lipid rafts assembly and formation. This prompt to an indirect effect of GSLs on fate determination in the context of brain development. Furthermore, GSL are known to mediate apical sorting and help maintaining apicobasal polarity. It is thus tempting to speculate that alteration in the composition of GSLs has implications on the maintenance of the correct polarity and protein sorting that could further explain the defects that we observe.

Conclusions

In this work, we have here identified a link between the cell biology of Golgi apparatus and its influence on brain development. We think we have proven that mutations on components of the GA machinery, such as COG5, cause defects in the correct sequence and timing of NPCs occurrence, in turn effecting also the neuronal population.
In the attempt to gain mechanistic insights into the interplay between the GA and cell fate, we showed that the Notch pathway is affected in our COG5-CDG, affecting NPCs progeny identity and abundance.
Our working hypothesis is that GA structural impairments lead to defects in trafficking and sorting of fate and polarity determinants affecting the outcome of cell division. Furthermore, data on ACBD3 further support the existence of alterations on the trafficking dynamics, differentially caused by COG5 mutation or complete absence. Finally, we describe a selective effect on sialylated lipids as a consequence of COG5 mutation.
Collectively, we believe we have contributed to gain insights into the relevance of Golgi apparatus in brain development.

APPENDIX

Protocol development for cryopreservation of human brain organoids

Introduction

Organoids represent nowadays a widely used system to model organogenesis and diseases in vitro. Compared to 2D model systems, organoids allow to recapitulate the 3D structure that confers the complexity of an organ and tissue, without the ethical concerns of using primary human tissue (Camp et al. 2015).

Different organs growth and functionality can be efficiently modeled and recapitulated using specific organoid protocols (Agboola et al. 2021; Lancaster and Knoblich 2014; Qian et al. 2020). Organoids are in fact crucial to reconstruct the developmental history of an organ, as in the case of brain organoids that are widely used to study neurodevelopment of the whole brain or of specific brain regions. Furthermore they are used as tools for studying diseases and testing drugs on more complex in vitro systems.

Though incredibly powerful organoids need time to grow, thus affecting the experimental rate of the user. To overcome this limitation several protocols for organoid cryopreservation have been developed that allow to store organoids for medium to long amout of time, thus allowing to have a storage of samples for the different analysis to be performed.

Brain organoids are more difficult to cryopreserve because of their very complex architecture that needs to be maintained in order to have functional brain organoids even after thawing. Furthermore neurons cannot be replaced upon death, that eventually happens during the thawing process.

Neocortex develops from two different classes of neural progenitor cells, apical progenitors and basal progenitors. These cells are able to proliferate to form the pool of cells necessary to sustain the formation of the whole thickness of the neocortex. Apical progenitors, the first to appear during brain development, will start differentiationg during mid neurogenesis into basal progenitors that will then give rise to most of the neurons of the 6-layered cortical plate. Brain organoids are capable of recapitulating these developmental steps forming structures called ventricles. In these ventricles APs and BPs are nicely organized in two regions, the ventricular zone and the subventricular zone, as in human brain development and basally there will be the neurons. It is thus crucial to ensure that the cryopreservation maintains this structure to allow thawed organoids to recover and to keep on developing the organoid and the neurons starting from the neural progenitor cells.

One cryopreservation protocol has been recently published by Xue and colleagues (Xue et al. 2024), who successfully managed to use MEDY to cryopreserve brain organoids without losing their internal structure.

Here we propose another protocol that makes use of mFreSR to cryopreserve organoids at different ages and then successfully recover them after thawing. This protocol allowed us to maintain the structural integrity of the ventricles within the organoid and to use this model system to form 2D cultures of viable neurons and NPCs.

Materials and methods

Organoids

Human brain organoids are generated from WTC11 iPSCs following Lancaster et al. protocol (2014) with some modifications. Briefly, iPSC at 70-80% of confluency were detached with Accutase (Sigma) for 5 minutes at 37°C; 2 mL of mTeSR1 were added to detach and resuspend in single cells. Cells were centrifuged for 5 minutes at 300g and resuspended in 1mL of mTeSR1 supplemented with RI (Tebu-bio srl). Cells were then counted and 9000 cells per well of a U-bottom 96 well plate were added to mTeSR1 with RI medium. Cells were then seeded adding 200uL of suspension to each well of the 96 well plate to form Embryoid bodies (EBs). Media change was done every other day using mTeSR1 without RI. At day 4, medium was changed to Neural induction medium (NIM DM-VitA was prepared with DMEM F12 (Gibco) in ratio 1:1, N2 1:200 (Thermofisher), 1:100 Glutamax (Thermofisher), 1ug/mL of heparin, 0.5% of MEM NEAA (Sigma) and 1:100P/S) with a volume of 150uL per well. Media change was done every other day. At day 7 the EBs were embedded in Geltrex droplets and put in 6cm petri dishes in Differentiation medium without Vitamin A (DM-VitA was prepared with DMEM F12 and Neurobasal (Gibco) in ratio 1:1, B27 -VitA 1:100 (Thermofisher), N2 1:200, 1:100 Glutamax, 2.5ug/mL insulin (Sigma), 50uM 2-mercaptoethanol (Merck) and 0.5% of MEM NEAA and 1:100 P/S). Media change was done every other day until day 13 when the embedded Ebs were transferred in DM+VitA (DM-VitA was prepared with DMEM F12 and Neurobasal in ratio 1:1, B27 +VitA 1:100, N2 1:200, 1:100 Glutamax, 2.5ug/mL insulin, 50uM 2-mercaptoethanol and 0.5% of MEM NEAA and 1:100P/S). Organoids were then kept in culture until the desired age in shaking at 70rpm at 37°C.

Cryopreservation protocol

Human brain organoids are collected and added to a 15mL falcon tube and let soaking to the bottom of the falcon. Organoids are then washed once in PBS to remove the medium and all leftover media is removed. If difficult to remove a 30s centrifugation at 300g can be used. Organoids are resuspended in 500uL of mRfreSR and added to a cryovial. A 500uL to 1mL of mFreSR are added to each cyovial, basing on the amount of organoids per each cryovial. Organoids are finally put at -80° following maintenance in liquid nitrogen.

Thawing cryopreserved organoids

Cryovials are thawed for 1 minute in waterbath at 37°C and the organoids are collected by adding up to 1mL of warm DMEM F12 to the cryovial and then transferring the organoids with a cut tip of a P1000 pipette into a 15mL falcon tube. A brief centrifuge (30s at 300xg) allows to completely discard leftover cryopreservation medium. Organoids are finally added to a petri dish with organoids medium. The medium can change accordingly to the stage the organoids were at when cryopreserved. For the development of his protocol DM+VitA medium was used.

Organoids dissociation

For organoids dissociation MACS neural tissue dissociation kit from Milteny was used, following manifacturer's instructions. Briefly, 200uL of enzyme P for 1-3 organoids was used and organoids were incubated for maximum of 30 minutes in waterbath at 37°C. At the end of the incubation dissociated tissue was added with 6uL of enzyme A to stop the reaction and harsh pipetting for up to 20 times was used to fully dissociate the organoids. A 70um cell strainer was used to filter out the undissociated debris and the filtered cells were pelleted by centrifugating at 300g for 5 minutes. Finally the pellet was resuspended in neuronal medium (Neurobasal, 2,5% FBS, B27 1X, L-glutamine (2mM) and P/S 1X). Cells were counted and plated on pre coated coverslips at a variable concentration, from 150 000 cells/well of a 6 well plate up to 500000 cells/well. If instead plating dissociated neural progenitors StemCell Neural Progenitors medium was used.

Fixation, embedding, and sectioning of microinjected organoids

All slices were collected in PBS and stored at 4°C for subsequent immunofluorescence staining. For cryosectioning, organoid slices were infiltrated with 30% sucrose at 4°C overnight prior to embedding in TissueTek tissue freezing medium (Leica Biosystems, Germany). 20µm-thick sections were cut using a cryostat (Leica Biosystems) and resulting sections were stored at -20°C for further processing.

Immunofluorescence

Cryosections were processed for IF staining as follows. Sections were dried for 5 min in a chemical hood then washed twice with 1X PBS, followed by permeabilization with 0.5% Triton-X100 (Sigma) in PBS for 30 min. Subsequently, sections were incubated with blocking solution (10% Gelatin, in 0.3% TritonX-100/PBS) for 1 h at room temperature in a humidified chamber. Primary antibodies diluted in blocking solution were incubated with the sections overnight at 4°C, followed by washing 5 times for 5 min each time with PBS. Sections were then incubated with secondary antibodies diluted in blocking solution with DAPI as nuclear counterstain for 1 h at room temperature followed by washing for 5 times 5 min each time. For EdU labeled organoids, EdU was added to the culture medium for 1h before fixation. For processing of the slices after the immunofluorescence protocol, Click-iT EdU cell proliferation kit was used following manifacturer's protocol. Briefly, after the last wash in PBS, the slices were fixed in PFA 4% for 15 minutes, following by BSA 3% washes. Slices were then incubated with Triton 0.5% for 20 minutes and then washed again in BSA 3%. The 1X lick-iT EdU reaction mix was then added to the slices for 45 minutes. Followed an incubation with DAPI (1:1000) for 15 minutes and PBS washes before mounting with Mowiol.

For immunofluorescence staining on cells permeabilization with Triton 0.3% in PBS for 10 minutes was done, followed by 2h incubation with primary antobodies at RT. Cells were then washed 3 times for 5 minutes each in PBS and the secondary antibodies were added for 1h at RT. Cells were washed in PBS and, if on coverslips, the sample was mounted with Mowiol.

A complete list of all primary and secondary antibodies used together with corresponding concentrations are listed in table 2.

Antibodies		
Goat anti SOX2 polyclonal antibody (1:200)	BioTechne	AF2018
Rabbit anti Ki67 polyclonal antibody (1:200)	Abcam	ab15580
Rabbit anti TBR2 polyclonal antibody (1:200)	Abcam	ab261913
Mouse Anti-tubulin b 3 (TUJ1) (1:500)	BioLegend	801202
Mouse anti Arl13b (1:400)	Proteintech Group	66739-1-IG
Rabbit Anti-HOPX (1:200)	SIGMA	HPA030180
Mouse anti Nestin monoclonal antibody (10C2) (1:200)	Thermofisher	MA1-110
Rabbit Anti-phospho-Histone H3 (Ser10) Antibody (1:200)	SIGMA MERCK	06-570
Donkey anti-Goat IgG (H+L) Highly Cross-Adsorbed Secondary Antibody, Alexa Fluor™ Plus 488 (1:500)	Invitrogen™/Thermofisher	A32814
Donkey anti-Goat IgG (H+L) Highly Cross-Adsorbed Secondary Antibody, Alexa Fluor™ Plus 555 (1:500)	Invitrogen™/Thermofisher	A32816
Donkey anti-Goat IgG (H+L) Highly Cross-Adsorbed Secondary Antibody, Alexa Fluor™ Plus647 (1:500)	Invitrogen™/Thermofisher	A32849
Donkey anti-Rabbit IgG (H+L) Highly Cross-Adsorbed Secondary Antibody, Alexa Fluor™ Plus 647 (1:500)	Invitrogen™/Thermofisher	A32795
Donkey anti-Rabbit IgG (H+L) Highly Cross-Adsorbed Secondary Antibody, Alexa Fluor™ Plus 555 (1:500)	Invitrogen™/Thermofisher	A32794
Donkey anti-Rabbit IgG (H+L) Highly Cross-Adsorbed Secondary Antibody, Alexa Fluor™ Plus 488 (1:500)	Invitrogen™/Thermofisher	A32790

Donkey anti-Mouse IgG (H+L) Highly Cross-Adsorbed Secondary Antibody, Alexa Fluor™ Plus 647 (1:500)	Invitrogen™/Thermofisher	A32787
Donkey anti-Mouse IgG (H+L) Highly Cross-Adsorbed Secondary Antibody, Alexa Fluor™ Plus 555 (1:500)	Invitrogen™/Thermofisher	A32773
Donkey anti-Mouse IgG (H+L) Highly Cross-Adsorbed Secondary Antibody, Alexa Fluor™ Plus 488 (1:500)	Invitrogen™/Thermofisher	A32766

Table 2. Antibodies used for protocol set up.

Preliminary Results

Characterization of thawed organoids

To validate our protocol we first assessed whether the internal brain organoid structure could be maintained despite the freezing and thawing process (Fig. 39A-B). We stained for DAPI organoids cryopreserved at d33 then thawed and kept in culture until day 41 and we observed that multiple ventricular structures were present inside the organoid. This, combined with the observation on Sox2+ cells suggests that the freezing and thawing process allows neural progenitor cells to survive and to maintain their structural organization into ventricles.

We then also stained for other cell types that have been reported to be present in d41 organoids, such as neurons and intermediate progenitors Tbr2+. Indeed, we could observe Tbr2+ cells around the ventricles with the expected position and organization in the putative SVZ as well as layers of TuJ1+ neurons in the basal most part of the ventricle. These results, though still preliminary, point at the possibility to efficiently cryopreserve human brain organoids without losing the structural integrity and cellular organization within each ventricle.

Furthermore, we also stained for PH3 to label cycling cells, to address the question whether the freezing and thawing process could impair the ability of NPCs to proliferate and self-renew. Interestingly we observed PH3+ cycling progenitors meaning that the protocol doesn't affect the capability of APs to get into cell cycle (Fig. 39B). This is also consistent with the fact that the more time we kept the organoids in culture, the more they grew (data not shown). It would be interesting to pursue further analysis and investigate on the growth of the ventricles over multiple timepoints successive to the thawing.

We also observed that the ventricles structure was better preserved when the organoids underwent cryopreservation at earlier stages. In fact, when examining older organoids that had been cryopreserved, it was more difficult to find ventricles within the thawed organoid. This is consistent with the fact that the NPCs populations are decreased with increased age of the organoid, in older organoids less progenitors can sustain the regrowth of the ventricles and of the whole organoid, replacing cells that died during the freezing-thawing cycle.

However, despite the difficulties in finding ventricles withing older thawed organoids, when labelling them with EdU and co staining with PH3 at d60, it was possible to observe the presence of cells committed to cell cycle, at least in S phase, suggesting that still cycling progenitors are present even at older timepoints (Fig. 39C). We cannot exclude, given the lower number of d60 organoids that we have analysed that the paucity of found ventricles is because of organoid specific features of technical reasons.

Then, we also examined the thawed organoids for Golgi apparatus, given the interest for my thesis project and we observed that Golgi maintained the expected localization and pattern within the observed ventricles, pointing us even more to believe that our protocol can efficiently maintain the structural, organizational and intracellular architecture of all the cell types that populate our brain organoids.

Finally, we stained for HopX+ basal radial glia cells, investigating at two different timepoints, d50 and d73. With the organoid protocol that we are using few HopX+ cells appear only at later stages, around d70. Thus, we investigated whether the cryopreserved organoids could grow and form late cell types. We observed that Hopx staining was negative in d50 thawed organoids, while they were present in d73 thawed organoids. Of course, these are preliminary data and we can't exclude an organoid related difference, however collecting together all of our data, we firmly believe that our protocol allows organoids to grow when thawed and maintained in culture.

Neurons from cryopreserved organoids

To understand whether the neurons inside the thawed organoids were living cells and whether they could be maintained in culture, we dissociated the thawed organoid after a short period of recovery and we plated the dissociated cells in a neuronal media. We then stained for general neuronal markers such as TuJ1 and Map2 for the dendrites and we could recognize that neuronal culture from dissociated organoids at different timepoints could be successfully maintained for up to 28 days (Fig. 40A).

On a similar investigation line, we also wanted to check more closely the neural progenitor cells. We thus dissociated the thawed organoids and plated NPCs using a media-based selection. We stained the 2D NPCs cultures for fate markers such as Pax6 and SOX2 for APs, Tbr2 for IPs and TuJ1 for newly born neurons (Fig. 40B-C). We assessed not only the presence of NPCs in culture but also their ability to differentiate and form neurons that were positive for Tuj1 staining. We finally stained for intracellular architecture related markers such as Arl13b for the cilium and Nestin and we could find all these structures on the plated NPCs (Fig. 40D).

Taken together these results support the fact that cell inside the thawed organoids are actually healthy and can be maintained as in the case of neurons, and be able to replicate and differentiate as in the case of NPCs.

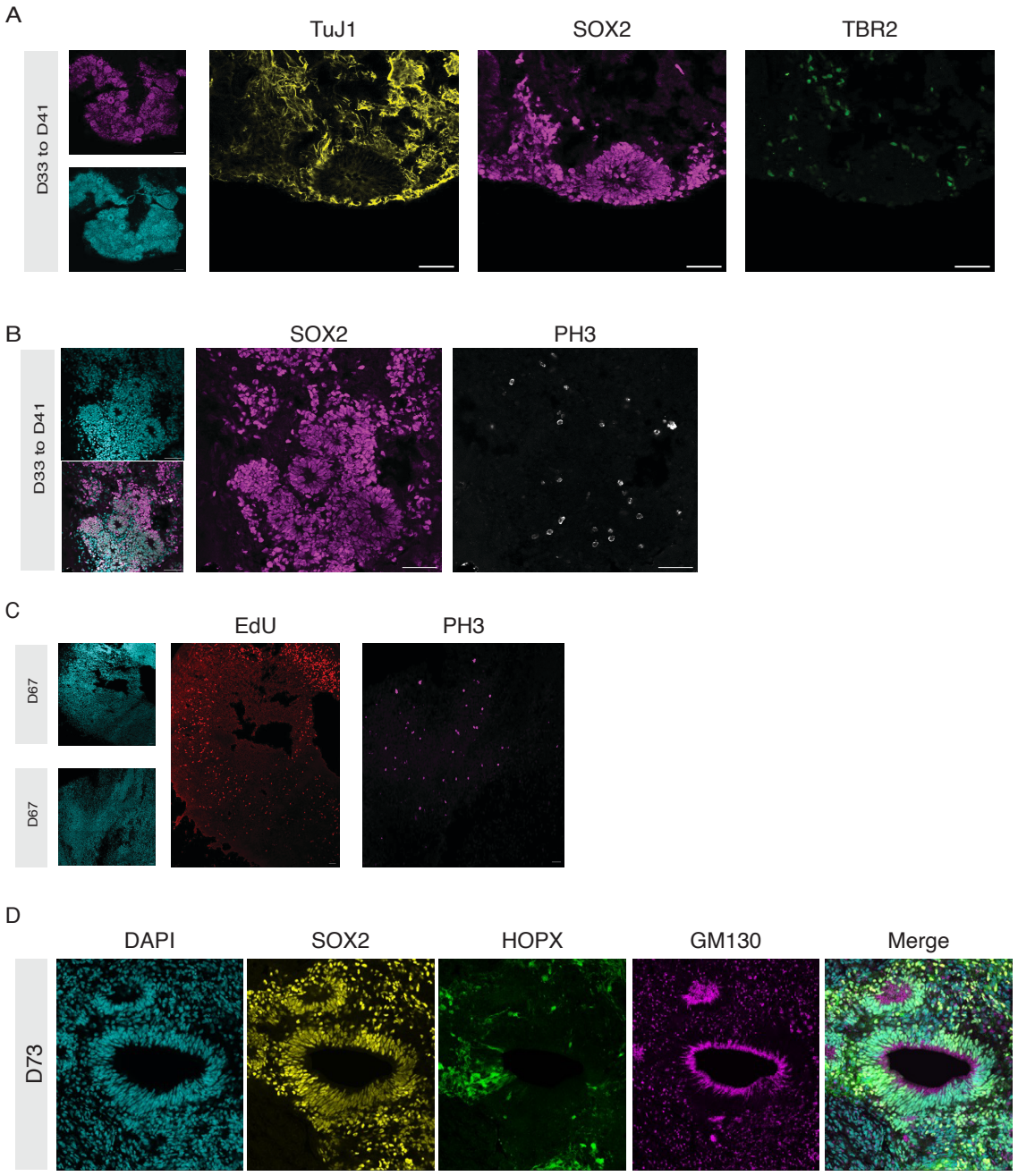


Figure 39. Cryopreserved organoids maintain the internal structure and cellular composition after thawing.

(A) Immunofluorescence staining of organoids cryopreserved at d33, thawed and cultured until d41. Tuj1 for neurons (yellow), Sox2 for APs (magenta) and Tbr2 for BPs (green). (B) The internal ventricles are maintained after thawing and cycling cells repopulate the ventricle (Sox2 in magenta, PH3 in grey). (C) d67 thawed organoids show less structural integrity, but cycling cells are present (EdU in red, PH3 in magenta). (C) d73 organoid show smaller ventricles, with Sox2+ APs (yellow) and Hopx+ bRGs (green); the intracellular organization of Golgi apparatus is maintained in thawed organoids (GM130, magenta).

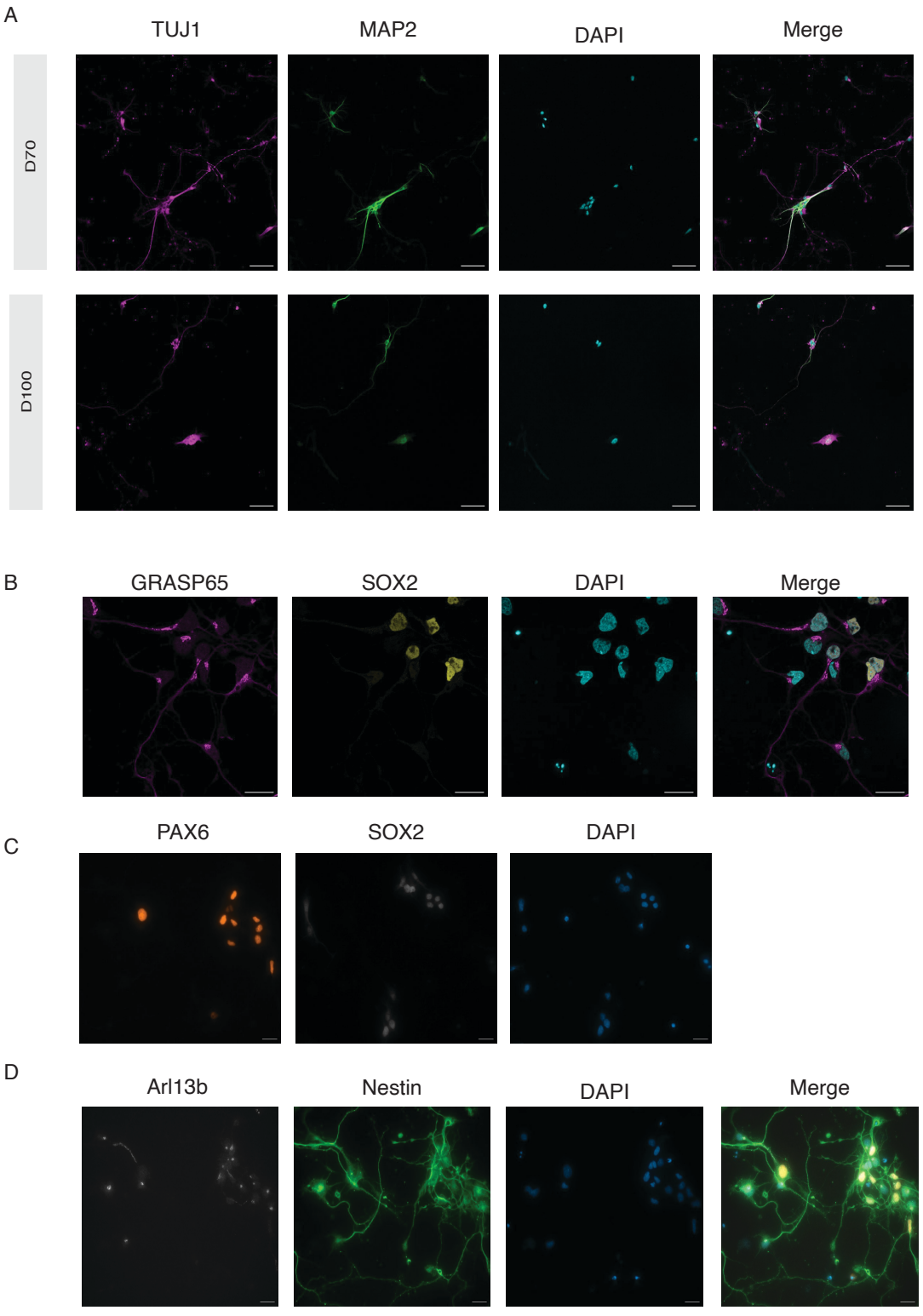


Figure 40. Cryopreserved organoids can be dissociated into NPCs and neurons.

(A) IF showing neurons from dissociated organoids at d70 and d100; staining for TuJ1 (magenta), MAP2 (green) and DAPI (cyan) allowed to assess the neuronal identity of the plated cells. (B-C) NPCs dissociated from cryopreserved organoids. Staining for GRASP65 (GA, magenta), Sox2 (APs, yellow in B and grey in C), Pax6 (APs in red). (D) IF staining of NPCs; markers used Arl13b (cilium, grey), Nestin (green). Scale bar 20μm.

Conclusions and discussion

The advent of human brain organoids allowed neurodevelopmental studies to raise and to tackle fundamental questions on how human brain forms and functions.

One of the limitations of human brain organoids protocol that are available to date is represented by the relative long amount of time required for the organoids to grow and thus to form structures such as brain ventricular-like structures. Moreover, for some experimental purposes it is necessary to have multiple biological replicates at a time, which can be complicated for human brain organoid maintenance reasons. Furthermore the possibility of creating biobanks of human brain organoids, similar to the existent ones for human primary tissue pave the way to studies on how to preserve the organoids in a way to always have material available for further studies.

While working on the current protocol, Xue and colleagues (Xue et al. 2024), successfully used a non commericial freezing medium called MEDY to cryopreserve brain organoids without losing their internal structure.

Here we propose a quick protocol that makes use of a commericial freezing medium, mFreSR, to cryopreserve human brain organoids maintaining the internal architecture and cellular composition.

We first characterized cryopreserved organoids using fate markers for NPCs and neurons and we observed that our thawed organoids maitained the cellular composition and localization as in non cryopreserved organoids. Furthermore the organoid internal ventricle-like structure was detectable when observing DAPI and SOX2 and staining. Thus our protocol allows to efficiently thaw the organoids, let them grow and observe internal structures similar to non cryopreserved organoids.

The presence ofcycling NPCs suggested that those organoids could grow and form cell types that usually appear at later timepoints, as in the case for HopX+ basal radial glia cells, that were not detected at d50 thawed organoids, but were present in d73 thawed organoids, suggesting that organoids not only mature, but NPCs that survived the thaweing process are healthy cells maintaining their proliferation and differentiation potential.

Apical progenitors have a very peculiar polarization of Golgi apparatus, being only present in the apical process of these cells; this feature that is an hallmark of APs identity is not impaired by the cryopreservation protocol. Thus, this pipeline allowed us not only to store human brain organoids, but also to thaw them without losing the main feauters of the organoid itself and of its component cells.

Finally we also assessed whether these organoids, when dissociated, could allow the creation of a 2D neuronal or NPCs culture. Indeed we observed that neurons were present and were maintained in a healthy state for up to 28 days. Also NPCs could be maintained in culture and did't lose the ability to proliferate and differentiate as they normally do in a more complex architecture such as that of the organoid.

In conclusions, these preliminary data suggest that the cryopreservation protocol that we developed have an enormous potential for multiple applications, from allowing to process experimental replicates together, to creating human brain organoids biobanks.

Bibliography

Agboola, Oluwafemi Solomon, Xinglin Hu, Zhiyan Shan, Yanshuang Wu, and Lei Lei. 2021. "Brain Organoid: A 3D Technology for Investigating Cellular Composition and Interactions in Human Neurological Development and Disease Models in Vitro." Stem Cell Research & Therapy 12 (1): 430. https://doi.org/10.1186/s13287-021-02369-8.

Alegria, Andrew D, Amey S Joshi, Jorge Blanco Mendana, et al. 2024. "High-Throughput Genetic Manipulation of Multicellular Organisms Using a Machine-Vision Guided Embryonic Microinjection Robot." GENETICS 226 (4): iyae025. https://doi.org/10.1093/genetics/iyae025.

Altassan, Ruqaiah, Romain Péanne, Jaak Jaeken, et al. 2019. "International Clinical Guidelines for the Management of Phosphomannomutase 2-congenital Disorders of Glycosylation: Diagnosis, Treatment and Follow Up." Journal of Inherited Metabolic Disease 42 (1): 5–28. https://doi.org/10.1002/jimd.12024.

Appenzeller-Herzog, Christian, and Hans-Peter Hauri. 2006. "The ER-Golgi Intermediate Compartment (ERGIC): In Search of Its Identity and Function." Journal of Cell Science 119 (11): 2173–83. https://doi.org/10.1242/jcs.03019.

Arai, Yoko, and Elena Taverna. 2017. "Neural Progenitor Cell Polarity and Cortical Development." Frontiers in Cellular Neuroscience 11 (December): 384. https://doi.org/10.3389/fncel.2017.00384.

Ayala, Inmaculada, and Antonino Colanzi. 2017. "Mitotic Inheritance of the Golgi Complex and Its Role in Cell Division." Biology of the Cell 109 (10): 364–74. https://doi.org/10.1111/boc.201700032.

Bagley, Joshua A, Daniel Reumann, Shan Bian, Julie Lévi-Strauss, and Juergen A Knoblich. 2017. "Fused Cerebral Organoids Model Interactions between Brain Regions." Nature Methods 14 (7): 743–51. https://doi.org/10.1038/nmeth.4304.

Bailey Blackburn, Jessica, Irina Pokrovskaya, Peter Fisher, Daniel Ungar, and Vladimir V. Lupashin. 2016. "COG Complex Complexities: Detailed Characterization of a Complete Set of HEK293T Cells Lacking Individual COG Subunits." Frontiers in Cell and Developmental Biology 4 (March). https://doi.org/10.3389/fcell.2016.00023.

Banworth, Marcellus J., and Guangpu Li. 2018. "Consequences of Rab GTPase Dysfunction in Genetic or Acquired Human Diseases." Small GTPases 9 (1–2): 158–81. https://doi.org/10.1080/21541248.2017.1397833.

Blackburn, Jessica B., Zinia D'Souza, and Vladimir V. Lupashin. 2019. "Maintaining Order: COG Complex Controls Golgi Trafficking, Processing, and Sorting." FEBS Letters 593 (17): 2466–87. https://doi.org/10.1002/1873-3468.13570.

Bonifacino, Juan S., and Jennifer Lippincott-Schwartz. 2003. "Coat Proteins: Shaping Membrane Transport." Nature Reviews Molecular Cell Biology 4 (5): 409–14. https://doi.org/10.1038/nrm1099.

Breitling, J., and M. Aebi. 2013. "N-Linked Protein Glycosylation in the Endoplasmic Reticulum." Cold Spring Harbor Perspectives in Biology 5 (8): a013359–a013359. https://doi.org/10.1101/cshperspect.a013359.

Breuza, Lionel, Regula Halbeisen, Paul Jenö, et al. 2004. "Proteomics of Endoplasmic Reticulum-Golgi Intermediate Compartment (ERGIC) Membranes from Brefeldin A-Treated HepG2 Cells Identifies ERGIC-32, a New Cycling Protein That Interacts with Human Erv46." Journal of Biological Chemistry 279 (45): 47242–53. https://doi.org/10.1074/jbc.M406644200.

Brunet, Stephanie, and Michael Sacher. 2014. “Are All Multisubunit Tethering Complexes Bona Fide Tethers?” Traffic 15 (11): 1282–87. https://doi.org/10.1111/tra.12200.

Buckley, Clare E., and Daniel St Johnston. 2022. “Apical–Basal Polarity and the Control of Epithelial Form and Function.” Nature Reviews Molecular Cell Biology 23 (8): 559–77. https://doi.org/10.1038/s41580-022-00465-y.

Budday, Silvia, Paul Steinmann, and Ellen Kuhl. 2015. “Physical Biology of Human Brain Development.” Frontiers in Cellular Neuroscience 9 (July). https://doi.org/10.3389/fncel.2015.00257.

Camp, J. Gray, Farhath Badsha, Marta Florio, et al. 2015. “Human Cerebral Organoids Recapitulate Gene Expression Programs of Fetal Neocortex Development.” Proceedings of the National Academy of Sciences 112 (51): 15672–77. https://doi.org/10.1073/pnas.1520760112.

Chang, Irene J., Miao He, and Christina T. Lam. 2018. “Congenital Disorders of Glycosylation.” Annals of Translational Medicine 6 (24): 477–477. https://doi.org/10.21037/atm.2018.10.45.

Chow, Yu Ting, Shuxun Chen, Ran Wang, et al. 2016. “Single Cell Transfection through Precise Microinjection with Quantitatively Controlled Injection Volumes.” Scientific Reports 6 (1): 24127. https://doi.org/10.1038/srep24127.

Colanzi, Antonino, Christine Suetterlin, and Vivek Malhotra. 2003. “Cell-Cycle-Specific Golgi Fragmentation: How and Why?” Current Opinion in Cell Biology 15 (4): 462–67. https://doi.org/10.1016/S0955-0674(03)00067-X.

De Bie, P, P Muller, C Wijmenga, and L W J Klomp. 2007. “Molecular Pathogenesis of Wilson and Menkes Disease: Correlation of Mutations with Molecular Defects and Disease Phenotypes.” Journal of Medical Genetics 44 (11): 673–88. https://doi.org/10.1136/jmg.2007.052746.

De Los Ángeles Juricic Urzúa, María, Javiera Gallardo Rojas, Andrés Couve Correa, Mauricio Cerda, Steffen Härtel Gründler, and Carolina González-Silva. 2021. “The Dendritic Ergic: Microtubule and Actin Cytoskeletons Mediate Stop-and-Go Movement of Mobile Carriers Between Stable Structures.” Preprint, Cell Biology, April 2. https://doi.org/10.1101/2021.03.31.437880.

Del Rio, J. A. 2000. “Developmental History of the Subplate and Developing White Matter in the Murine Neocortex. Neuronal Organization and Relationship with the Main Afferent Systems at Embryonic and Perinatal Stages.” Cerebral Cortex 10 (8): 784–801. https://doi.org/10.1093/cercor/10.8.784.

Dingle, Yu-Ting L., Molly E. Boutin, Anda M. Chirila, et al. 2015. “Three-Dimensional Neural Spheroid Culture: An In Vitro Model for Cortical Studies.” Tissue Engineering Part C: Methods 21 (12): 1274–83. https://doi.org/10.1089/ten.tec.2015.0135.

Dinter, André, and E. G. Berger. 1998. “Golgi-Disturbing Agents.” Histochemistry and Cell Biology 109 (5–6): 571–90. https://doi.org/10.1007/s004180050256.

D’Souza, Zinia, Farhana S. Taher, and Vladimir V. Lupashin. 2020. “Golgi inCOGnito: From Vesicle Tethering to Human Disease.” Biochimica et Biophysica Acta (BBA) - General Subjects 1864 (11): 129694. https://doi.org/10.1016/j.bbagen.2020.129694.

D’Souza-Schorey, Crislyn, and Philippe Chavrier. 2006. “ARF Proteins: Roles in Membrane Traffic and Beyond.” Nature Reviews Molecular Cell Biology 7 (5): 347–58. https://doi.org/10.1038/nrm1910.

Esmail, Sally, and Morris F. Manolson. 2021. “Advances in Understanding N-Glycosylation Structure, Function, and Regulation in Health and Disease.” European Journal of Cell Biology 100 (7–8): 151186. https://doi.org/10.1016/j.ejcb.2021.151186.

Ferent, Julien, Donia Zaidi, and Fiona Francis. 2020. “Extracellular Control of Radial Glia Proliferation and Scaffolding During Cortical Development and Pathology.” Frontiers in Cell and Developmental Biology 8 (October): 578341. https://doi.org/10.3389/fcell.2020.578341.

Ferreira, Carlos R., Zhi-Jie Xia, Aurélie Clément, et al. 2018. “A Recurrent De Novo Heterozygous COG4 Substitution Leads to Saul-Wilson Syndrome, Disrupted Vesicular Trafficking, and Altered Proteoglycan Glycosylation.” The American Journal of Human Genetics 103 (4): 553–67. https://doi.org/10.1016/j.ajhg.2018.09.003.

Fietz, Simone A, and Wieland B Huttner. 2011. “Cortical Progenitor Expansion, Self-Renewal and Neurogenesis—a Polarized Perspective.” Current Opinion in Neurobiology 21 (1): 23–35. https://doi.org/10.1016/j.conb.2010.10.002.

Fish, Jennifer L., Colette Dehay, Henry Kennedy, and Wieland B. Huttner. 2008. “Making Bigger Brains–the Evolution of Neural-Progenitor-Cell Division.” Journal of Cell Science 121 (17): 2783–93. https://doi.org/10.1242/jcs.023465.

Florio, Marta, and Wieland B. Huttner. 2014. “Neural Progenitors, Neurogenesis and the Evolution of the Neocortex.” Development 141 (11): 2182–94. https://doi.org/10.1242/dev.090571.

Florio, Marta, Albert Mareike, Taverna Elena, Namba Takashi, Brandl Holger, Lewitus Eric, Haffner Christiane, Skyes Alex, Paabo Svante and Huttner Wieland B. 2015. "Human-specific gene ARHFAP11B promotes basal progenitor amplification and neocortex expansion". Science DOI: 10.1126/science.aaa1975.

Flynn, Kaitlyn, Candice Feben, Lindiwe Lamola, et al. 2021. “Ending a Diagnostic Odyssey—The First Case of Takenouchi–Kosaki Syndrome in an African Patient.” Clinical Case Reports 9 (4): 2144–48. https://doi.org/10.1002/ccr3.3966.

Fotso, Pierre, Yulia Koryakina, Oleksandra Pavliv, Arnold B. Tsiomenko, and Vladimir V. Lupashin. 2005. “Cog1p Plays a Central Role in the Organization of the Yeast Conserved Oligomeric Golgi Complex.” Journal of Biological Chemistry 280 (30): 27613–23. https://doi.org/10.1074/jbc.M504597200.

Foulquier, François, Daniel Ungar, Ellen Reynders, et al. 2007. “A New Inborn Error of Glycosylation Due to a Cog8 Deficiency Reveals a Critical Role for the Cog1–Cog8 Interaction in COG Complex Formation.” Human Molecular Genetics 16 (7): 717–30. https://doi.org/10.1093/hmg/ddl476.

Francisco, Rita, Sandra Brasil, Joana Poejo, et al. 2023. “Congenital Disorders of Glycosylation (CDG): State of the Art in 2022.” Orphanet Journal of Rare Diseases 18 (1): 329. https://doi.org/10.1186/s13023-023-02879-z.

Freeze, Hudson H., Jaak Jaeken, and Gert Matthijs. 2022. “CDG or Not CDG.” Journal of Inherited Metabolic Disease 45 (3): 383–85. https://doi.org/10.1002/jimd.12498.

Freeze, Hudson H., Jessica X. Chong, Michael J. Bamshad, and Bobby G. Ng. 2014. “Solving Glycosylation Disorders: Fundamental Approaches Reveal Complicated Pathways.” The American Journal of Human Genetics 94 (2): 161–75. https://doi.org/10.1016/j.ajhg.2013.10.024.

Galea, George, Karolina Kuodyte, Muzamil M. Khan, et al. 2022. “Spatiotemporal Dynamics of RAD51C between the Golgi and Nucleus Regulates Homologous Recombination and Genomic Stability.” Preprint, Cell Biology, October 17. https://doi.org/10.1101/2022.10.17.512236.

Gandini, Rosaria, Tom Reichenbach, Tien-Chye Tan, and Christina Divne. 2017. “Structural Basis for Dolichylphosphate Mannose Biosynthesis.” Nature Communications 8 (1): 120. https://doi.org/10.1038/s41467-017-00187-2.

Gavilan, Maria P, Pablo Gandolfo, Fernando R Balestra, Francisco Arias, Michel Bornens, and Rosa M Rios. 2018. “The Dual Role of the Centrosome in Organizing the Microtubule Network in Interphase.” EMBO Reports 19 (11): e45942. https://doi.org/10.15252/embr.201845942.

Gillingham, Alison K, and Sean Munro. 2003. “Long Coiled-Coil Proteins and Membrane Traffic.” Biochimica et Biophysica Acta (BBA) - Molecular Cell Research 1641 (2–3): 71–85. https://doi.org/10.1016/S0167-4889(03)00088-0.

Glick, B. S., and A. Luini. 2011. “Models for Golgi Traffic: A Critical Assessment.” Cold Spring Harbor Perspectives in Biology 3 (11): a005215–a005215. https://doi.org/10.1101/cshperspect.a005215.

Glotzer, Michael, and Anthony A Hyman. n.d. The Importance of Being Polar.

Götz, Magdalena, and Wieland B. Huttner. 2005. “The Cell Biology of Neurogenesis.” Nature Reviews Molecular Cell Biology 6 (10): 777–88. https://doi.org/10.1038/nrm1739.

Greig, Luciano Custo, Mollie B. Woodworth, Maria J. Galazo, Hari Padmanabhan, and Jeffrey D. Macklis. 2013. “Molecular Logic of Neocortical Projection Neuron Specification, Development and Diversity.” Nature Reviews Neuroscience 14 (11): 755–69. https://doi.org/10.1038/nrn3586.

Guet, David, Kalpana Mandal, Mathieu Pinot, et al. 2014. “Mechanical Role of Actin Dynamics in the Rheology of the Golgi Complex and in Golgi-Associated Trafficking Events.” Current Biology 24 (15): 1700–1711. https://doi.org/10.1016/j.cub.2014.06.048.

Guillard, Mailys, Yoshinao Wada, Hana Hansikova, et al. 2011. “Transferrin Mutations at the Glycosylation Site Complicate Diagnosis of Congenital Disorders of Glycosylation Type I.” Journal of Inherited Metabolic Disease 34 (4): 901–6. https://doi.org/10.1007/s10545-011-9311-y.

Haenseler, Walther, Stephen N. Sansom, Julian Buchrieser, et al. 2017. “A Highly Efficient Human Pluripotent Stem Cell Microglia Model Displays a Neuronal-Co-Culture-Specific Expression Profile and Inflammatory Response.” Stem Cell Reports 8 (6): 1727–42. https://doi.org/10.1016/j.stemcr.2017.05.017.

Hanus, Cyril, Helene Geptin, Georgi Tushev, et al. 2016. “Unconventional Secretory Processing Diversifies Neuronal Ion Channel Properties.” eLife 5 (September): e20609. https://doi.org/10.7554/eLife.20609.

Harris, James, Giulio Srubek Tomassy, and Paola Arlotta. 2015. “Building Blocks of the Cerebral Cortex: From Development to the Dish.” WIREs Developmental Biology 4 (5): 529–44. https://doi.org/10.1002/wdev.192.

Haynes, Cole M., Eric A. Titus, and Antony A. Cooper. 2004. “Degradation of Misfolded Proteins Prevents ER-Derived Oxidative Stress and Cell Death.” Molecular Cell 15 (5): 767–76. https://doi.org/10.1016/j.molcel.2004.08.025.

He, Mengyuan, Xiangxiang Zhou, and Xin Wang. 2024a. “Glycosylation: Mechanisms, Biological Functions and Clinical Implications.” Signal Transduction and Targeted Therapy 9 (1): 194. https://doi.org/10.1038/s41392-024-01886-1.

He, Mengyuan, Xiangxiang Zhou, and Xin Wang. 2024b. “Glycosylation: Mechanisms, Biological Functions and Clinical Implications.” Signal Transduction and Targeted Therapy 9 (1): 194. https://doi.org/10.1038/s41392-024-01886-1.

Hirata, Tetsuya, Jing Yang, Seita Tomida, et al. 2022. “ER Entry Pathway and Glycosylation of GPI-Anchored Proteins Are Determined by N-Terminal Signal Sequence and C-Terminal GPI-Attachment Sequence.” Journal of Biological Chemistry 298 (10): 102444. https://doi.org/10.1016/j.jbc.2022.102444.

Hong, Wanjin. 2005. “SNAREs and Traffic.” Biochimica et Biophysica Acta (BBA) - Molecular Cell Research 1744 (2): 120–44. https://doi.org/10.1016/j.bbamcr.2005.03.014.

Jaeken, J., T. Hennet, H. H. Freeze, and G. Matthijs. 2008. “On the Nomenclature of Congenital Disorders of Glycosylation (CDG).” Journal of Inherited Metabolic Disease 31 (6): 669–72. https://doi.org/10.1007/s10545-008-0983-x.

Jaeken, Jaak, Thierry Hennet, Gert Matthijs, and Hudson H. Freeze. 2009. “CDG Nomenclature: Time for a Change!” Biochimica et Biophysica Acta (BBA) - Molecular Basis of Disease 1792 (9): 825–26. https://doi.org/10.1016/j.bbadis.2009.08.005.

Jaeken, Jaak, and Gert Matthijs. n.d. Congenital Disorders of Glycosylation.

Jahn, Reinhard, David C. Cafiso, and Lukas K. Tamm. 2024. “Mechanisms of SNARE Proteins in Membrane Fusion.” Nature Reviews Molecular Cell Biology 25 (2): 101–18. https://doi.org/10.1038/s41580-023-00668-x.

Jahn, Reinhard, and Richard H. Scheller. 2006. “SNAREs — Engines for Membrane Fusion.” Nature Reviews Molecular Cell Biology 7 (9): 631–43. https://doi.org/10.1038/nrm2002.

Janesick, Amanda, Stephanie Cherie Wu, and Bruce Blumberg. 2015. “Retinoic Acid Signaling and Neuronal Differentiation.” Cellular and Molecular Life Sciences 72 (8): 1559–76. https://doi.org/10.1007/s00018-014-1815-9.

Jáñez Pedrayes, Andrea, Daisy Rymen, Bart Ghesquière, and Peter Witters. 2024. “Glycosphingolipids in Congenital Disorders of Glycosylation (CDG).” Molecular Genetics and Metabolism 142 (1): 108434. https://doi.org/10.1016/j.ymgme.2024.108434.

Kalebic, Nereo, Carlotta Gilardi, Barbara Stepien, et al. 2019. “Neocortical Expansion Due to Increased Proliferation of Basal Progenitors Is Linked to Changes in Their Morphology.” Cell Stem Cell 24 (4): 535-550.e9. https://doi.org/10.1016/j.stem.2019.02.017.

Kalebic, Nereo, and Wieland B. Huttner. 2020. “Basal Progenitor Morphology and Neocortex Evolution.” Trends in Neurosciences 43 (11): 843–53. https://doi.org/10.1016/j.tins.2020.07.009.

Kintner, Chris. 2002. “Neurogenesis in Embryos and in Adult Neural Stem Cells.” The Journal of Neuroscience 22 (3): 639–43. https://doi.org/10.1523/JNEUROSCI.22-03-00639.2002.

Kodandaramaiah, Suhasa B, Francisco J Flores, Gregory L Holst, et al. 2018. “Multi-Neuron Intracellular Recording in Vivo via Interacting Autopatching Robots.” eLife 7 (January): e24656. https://doi.org/10.7554/eLife.24656.

Kosodo, Yoichi, Taeko Suetsugu, Masumi Suda, et al. 2011. “Regulation of Interkinetic Nuclear Migration by Cell Cycle-Coupled Active and Passive Mechanisms in the Developing Brain: Mechanisms of Interkinetic Nuclear Migration.” The EMBO Journal 30 (9): 1690–704. https://doi.org/10.1038/emboj.2011.81.

Kyrousi, Christina, Adam C. O’Neill, Agnieska Brazovskaja, et al. 2021. “Extracellular LGALS3BP Regulates Neural Progenitor Position and Relates to Human Cortical

Complexity." Nature Communications 12 (1): 6298. https://doi.org/10.1038/s41467-021-26447-w.

Laguesse, Sophie, Catherine Creppe, Danny D. Nedialkova, et al. 2015. "A Dynamic Unfolded Protein Response Contributes to the Control of Cortical Neurogenesis." Developmental Cell 35 (5): 553–67. https://doi.org/10.1016/j.devcel.2015.11.005.

Lamprecht, Sebastian, Eva Marina Schmidt, Cristina Blaj, et al. 2017. "Multicolor Lineage Tracing Reveals Clonal Architecture and Dynamics in Colon Cancer." Nature Communications 8 (1): 1406. https://doi.org/10.1038/s41467-017-00976-9.

Lancaster, Madeline A, and Juergen A Knoblich. 2014. "Generation of Cerebral Organoids from Human Pluripotent Stem Cells." Nature Protocols 9 (10): 2329–40. https://doi.org/10.1038/nprot.2014.158.

Lee, Byeong Eun, Pann-Ghill Suh, and Jae-Ick Kim. 2021. "O-GlcNAcylation in Health and Neurodegenerative Diseases." Experimental & Molecular Medicine 53 (11): 1674–82. https://doi.org/10.1038/s12276-021-00709-5.

Lehtinen, Maria K., Mauro W. Zappaterra, Xi Chen, et al. 2011. "The Cerebrospinal Fluid Provides a Proliferative Niche for Neural Progenitor Cells." Neuron 69 (5): 893–905. https://doi.org/10.1016/j.neuron.2011.01.023.

Liu, Jianyang, Yan Huang, Ting Li, Zheng Jiang, Liuwang Zeng, and Zhiping Hu. 2021. "The Role of the Golgi Apparatus in Disease (Review)." International Journal of Molecular Medicine 47 (4): 38. https://doi.org/10.3892/ijmm.2021.4871.

Long, K., L. Moss, L. Laursen, L. Boulter, and C. ffrench-Constant. 2016. "Integrin Signalling Regulates the Expansion of Neuroepithelial Progenitors and Neurogenesis via Wnt7a and Decorin." Nature Communications 7 (1): 10354. https://doi.org/10.1038/ncomms10354.

Lui, Jan H., David V. Hansen, and Arnold R. Kriegstein. 2011. "Development and Evolution of the Human Neocortex." Cell 146 (1): 18–36. https://doi.org/10.1016/j.cell.2011.06.030.

Lürick, Anna, Daniel Kümmel, and Christian Ungermann. 2018. "Multisubunit Tethers in Membrane Fusion." Current Biology 28 (8): R417–20. https://doi.org/10.1016/j.cub.2017.12.012.

Malsam, J., and T. H. Sollner. 2011. "Organization of SNAREs within the Golgi Stack." Cold Spring Harbor Perspectives in Biology 3 (10): a005249–a005249. https://doi.org/10.1101/cshperspect.a005249.

Marin-Valencia, Isaac, Gaia Novarino, Anide Johansen, et al. 2018. "A Homozygous Founder Mutation in TRAPPC6B Associates with a Neurodevelopmental Disorder Characterised by Microcephaly, Epilepsy and Autistic Features." Journal of Medical Genetics 55 (1): 48–54. https://doi.org/10.1136/jmedgenet-2017-104627.

Milev, Miroslav P., Megan E. Grout, Djenann Saint-Dic, et al. 2017. "Mutations in TRAPPC12 Manifest in Progressive Childhood Encephalopathy and Golgi Dysfunction." The American Journal of Human Genetics 101 (2): 291–99. https://doi.org/10.1016/j.ajhg.2017.07.006.

Miyata, Shingo, Tatsunori Mizuno, Yoshihisa Koyama, Taiichi Katayama, and Masaya Tohyama. 2013. "The Endoplasmic Reticulum-Resident Chaperone Heat Shock Protein 47 Protects the Golgi Apparatus from the Effects of O-Glycosylation Inhibition." PLoS ONE 8 (7): e69732. https://doi.org/10.1371/journal.pone.0069732.

Mochida, Ganeshwaran H., Muhammad Mahajnah, Anthony D. Hill, et al. 2009. "A Truncating Mutation of TRAPPC9 Is Associated with Autosomal-Recessive

Intellectual Disability and Postnatal Microcephaly." The American Journal of Human Genetics 85 (6): 897–902. https://doi.org/10.1016/j.ajhg.2009.10.027.

Mukhtar, Tanzila, and Verdon Taylor. 2018. "Untangling Cortical Complexity During Development." Journal of Experimental Neuroscience 12 (January): 1179069518759332. https://doi.org/10.1177/1179069518759332.

Nakagawa, Naoki. 2024. "The Neuronal Golgi in Neural Circuit Formation and Reorganization." Frontiers in Neural Circuits 18 (December): 1504422. https://doi.org/10.3389/fncir.2024.1504422.

Nakamura, Nobuhiro. 2010. "Emerging New Roles of GM130, a Cis-Golgi Matrix Protein, in Higher Order Cell Functions." Journal of Pharmacological Sciences 112 (3): 255–64. https://doi.org/10.1254/jphs.09R03CR.

Namba, Takashi, and Wieland B. Huttner. 2017. "Neural Progenitor Cells and Their Role in the Development and Evolutionary Expansion of the Neocortex." WIREs Developmental Biology 6 (1): e256. https://doi.org/10.1002/wdev.256.

Ng, Bobby G., Gege Xu, Nandini Chandy, et al. 2018. "Biallelic Mutations in FUT8 Cause a Congenital Disorder of Glycosylation with Defective Fucosylation." The American Journal of Human Genetics 102 (1): 188–95. https://doi.org/10.1016/j.ajhg.2017.12.009.

Nguyen, Huy, Adam P Ostendorf, Jakob S Satz, et al. 2013. "Glial Scaffold Required for Cerebellar Granule Cell Migration Is Dependent on Dystroglycan Function as a Receptor for Basement Membrane Proteins." Acta Neuropathologica Communications 1 (1): 58. https://doi.org/10.1186/2051-5960-1-58.

Nickel, Walter, and Catherine Rabouille. 2018. "Unconventional Protein Secretion: Diversity and Consensus." Seminars in Cell & Developmental Biology 83 (November): 1–2. https://doi.org/10.1016/j.semcdb.2018.03.007.

Ninagawa, Satoshi, Ginto George, and Kazutoshi Mori. 2021. "Mechanisms of Productive Folding and Endoplasmic Reticulum-Associated Degradation of Glycoproteins and Non-Glycoproteins." Biochimica et Biophysica Acta (BBA) - General Subjects 1865 (3): 129812. https://doi.org/10.1016/j.bbagen.2020.129812.

Noctor, Stephen C, Verónica Martínez-Cerdeño, Lidija Ivic, and Arnold R Kriegstein. 2004. "Cortical Neurons Arise in Symmetric and Asymmetric Division Zones and Migrate through Specific Phases." Nature Neuroscience 7 (2): 136–44. https://doi.org/10.1038/nn1172.

Oka, Toshihiko, Daniel Ungar, Frederick M Hughson, and Monty Krieger. n.d. The COG and COPI Complexes Interact to Control the Abundance of GEARs, a Subset of Golgi Integral Membrane Proteins□D.

Oka, Toshihiko, Eliza Vasile, Marsha Penman, et al. 2005. "Genetic Analysis of the Subunit Organization and Function of the Conserved Oligomeric Golgi (COG) Complex." Journal of Biological Chemistry 280 (38): 32736–45. https://doi.org/10.1074/jbc.M505558200.

Ori-McKenney, Kassandra M., Lily Yeh Jan, and Yuh-Nung Jan. 2012. "Golgi Outposts Shape Dendrite Morphology by Functioning as Sites of Acentrosomal Microtubule Nucleation in Neurons." Neuron 76 (5): 921–30. https://doi.org/10.1016/j.neuron.2012.10.008.

Paprocka, Justyna, Aleksandra Jezela-Stanek, Anna Tylki-Szymańska, and Stephanie Grunewald. 2021. "Congenital Disorders of Glycosylation from a Neurological Perspective." Brain Sciences 11 (1): 88. https://doi.org/10.3390/brainsci11010088.

Paridaen, Judith Tml, and Wieland B Huttner. 2014. “Neurogenesis during Development of the Vertebrate Central Nervous System.” EMBO Reports 15 (4): 351–64. https://doi.org/10.1002/embr.201438447.

Park, Kunyou, Sungeun Ju, Nari Kim, and Seung-Yeol Park. 2021. “The Golgi Complex: A Hub of the Secretory Pathway.” BMB Reports 54 (5): 246–52. https://doi.org/10.5483/BMBRep.2021.54.5.270.

Passemard, Sandrine, Franck Perez, Pierre Gressens, and Vincent El Ghouzzi. 2019. “Endoplasmic Reticulum and Golgi Stress in Microcephaly.” Cell Stress 3 (12): 369–84. https://doi.org/10.15698/cst2019.12.206.

Paumet, Fabienne, Vahid Rahimian, and James E. Rothman. 2004. “The Specificity of SNARE-Dependent Fusion Is Encoded in the SNARE Motif.” Proceedings of the National Academy of Sciences 101 (10): 3376–80. https://doi.org/10.1073/pnas.0400271101.

Penisson, Maxime, Julia Ladewig, Richard Belvindrah, and Fiona Francis. 2019. “Genes and Mechanisms Involved in the Generation and Amplification of Basal Radial Glial Cells.” Frontiers in Cellular Neuroscience 13 (August): 381. https://doi.org/10.3389/fncel.2019.00381.

Pokrovskaya, Irina D, Rose Willett, Richard D Smith, Willy Morelle, Tetyana Kudlyk, and Vladimir V Lupashin. 2011. “Conserved Oligomeric Golgi Complex Specifically Regulates the Maintenance of Golgi Glycosylation Machinery.” Glycobiology 21 (12): 1554–69. https://doi.org/10.1093/glycob/cwr028.

Polenghi, Martina, and Elena Taverna. 2023. “Intracellular Traffic and Polarity in Brain Development.” Frontiers in Neuroscience 17 (October): 1172016. https://doi.org/10.3389/fnins.2023.1172016.

Polioudakis, Damon, Luis De La Torre-Ubieta, Justin Langerman, et al. 2019. “A Single-Cell Transcriptomic Atlas of Human Neocortical Development during Mid-Gestation.” Neuron 103 (5): 785-801.e8. https://doi.org/10.1016/j.neuron.2019.06.011.

Pucadyil, Thomas J., and Sandra L. Schmid. 2009. “Conserved Functions of Membrane Active GTPases in Coated Vesicle Formation.” Science 325 (5945): 1217–20. https://doi.org/10.1126/science.1171004.

Qian, Xuyu, Yijing Su, Christopher D. Adam, et al. 2020. “Sliced Human Cortical Organoids for Modeling Distinct Cortical Layer Formation.” Cell Stem Cell 26 (5): 766-781.e9. https://doi.org/10.1016/j.stem.2020.02.002.

Quelhas, Dulce, Joana Correia, Jaak Jaeken, et al. 2021. “SLC35A2-CDG: Novel Variant and Review.” Molecular Genetics and Metabolism Reports 26 (March): 100717. https://doi.org/10.1016/j.ymgmr.2021.100717.

Rakic, Pasko. 1995. “A Small Step for the Cell, a Giant Leap for Mankind: A Hypothesis of Neocortical Expansion during Evolution.” Trends in Neurosciences 18 (9): 383–88. https://doi.org/10.1016/0166-2236(95)93934-P.

Rakic, Pasko. 2009. “Evolution of the Neocortex: A Perspective from Developmental Biology.” Nature Reviews Neuroscience 10 (10): 724–35. https://doi.org/10.1038/nrn2719.

Rasika, Sowmyalakshmi, Sandrine Passemard, Alain Verloes, Pierre Gressens, and Vincent El Ghouzzi. 2018. “Golgipathies in Neurodevelopment: A New View of Old Defects.” Developmental Neuroscience 40 (5–6): 396–416. https://doi.org/10.1159/000497035.

Rymen, Daisy, Liesbeth Keldermans, Valérie Race, et al. 2012. “COG5-CDG: Expanding the Clinical Spectrum.” Orphanet Journal of Rare Diseases 7 (1): 94. https://doi.org/10.1186/1750-1172-7-94.

Sakamoto, Masamune, Kazunori Sasaki, Atsushi Sugie, et al. 2021. “De Novo ARF3 Variants Cause Neurodevelopmental Disorder with Brain Abnormality.” Human Molecular Genetics 31 (1): 69–81. https://doi.org/10.1093/hmg/ddab224.

Sasaki, Kanae, Ryota Komori, Mai Taniguchi, et al. 2019. “PGSE Is a Novel Enhancer Regulating the Proteoglycan Pathway of the Mammalian Golgi Stress Response.” Cell Structure and Function 44 (1): 1–19. https://doi.org/10.1247/csf.18031.

Sato, Ken, and Akihiko Nakano. 2007. “Mechanisms of COPII Vesicle Formation and Protein Sorting.” FEBS Letters 581 (11): 2076–82. https://doi.org/10.1016/j.febslet.2007.01.091.

Schindelin, Johannes, Ignacio Arganda-Carreras, Erwin Frise, et al. 2012. “Fiji: An Open-Source Platform for Biological-Image Analysis.” Nature Methods 9 (7): 676–82. https://doi.org/10.1038/nmeth.2019.

Shaheen, Ranad, Shinu Ansari, Muneera J Alshammari, et al. 2013. “A Novel Syndrome of Hypohidrosis and Intellectual Disability Is Linked to COG6 Deficiency.” Journal of Medical Genetics 50 (7): 431–36. https://doi.org/10.1136/jmedgenet-2013-101527.

Shamseldin, Hanan E., Alexis H. Bennett, Majid Alfadhel, Vandana Gupta, and Fowzan S. Alkuraya. 2016. “GOLGA2, Encoding a Master Regulator of Golgi Apparatus, Is Mutated in a Patient with a Neuromuscular Disorder.” Human Genetics 135 (2): 245–51. https://doi.org/10.1007/s00439-015-1632-8.

Shan, Qing-Hong, Xin-Ya Qin, Nan Zhou, et al. 2022. “A Method for Ultrafast Tissue Clearing That Preserves Fluorescence for Multimodal and Longitudinal Brain Imaging.” BMC Biology 20 (1): 77. https://doi.org/10.1186/s12915-022-01275-6.

Shestakova, Anna, Sergey Zolov, and Vladimir Lupashin. 2006a. “COG Complex-Mediated Recycling of Golgi Glycosyltransferases Is Essential for Normal Protein Glycosylation.” Traffic 7 (2): 191–204. https://doi.org/10.1111/j.1600-0854.2005.00376.x.

Shestakova, Anna, Sergey Zolov, and Vladimir Lupashin. 2006b. “COG Complex-Mediated Recycling of Golgi Glycosyltransferases Is Essential for Normal Protein Glycosylation.” Traffic 7 (2): 191–204. https://doi.org/10.1111/j.1600-0854.2005.00376.x.

Short, Benjamin, Alexander Haas, and Francis A. Barr. 2005. “Golgins and GTPases, Giving Identity and Structure to the Golgi Apparatus.” Biochimica et Biophysica Acta (BBA) - Molecular Cell Research 1744 (3): 383–95. https://doi.org/10.1016/j.bbamcr.2005.02.001.

Short, Spencer, Rodrigo García-Tejera, Linus J. Schumacher, and Daniel L. Coutu. 2025. “Next Generation Lineage Tracing and Its Applications to Unravel Development.” Npj Systems Biology and Applications 11 (1): 60. https://doi.org/10.1038/s41540-025-00542-w.

Shull, Gabriella, Christiane Haffner, Wieland B Huttner, Suhasa B Kodandaramaiah, and Elena Taverna. 2019. “Robotic Platform for Microinjection into Single Cells in Brain Tissue.” EMBO Reports 20 (10): e47880. https://doi.org/10.15252/embr.201947880.

Siegenthaler, Julie A., Amir M. Ashique, Konstantinos Zarbalis, et al. 2009. “Retinoic Acid from the Meninges Regulates Cortical Neuron Generation.” Cell 139 (3): 597–609. https://doi.org/10.1016/j.cell.2009.10.004.

Sloan, Steven A., Jimena Andersen, Anca M. Pașca, Fikri Birey, and Sergiu P. Pașca. 2018. "Generation and Assembly of Human Brain Region–Specific Three-Dimensional Cultures." Nature Protocols 13 (9): 2062–85. https://doi.org/10.1038/s41596-018-0032-7.

Soares, Rita, FilipaF Ribeiro, DiogoM Lourenço, et al. 2021. "The Neurosphere Assay: An Effective in Vitro Technique to Study Neural Stem Cells." Neural Regeneration Research 16 (11): 2229. https://doi.org/10.4103/1673-5374.310678.

Sokpor, Godwin, Beate Brand-Saberi, Huu Phuc Nguyen, and Tran Tuoc. 2022. "Regulation of Cell Delamination During Cortical Neurodevelopment and Implication for Brain Disorders." Frontiers in Neuroscience 16 (February): 824802. https://doi.org/10.3389/fnins.2022.824802.

Stukalov, Alexey, Virginie Girault, Vincent Grass, et al. 2021. "Multilevel Proteomics Reveals Host Perturbations by SARS-CoV-2 and SARS-CoV." Nature 594 (7862): 246–52. https://doi.org/10.1038/s41586-021-03493-4.

Swingler, Michael, Martina Donadoni, Anna Bellizzi, Senem Cakir, and Ilker K. Sariyer. 2023. "iPSC-Derived Three-Dimensional Brain Organoid Models and Neurotropic Viral Infections." Journal of NeuroVirology 29 (2): 121–34. https://doi.org/10.1007/s13365-023-01133-3.

Takahashi, Kazutoshi, and Shinya Yamanaka. 2006. "Induction of Pluripotent Stem Cells from Mouse Embryonic and Adult Fibroblast Cultures by Defined Factors." Cell 126 (4): 663–76. https://doi.org/10.1016/j.cell.2006.07.024.

Takano, Tetsuya, Yasuhiro Funahashi, and Kozo Kaibuchi. 2019. "Neuronal Polarity: Positive and Negative Feedback Signals." Frontiers in Cell and Developmental Biology 7 (April): 69. https://doi.org/10.3389/fcell.2019.00069.

Taniguchi, Mai, and Hiderou Yoshida. 2017. "TFE3, HSP47, and CREB3 Pathways of the Mammalian Golgi Stress Response." Cell Structure and Function 42 (1): 27–36. https://doi.org/10.1247/csf.16023.

Tavano, Stefania, Elena Taverna, Nereo Kalebic, et al. 2018. "Insm1 Induces Neural Progenitor Delamination in Developing Neocortex via Downregulation of the Adherens Junction Belt-Specific Protein Plekha7." Neuron 97 (6): 1299-1314.e8. https://doi.org/10.1016/j.neuron.2018.01.052.

Taverna, Elena, Christiane Haffner, Rainer Pepperkok, and Wieland B Huttner. 2012. "A New Approach to Manipulate the Fate of Single Neural Stem Cells in Tissue." Nature Neuroscience 15 (2): 329–37. https://doi.org/10.1038/nn.3008.

Taverna, Elena, and Wieland B. Huttner. 2010. "Neural Progenitor Nuclei IN Motion." Neuron 67 (6): 906–14. https://doi.org/10.1016/j.neuron.2010.08.027.

Taverna, Elena, and Wieland B. Huttner. 2019. "The Golgi Apparatus in Polarized Neuroepithelial Stem Cells and Their Progeny: Canonical and Noncanonical Features." In The Golgi Apparatus and Centriole, edited by Malgorzata Kloc, vol. 67. Results and Problems in Cell Differentiation. Springer International Publishing. https://doi.org/10.1007/978-3-030-23173-6_15.

Taverna, Elena, Felipe Mora-Bermúdez, Paulina J. Strzyz, et al. 2016. "Non-Canonical Features of the Golgi Apparatus in Bipolar Epithelial Neural Stem Cells." Scientific Reports 6 (1): 21206. https://doi.org/10.1038/srep21206.

Travis, Sophie M., Kevin DAmico, I-Mei Yu, et al. 2020. "Structural Basis for the Binding of SNAREs to the Multisubunit Tethering Complex Dsl1." Journal of Biological Chemistry 295 (30): 10125–35. https://doi.org/10.1074/jbc.RA120.013654.

Ungar, Daniel, Toshihiko Oka, Elizabeth E. Brittle, et al. 2002. “Characterization of a Mammalian Golgi-Localized Protein Complex, COG, That Is Required for Normal Golgi Morphology and Function.” The Journal of Cell Biology 157 (3): 405–15. https://doi.org/10.1083/jcb.200202016.

Vahsen, Björn F., Elizabeth Gray, Ana Candalija, et al. 2022. “Human iPSC Co-Culture Model to Investigate the Interaction between Microglia and Motor Neurons.” Scientific Reports 12 (1): 12606. https://doi.org/10.1038/s41598-022-16896-8.

Vajsar, Jiri, and Harry Schachter. 2006. “Walker-Warburg Syndrome.” Orphanet Journal of Rare Diseases 1 (1): 29. https://doi.org/10.1186/1750-1172-1-29.

Van Tol, Walinka, Hans Wessels, and Dirk J Lefeber. 2019. “O-Glycosylation Disorders Pave the Road for Understanding the Complex Human O-Glycosylation Machinery.” Current Opinion in Structural Biology 56 (June): 107–18. https://doi.org/10.1016/j.sbi.2018.12.006.

Varki, Ajit. 2017. “Biological Roles of Glycans.” Glycobiology 27 (1): 3–49. https://doi.org/10.1093/glycob/cww086.

Verheijen, Jan, Shawn Tahata, Tamas Kozicz, Peter Witters, and Eva Morava. 2020. “Therapeutic Approaches in Congenital Disorders of Glycosylation (CDG) Involving N-Linked Glycosylation: An Update.” Genetics in Medicine 22 (2): 268–79. https://doi.org/10.1038/s41436-019-0647-2.

Volchuk, Allen, Mariella Ravazzola, Alain Perrelet, et al. 2004. “Countercurrent Distribution of Two Distinct SNARE Complexes Mediating Transport within the Golgi Stack.” Molecular Biology of the Cell 15 (4): 1506–18. https://doi.org/10.1091/mbc.e03-08-0625.

Wang, Lei, Shirui Hou, and Young-Goo Han. 2016. “Hedgehog Signaling Promotes Basal Progenitor Expansion and the Growth and Folding of the Neocortex.” Nature Neuroscience 19 (7): 888–96. https://doi.org/10.1038/nn.4307.

Weixel, Tara, Lynne Wolfe, and Ellen F. Macnamara. 2024. “Genetic Counseling for Congenital Disorders of Glycosylation (CDG).” Journal of Genetic Counseling 33 (6): 1358–64. https://doi.org/10.1002/jgc4.1856.

Willett, Rose. n.d. “COG Lobe B Sub-Complex Engages v-SNARE GS15 and Functions via Regulated Interaction with Lobe A Sub-Complex.” SCIENTIFIC RepoRts.

Willett, Rose, Jessica Bailey Blackburn, Leslie Climer, et al. 2016. “COG Lobe B Sub-Complex Engages v-SNARE GS15 and Functions via Regulated Interaction with Lobe A Sub-Complex.” Scientific Reports 6 (1): 29139. https://doi.org/10.1038/srep29139.

Wilsch-Bräuninger, Michaela, Jula Peters, Judith T. M. L. Paridaen, and Wieland B. Huttner. 2012. “Basolateral Rather than Apical Primary Cilia on Neuroepithelial Cells Committed to Delamination.” Development 139 (1): 95–105. https://doi.org/10.1242/dev.069294.

Witkos, Tomasz M., and Martin Lowe. 2016. “The Golgin Family of Coiled-Coil Tethering Proteins.” Frontiers in Cell and Developmental Biology 3 (January). https://doi.org/10.3389/fcell.2015.00086.

Xie, Zhigang, Seong Kwon Hur, Liang Zhao, Charles S. Abrams, and Vytas A. Bankaitis. 2018. “A Golgi Lipid Signaling Pathway Controls Apical Golgi Distribution and Cell Polarity during Neurogenesis.” Developmental Cell 44 (6): 725-740.e4. https://doi.org/10.1016/j.devcel.2018.02.025.

Xue, Weiwei, Jiacheng Du, Yunteng Li, and Zhicheng Shao. 2024. “Protocol for Cryopreserving Neural Organoids and Human Living Brain Tissue Using MEDY.” STAR Protocols 5 (4): 103466. https://doi.org/10.1016/j.xpro.2024.103466.

Youn, Yong Ha, and Young-Goo Han. 2018. “Primary Cilia in Brain Development and Diseases.” The American Journal of Pathology 188 (1): 11–22. https://doi.org/10.1016/j.ajpath.2017.08.031.

Zeevaert, R., F. Foulquier, B. Dimitrov, et al. 2008. “Cerebrocostomandibular-like Syndrome and a Mutation in the Conserved Oligomeric Golgi Complex, Subunit 1.” Human Molecular Genetics 18 (3): 517–24. https://doi.org/10.1093/hmg/ddn379.

Zhang, Yong Ci, Yuan Zhou, Chun Zheng Yang, and Dong Sheng Xiong. n.d. A Review of ERGIC-53: Its Structure, Functions, Regulation and Relations with Diseases.

Zhou, Shuling, Karolina Szczesna, Anna Ochalek, et al. 2016. “Neurosphere Based Differentiation of Human iPSC Improves Astrocyte Differentiation.” Stem Cells International 2016 (1): 4937689. https://doi.org/10.1155/2016/4937689.

Zhou, Yan, Joshua B. Atkins, Santiago B. Rompani, et al. 2007. “The Mammalian Golgi Regulates Numb Signaling in Asymmetric Cell Division by Releasing ACBD3 during Mitosis.” Cell 129 (1): 163–78. https://doi.org/10.1016/j.cell.2007.02.037.

Zolov, Sergey N., and Vladimir V. Lupashin. 2005. “Cog3p Depletion Blocks Vesicle-Mediated Golgi Retrograde Trafficking in HeLa Cells.” The Journal of Cell Biology 168 (5): 747–59. https://doi.org/10.1083/jcb.200412003.